

Measurement of single top-quark production in association with a W boson in pp collisions at $\sqrt{s} = 13$ TeV with the ATLAS detector

G. Aad *et al.**
(ATLAS Collaboration)

 (Received 23 July 2024; accepted 11 September 2024; published 17 October 2024)

The inclusive cross section for the production of a single top quark in association with a W boson is measured using 140 fb^{-1} of proton-proton collision data collected with the ATLAS detector at $\sqrt{s} = 13$ TeV. Events containing two charged leptons and at least one jet identified as originating from a b -quark are selected. A multivariate discriminant is constructed to separate the tW signal from the $t\bar{t}$ background. The cross section is extracted using a profile likelihood fit to the signal and control regions and it is measured to be $\sigma_{tW} = 75_{-14}^{+15}$ pb, in good agreement with the Standard Model prediction. The measured cross section is used to extract a value for the left-handed form factor at the Wtb vertex times the Cabibbo-Kobayashi-Maskawa matrix element $|f_{LV}V_{tb}|$ of 0.97 ± 0.10 .

DOI: [10.1103/PhysRevD.110.072010](https://doi.org/10.1103/PhysRevD.110.072010)

I. INTRODUCTION

Top quarks are predominantly produced at the Large Hadron Collider (LHC) [1] in pairs via the strong interaction. However, they can also be produced singly through processes that involve the electroweak Wtb vertex, thus providing important tests of the electroweak interaction involving the third-generation quarks. In the Standard Model (SM), single top-quark production at leading-order (LO) can be classified as proceeding through three distinct channels: $qb \rightarrow tq'$ and $q\bar{q}' \rightarrow t\bar{b}$ (and their charge conjugates) via t -channel and s -channel W -boson propagators, respectively, and tW production, as shown in Fig. 1.

At the LHC, the tW -channel has the second largest single top-quark production cross section following the $qb \rightarrow tq'$ t -channel. It represents approximately 26% of the total single top-quark production rate at 13 TeV, which makes it experimentally accessible at the LHC. In addition, tW production is the only single top-quark production mechanism that can be measured in the dilepton final state with relatively clean signatures where the only significant background is from top-quark pair production ($t\bar{t}$).

The cross section for each of the three single top-quark production channels is primarily dominated by the coupling between the W boson and the top and bottom quarks, which

is proportional to the square of the Cabibbo-Kobayashi-Maskawa (CKM) matrix element $|V_{tb}|^2$ [2,3]. Single top-quark production therefore presents an opportunity to precisely test the structure of the SM, and to search for signs of physics beyond the SM (BSM) that can affect the Wtb vertex. The value of $|f_{LV}V_{tb}|^2$, where f_{LV} is the left-handed form factor, was measured to be 1.015 ± 0.031 in the $qb \rightarrow tq'$ t -channel [4]. In contrast to the t -channel and $q\bar{q}' \rightarrow t\bar{b}$ s -channel processes, where BSM effects can arise from both the existence of four-fermion operators and corrections to the Wtb vertex, the tW -channel solely relies on the latter. It is therefore crucial to investigate this channel independently to make a detailed comparison with the other channels [5,6]. Furthermore, a precise measurement and good modeling of the tW process is needed for many BSM searches [7,8] and in Higgs boson and other top-quark measurements, where it is one of the main background processes.

The predicted cross section of tW production in proton-proton (pp) collisions at a center-of-mass energy of 13 TeV is $\sigma_{tW}^{\text{theory}} = 79.3_{-1.8}^{+1.9}(\text{scale}) \pm 2.2(\text{PDF})$ pb and is computed at next-to-leading-order (NLO) in quantum chromodynamics (QCD) with the addition of third-order corrections from soft-gluon emissions by resumming next-to-next-to-leading-logarithmic (NNLL) terms [9]. The top-quark mass is set to 172.5 GeV and the PDF4LHC21 set of parton distribution functions (PDFs) [10] is used. The quoted uncertainty includes the uncertainty due to the choice of the renormalization scale μ_r and the factorization scale μ_f , as well as the uncertainty in the PDFs. The uncertainty in the scale choice is determined by varying the scales simultaneously up and down by a factor of two relative to the nominal value. The PDF uncertainties are

*Full author list given at the end of the article.

Published by the American Physical Society under the terms of the [Creative Commons Attribution 4.0 International license](https://creativecommons.org/licenses/by/4.0/). Further distribution of this work must maintain attribution to the author(s) and the published article's title, journal citation, and DOI. Funded by SCOAP³.

based on the Hessian method and include the uncertainty in the strong coupling constant α_s .

Accurate estimates of rates and kinematic distributions of the tW process are made more difficult at higher orders in α_s due to quantum interference with the $t\bar{t}$ process. Two commonly used approaches to separate tW and $t\bar{t}$ production beyond LO are diagram removal (DR) and diagram subtraction (DS) [11]. In the DR approach, all doubly resonant NLO diagrams are removed from the calculation of the tW amplitude. Instead, in the DS approach a subtraction term is implemented in the matrix-element calculation to locally cancel out the $t\bar{t}$ doubly resonant contributions. This interference effect was studied using 13 TeV collision data by the ATLAS collaboration [12] and the results provide an important constraint on interference models.

At the LHC, evidence for the tW process with 7 TeV collision data was presented by the ATLAS collaboration [13] (with a significance of 3.6σ), and by the CMS collaboration [14] (with a significance of 4.0σ). With 8 TeV collision data, CMS reported the observation of the tW -channel with a significance of 6.1σ [15] while ATLAS observed it with a significance of 7.7σ [16,17]. The tW cross section was also measured with 13 TeV collision data inclusively and differentially by the ATLAS [18,19] and CMS collaborations [20–22].

In this paper, a measurement of tW production is reported, extending previous measurements, by using a data sample collected with the ATLAS detector from 2015 to 2018 and corresponding to an integrated luminosity of 140 fb^{-1} of pp collisions at a center-of-mass energy of $\sqrt{s} = 13 \text{ TeV}$. After a brief introduction of the ATLAS detector in Sec. II, further details of the data sample and the simulated samples used for the measurement are given in Sec. III. The measurement is made using events containing at least one b -jet (identified as containing a b -hadron) and exactly one electron and one muon with opposite charge in the final state, produced either directly from the decay of a W boson or from the decay of an intermediate τ -lepton. The tW signal appears in this final state when the top quark decays into a W boson and a b -quark, with both the W bosons decaying leptonically, as shown in Fig. 1. The ee and $\mu\mu$ dilepton channels are not considered due to an additional large background from Drell-Yan $Z/\gamma^* \rightarrow e^+e^-$ (or $\mu^+\mu^-$) processes. The object and event selection details are provided in Sec. IV.

Selected events are grouped into three different regions based on jet and b -jet multiplicities. A boosted decision tree (BDT) analysis is performed in each of the three regions to build discriminants to separate the tW signal from the dominant $t\bar{t}$ background. Details of the input variables and the BDT training are given in Sec. V, while the systematic uncertainties considered are discussed in Sec. VI. A simultaneous fit to the three regions is used to extract the signal strength, defined as the measured tW cross

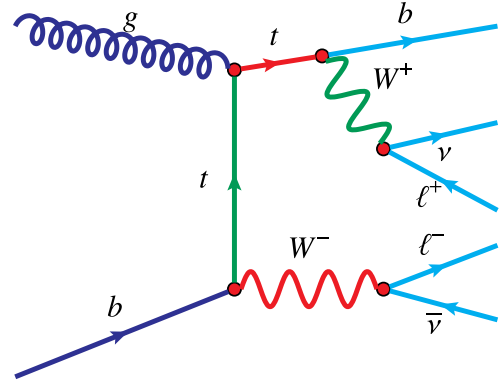


FIG. 1. A representative leading-order Feynman diagram for the production of a single top quark in the tW -channel and then the decay of the W boson and the top quark giving two leptons in the final state.

section over the SM prediction, and the $t\bar{t}$ normalization. The systematic uncertainties are included as nuisance parameters in the fit to data. To avoid overconstraining some systematic uncertainties in nonphysical ways, a limited range of the BDT discriminant is used in a profile-likelihood fit. This approach enhances the reliability of the measurement, at the cost of a slightly larger uncertainty. The fit procedure and the results are detailed in Secs. VII and VIII, respectively, and conclusions are given in Sec. IX.

II. ATLAS DETECTOR

The ATLAS detector [23] at the LHC covers nearly the entire solid angle around the collision point.¹ It consists of an inner tracking detector surrounded by a thin superconducting solenoid, electromagnetic and hadronic calorimeters, and a muon spectrometer incorporating three large superconducting air-core toroidal magnets.

The inner-detector system (ID) is immersed in a 2 T axial magnetic field and provides charged-particle tracking in the range $|\eta| < 2.5$. The high-granularity silicon pixel detector covers the vertex region and typically provides four measurements per track, the first hit generally being in the insertable B-layer installed before run 2 [24,25]. It is followed by the SemiConductor Tracker, which usually provides eight measurements per track. These silicon

¹ATLAS uses a right-handed coordinate system with its origin at the nominal interaction point in the center of the detector and the z axis along the beam pipe. The x axis points from the interaction point to the center of the LHC ring, and the y axis points upwards. Polar coordinates (r, ϕ) are used in the transverse plane, ϕ being the azimuthal angle around the z axis. The pseudorapidity is defined in terms of the polar angle θ as $\eta = -\ln \tan(\theta/2)$ and is equal to the rapidity $y = \frac{1}{2} \ln \left(\frac{E+p_z c}{E-p_z c} \right)$ in the relativistic limit. Angular distance is measured in units of $\Delta R \equiv \sqrt{(\Delta y)^2 + (\Delta \phi)^2}$.

detectors are complemented by the transition radiation tracker, which enables radially extended track reconstruction up to $|\eta| = 2.0$. The transition radiation tracker also provides electron identification information based on the fraction of hits (typically 30 in total) above a higher energy-deposit threshold corresponding to transition radiation.

The calorimeter system covers the pseudorapidity range $|\eta| < 4.9$. Within the region $|\eta| < 3.2$, electromagnetic calorimetry is provided by barrel and end cap high-granularity lead/liquid-argon (LAr) calorimeters, with an additional thin LAr presampler covering $|\eta| < 1.8$ to correct for energy loss in material upstream of the calorimeters. Hadronic calorimetry is provided by the steel/scintillator-tile calorimeter, segmented into three barrel structures within $|\eta| < 1.7$, and two copper/LAr hadronic end cap calorimeters. The solid angle coverage is completed with forward copper/LAr and tungsten/LAr calorimeter modules optimized for electromagnetic and hadronic energy measurements, respectively.

The muon spectrometer comprises separate trigger and high-precision tracking chambers measuring the deflection of muons in a magnetic field generated by the superconducting air-core toroidal magnets. The field integral of the toroids ranges between 2.0 and 6.0 Tm across most of the detector. Three layers of precision chambers, each consisting of layers of monitored drift tubes, cover the region $|\eta| < 2.7$, complemented by cathode-strip chambers in the forward region, where the background is highest. The muon trigger system covers the range $|\eta| < 2.4$ with resistive-plate chambers in the barrel, and thin-gap chambers in the end cap regions.

The luminosity is measured mainly by the LUCID-2 [26] detector that records Cherenkov light produced in the quartz windows of photomultipliers located close to the beam pipe.

Events are selected by the first-level trigger system implemented in custom hardware, followed by selections made by algorithms implemented in software in the high-level trigger [27]. The first-level trigger accepts events from the 40 MHz bunch crossings at a rate below 100 kHz, which the high-level trigger further reduces in order to record complete events to disk at about 1 kHz.

A software suite [28] is used in data simulation, in the reconstruction and analysis of real and simulated data, in detector operations, and in the trigger and data acquisition systems of the experiment.

III. DATA AND SIMULATION

Data were collected with the ATLAS detector from 2015 to 2018 in pp collisions at a center-of-mass energy of $\sqrt{s} = 13$ TeV delivered by the LHC. The full data sample corresponds to an integrated luminosity of 140 fb^{-1} .

Monte Carlo (MC) simulation is used to model the signal and background processes. The effect of multiple

interactions in the same and neighboring bunch crossings (pileup) is modeled by overlaying the original hard-scattering event with simulated minimum-bias events generated with PYTHIA8.186 [29] using the NNPDF2.3LO PDF set [30] and the A3 set of tuned parameters (tune) [31]. The MC simulated events are weighted to reproduce the distribution of the interactions per bunch crossing observed in the data, referred to as “pileup reweighting”. In all top-quark samples, the top-quark mass is set to $m_{\text{top}} = 172.5$ GeV. The decays of bottom and charm hadrons are simulated using the EVTGEN program [32] for all non-SHERPA samples.

Single-top tW production is modeled using the POWHEG BOX v2 [33–36] generator which provides matrix elements at NLO in the strong coupling constant α_s in the five-flavor scheme with the NNPDF3.0NLO PDF set. The functional form of the renormalization and factorization scale is set to the default scale, which is equal to the top-quark mass. The diagram-removal scheme is used to treat the interference with $t\bar{t}$ production [37]. The events are interfaced with PYTHIA8.230 [38] using the A14 tune [39] and the NNPDF2.3LO PDF set. The inclusive cross section is normalized to the theory prediction calculated at NLO in QCD with NNLL soft-gluon corrections [9].

The $t\bar{t}$ events are simulated using the POWHEG BOX v2 [34–36,40] generator at NLO with the NNPDF3.0NLO PDF and the h_{damp} parameter² set to $1.5 m_{\text{top}}$ [37]. The events are interfaced with PYTHIA8.230 using the A14 tune [39] and the NNPDF2.3LO PDF set. The NLO $t\bar{t}$ inclusive production cross section is corrected to the theory prediction at next-to-next-to-leading-order (NNLO) in QCD including the resummation of NNLL soft-gluon terms calculated using TOP++2.0 [41–47]. The $t\bar{t}$ samples are normalized to a reference cross section of $832_{-29}^{+20} \pm 35$ pb, where the first uncertainty corresponds to QCD scale uncertainties and the second to PDF uncertainties.

Various samples are simulated to evaluate the modeling uncertainties in the tW and $t\bar{t}$ production. Further variations are obtained from the baseline sample, by using event weights to change the QCD factorization and renormalization scales, and the amounts of initial and final state radiation. Alternative samples to evaluate the parton shower and hadronization uncertainties of tW and $t\bar{t}$ are produced with the POWHEG BOX v2 generator at NLO in QCD in the five-flavor scheme using the NNPDF3.0NLO PDF. The events are interfaced with HERWIG7.04 [48,49], using the H7UE tune [49] and the MMHT2014LO PDF set [50].

To assess the uncertainty in the hard scattering simulation and the matching scheme, additional tW and $t\bar{t}$ samples are generated with the MADGRAPH5_AMC@NLO

²The h_{damp} parameter controls the transverse momentum p_T of the first additional emission beyond the leading-order Feynman diagram in the parton shower and therefore regulates the high- p_T emission against which the $t\bar{t}$ system recoils.

generator at NLO in QCD in the five-flavor scheme, interfaced with PYTHIA8.230.

Previous studies have seen improved agreement between data and prediction in $t\bar{t}$ events, particularly for the top-quark p_T distribution, when comparing with NNLO calculations [51]. Therefore, all $t\bar{t}$ samples are reweighted to match their top-quark p_T distribution to that predicted at NNLO in QCD and NLO electroweak (EW) accuracy [52].

To estimate the uncertainty in the interference between tW and $t\bar{t}$ production, an alternative tW POWHEG+PYTHIA8 sample is simulated using the diagram-subtraction scheme.

Backgrounds with minor contributions, referred to as minor backgrounds in the following, are also simulated. The production of a vector boson in association with jets, $V + \text{jets}$ ($V = W, Z$) is simulated with the SHERPA v2.2.1 [53] generator. In this setup, NLO-accurate matrix elements for up to two jets, and LO-accurate matrix elements for up to four jets are calculated with the Comix [54] and OPENLOOPS [55,56] libraries. They are matched with the SHERPA parton shower [57] using the MEPS@NLO prescription [58–61]. Diboson samples, with fully leptonic and semileptonic decays, are simulated with the SHERPA v2.2.2 [53] generator. In this setup multiple matrix elements are matched and merged with the SHERPA parton shower based on Catani-Seymour dipole factorization [54,57] using the MEPS@NLO prescription. The virtual QCD corrections for matrix elements at NLO accuracy are provided by the OPENLOOPS library. These SHERPA samples are simulated using the NNPDF3.0NNLO set, along with the dedicated set of tuned parton-shower parameters developed by the SHERPA authors.

The MC simulated samples used for the nominal estimates were processed through a simulation [62] of the ATLAS detector based on GEANT [63], while those used for evaluating systematic uncertainties were processed with a fast simulation that relies on a parametrization of the calorimeter response [64].

IV. OBJECT AND EVENT SELECTION

This section describes the reconstruction of the basic objects used in the analysis and how events are selected using these objects. Events must first be selected by a single-electron trigger [65] or a single-muon trigger [66]. The lowest p_T threshold used for electrons was 24 GeV (26 GeV) in 2015 (2016–2018), while for muons the threshold was 20 GeV (26 GeV).

A. Object reconstruction

The primary vertex is selected as the pp vertex candidate that has at least two tracks and the highest sum of the squared transverse momenta of all the matched tracks with $p_T > 500$ MeV [67].

Electron candidates are reconstructed from energy deposits in the electromagnetic calorimeter matched with ID tracks [68]. The clusters are required to be in the

pseudorapidity range $|\eta| < 2.47$, with the transition region between the barrel and end cap electromagnetic calorimeters, $1.37 < |\eta| < 1.52$, excluded. The candidate electrons are required to have transverse energy $E_T > 20$ GeV. Further requirements on the electromagnetic shower shape, calorimeter energy to tracker momentum ratio, and other discriminating variables are combined into a likelihood-based object quality cut, to enhance electron selection efficiency while rejecting backgrounds from photon conversions and hadrons misidentified as electrons [68]. Furthermore, electrons are required to be isolated from other activity in the event using criteria based on the calorimeter energy in a cone of radius $\Delta R = 0.2$ around the electron, and the sum of the p_T of tracks in a cone with size varying with electron p_T . The efficiency of the isolation requirement depends on the electron p_T . For example, in $Z \rightarrow ee$ decays, it is 90% (99%) efficient for electrons with $p_T > 25$ GeV ($p_T > 60$ GeV). Electron tracks are also required to be consistent with coming from the primary vertex requiring $|d_0/\sigma_{d_0}| < 5$ and $|z_0 \sin \theta| < 0.5$ mm. Here d_0 and $\sigma(d_0)$ are the transverse impact parameter and its uncertainty, and z_0 is the longitudinal impact parameter relative to the primary vertex of the event along the beam line.

Muon candidates are identified by matching reconstructed ID tracks with tracks in the muon spectrometer [69], and are required to have $|\eta| < 2.5$ and $p_T > 20$ GeV. To reduce background from heavy flavor decays into muons inside jets, muons are required to satisfy analogous isolation requirements to electrons. Muon tracks are also required to be consistent with the primary vertex requiring $|d_0/\sigma_{d_0}| < 3$ and $|\Delta z_0 \sin \theta| < 0.5$ mm. Similarly to electrons, correction factors are applied to simulated muons to account for small differences between data and simulation in the identification efficiencies.

Jets are reconstructed using a particle-flow algorithm [70], using calorimeter measurements for the energies of neutral particles and ID track-momentum measurements for charged hadrons. Jet reconstruction starts with particle-flow objects and are formed using the anti- k_r algorithm with radius parameter of $R = 0.4$ [71,72]. These jets are then calibrated to the particle level by the application of a jet energy scale derived from simulation. The jet energy is further corrected by applying *in situ* corrections for the contribution from pileup events based on $\sqrt{s} = 13$ TeV data [73]. Selected jets are required to have $p_T > 20$ GeV and $|\eta| < 2.5$ to ensure all of the matched charged particles are inside the coverage of the ID. To suppress jets arising from pileup, a discriminant called the jet-vertex-tagger (JVT) [74] is constructed using a two-dimensional likelihood method. The JVT discriminates between jets produced in the hard-scatter and pileup processes, and is required to be larger than 0.59 for the jets with $p_T < 60$ GeV and $|\eta| < 2.4$, corresponding to 92% efficiency in $t\bar{t}$ events.

Jets containing b -hadrons (b -jets) are identified using the DL1r [75] algorithm, which uses a deep feed-forward neural network to calculate the probability that a jet is a b -jet, c -jet, or light jet (jets containing neither a b - or c -hadron). The inputs to this b -tagging algorithm include impact parameter and reconstructed secondary vertex information from tracks in the jet. Candidate b -jets are required to have a b -tagging discriminant value greater than a threshold that corresponds to a b -tagging efficiency of 77% in simulated $t\bar{t}$ events. With this requirement the rejection factors are 170 for light jets and five for c -jets. Correction factors are applied to account for remaining differences between data and simulation separately for b -jets, c -jets, and light jets.

The missing transverse momentum, with magnitude E_T^{miss} , serves as an indicator of the transverse momentum attributed to undetected neutrinos, computed as the magnitude of the negative vector sum of the momenta of all identified particles (electrons, photons, muons, τ -leptons, and jets) in the event transverse plane [76]. It also includes a contribution from soft hadronic activity by using reconstructed charged-particle tracks matched with the primary vertex but not with any of the reconstructed objects.

To avoid cases where the detector response to a single physical object is reconstructed as two separate final-state objects, an overlap-removal procedure is employed. First, if an electron candidate and a muon candidate share a track, the electron candidate is removed. Next, the closest jet to each electron within a ΔR distance of 0.2 is removed to reduce the portion of electrons being reconstructed as jets. Electrons within distances of $0.2 \leq \Delta R < 0.4$ from any of the remaining nonpileup jets are removed to reduce backgrounds from nonprompt, nonisolated electrons resulting from heavy flavor hadron decays. Jets with fewer than three matched tracks and a distance $\Delta R < 0.2$ from a muon candidate are then removed to reduce fake jets from muons depositing energy in the calorimeters. Finally muons that are a distance of $0.2 \leq \Delta R < 0.4$ from any of the surviving jets are removed to avoid contamination with nonprompt muons from heavy flavor hadron decays.

B. Event selection and categorization

After the objects are identified, a selection is applied to maximize the purity of tW signal events while reducing major background contributions from $t\bar{t}$ and minor contributions from $Z + \text{jets}$, $W + \text{jets}$, and diboson production. Simulated events with at least one selected electron or muon which is misidentified or nonprompt (i.e., matched to a b - or c -hadron decay, a misidentified jet, a kaon or pion decay, or an electron from a photon conversion) are separated out from all available MC samples and are merged to estimate the misidentified/nonprompt background. The contribution where both the leptons are misidentified/nonprompt was determined to be negligible. The misidentified/nonprompt background estimate is

validated using $e^\pm\mu^\pm$ same-charge regions with the same jet multiplicities, where a larger contribution of such background is present.

The tW final state used for this measurement comprises two oppositely charged leptons ($e^\pm\mu^\mp$ events) and missing transverse momentum from the two W boson decays, and one b -jet from the top-quark decay. The event preselection begins by requiring an oppositely charged electron-muon pair (dilepton $e^\pm\mu^\mp$ events). The leading lepton in the event must satisfy $p_T > 27$ GeV, while an event is rejected if a third lepton is present with $p_T > 20$ GeV. One of the selected leptons must be matched to the trigger object used to select the event. At least one jet with $p_T > 25$ GeV, $|\eta| < 2.5$, and b -tagged at the 77% efficiency criterion discussed above, is required in each event.

After preselection, the dilepton events are categorized based on the jet and b -jet multiplicities. At LO the signal process results in a final state with one b -jet arising from the top-quark decay, while the $t\bar{t}$ process results in two b -jets from the two top-quark decays. Events with one additional jet are also considered due to the expected contributions to the tW signal mostly from QCD radiation in higher-order processes.

Based on the expected final states, three orthogonal event categories are defined: events with exactly one selected jet that is also b -tagged (denoted 1j1b), events with exactly two selected jets one of which is b -tagged (2j1b), and events with exactly two jets where each are b -tagged (2j2b). The third category helps to constrain the $t\bar{t}$ background normalization. These three categories, 1j1b, 2j1b, and 2j2b, are referred to as fit regions, as they are used in the simultaneous fit procedure described in Sec. VII.

The expected event yields after preselection, separated according to fit region, for the signal and background processes with their total uncertainties before fit, are shown in Table I. Also shown is the number of observed data events in each fit region. Agreement between data and simulation in all regions is observed.

V. SEPARATION OF SIGNAL FROM BACKGROUND

After the event preselection described in Sec. IV, the selected dilepton events consist primarily of $t\bar{t}$ and tW with minor contributions from other processes as listed in Table I.

To better separate events from tW production and those from $t\bar{t}$, BDTs are used, based on the implementation provided by the LightGBM software package [77]. One BDT is trained for each analysis fit region, with simulated tW events serving as signal and simulated $t\bar{t}$ events serving as background. Other minor backgrounds are not included in the training procedure.

Reconstructed final-state objects (jets, leptons, E_T^{miss}) are used to construct various kinematic quantities.

TABLE I. Expected and observed number of events in each fit region of the analysis after preselection. The tW and $t\bar{t}$ processes are normalized to their respective theoretical cross sections. The uncertainties include statistical and systematic uncertainties while the uncertainties stemming from the theoretical calculation of the tW and $t\bar{t}$ processes are not included.

	1j1b	2j1b	2j2b
tW	$27\,500 \pm 2\,400$	$17\,500 \pm 1\,900$	$5\,400 \pm 900$
$t\bar{t}$	$111\,000 \pm 11\,000$	$182\,000 \pm 12\,000$	$155\,000 \pm 14\,000$
Z + jets	$1\,810 \pm 230$	$1\,000 \pm 120$	87 ± 19
Diboson	820 ± 180	840 ± 190	23.2 ± 3.2
Misidentified/nonprompt lepton	430 ± 220	800 ± 400	180 ± 90
Total prediction	$141\,000 \pm 12\,000$	$202\,000 \pm 12\,000$	$160\,000 \pm 14\,000$
Data	139349	199095	158314

TABLE II. Definitions of variable names constructed from the set of final-state objects $s = (o_1, \dots, o_n)$ for $n \geq 1$. For variables that compare two sets of objects, s_1 and s_2 , \vec{s}_i is the momentum-vector sum of the objects in set s_i .

Variable	Definition
$p_T(s)$	Transverse component of the vector sum of momenta
$m(s)$	Invariant mass of the system of multiple objects s
$H(s)$	Scalar sum of momenta
$H_T(s)$	Scalar sum of transverse momenta
Centrality(s)	Centrality of the system s , given by $H_T(s)/H(s)$
$\Delta R(\vec{s}_1, \vec{s}_2)$	$\eta - \phi$ separation between \vec{s}_1 and \vec{s}_2
$\Delta p_T(\vec{s}_1, \vec{s}_2)$	Magnitude of the transverse component of $\vec{s}_1 - \vec{s}_2$
$H_T^{\text{ratio}}(s_1, s_2)$	Ratio of the H_T of the two systems: $H_T(s_1)/H_T(s_2)$
$p_T(j_{S1})$	p_T of the leading soft jet
$m_T(o_1 E_T^{\text{miss}})$	Transverse mass of object o_1 and E_T^{miss} : $m_T = \sqrt{2p_T(o_1)E_T^{\text{miss}}(1 - \cos \Delta\phi(o_1, E_T^{\text{miss}}))}$

The definitions of these variables are given in Table II. For a given object type, the subscript 1 is used to denote the object with highest p_T , referred to as the leading object. For example, $p_T(\ell_1 \ell_2 j_1 E_T^{\text{miss}})$ is the p_T of the vector sum of momenta of the leading lepton, subleading lepton, leading jet, and E_T^{miss} . Although jets are required to have $p_T > 25$ GeV to define the fit regions, the transverse momentum of additional soft jets (j_S) in events is considered, where the soft jets are defined by having $20 \text{ GeV} < p_T < 25 \text{ GeV}$. In cases where no soft jet is present, a value of zero is used.

For each fit region, an optimization procedure maximizes the area under the receiver operating characteristic curve value while reducing overtraining. The signal and background samples are separated into three categories for the optimization procedure: training set (40% of each sample), validation set (20% of each sample), and testing set (40% of each sample). A grid search is performed to find the optimal hyperparameters of the BDT model.

Two strategies are used to prevent overtraining in parallel with the grid search optimization. The first strategy is the practice of early stopping. Early stopping is a mechanism to end the training procedure if the area under the receiver operating characteristic curve value of the validation set stops improving. The second strategy is to do a two-sample Kolmogorov-Smirnov (KS) test [78,79] on the training and

test sets. The KS test is performed on the signal and background samples (comparing the training and testing distributions). If one of the signal or background KS-test p values is less than 0.05, then the specific grid point is rejected. The final hyperparameter configuration is chosen by selecting the training configuration with the highest area under the curve after rejecting any overtrained models. The final hyperparameter configuration for each region is reported in Table III.

The list of variables used and their rank for all fit regions is given in Table IV. The number of variables is significantly smaller and thus the training procedure is simplified; compared with using the complete set of variables, a performance loss of less than 2% of the maximum

TABLE III. The final hyperparameter settings of the BDTs trained in each analysis region.

Region	Learning rate	Number of leaves	Minimum data in a leaf	Maximum depth
1j1b	0.2	20	50	4
2j1b	0.1	20	120	7
2j2b	0.2	20	50	4

TABLE IV. Importance ranks for the variables used in the BDT for all three regions. The variable name definitions are given in Table II. The variables without a rank are not used in that region and “–” indicates undefined variables in that region.

Variable	1j1b	2j1b	2j2b
$p_T(\ell_1 \ell_2 j_1 E_T^{\text{miss}})$	1	3	
$p_T(j_{S1})$	2		
Centrality($\ell_1 \ell_2$)	3		
$m_T(j_1 E_T^{\text{miss}})$	4		
$m(\ell_1 j_1)$	5	2	1
$m(\ell_2 j_1)$	6		4
$\Delta p_T(\ell_1, \ell_2)$	7		
$p_T(\ell_1 \ell_2)$	8	5	
$m(\ell_2 j_1 E_T^{\text{miss}})$	9		
$p_T(j_1 E_T^{\text{miss}})$	10		
$\Delta R(\ell_2, j_1)$		6	
$p_T(\ell_1 \ell_2 E_T^{\text{miss}})$			6
$m(\ell_1 j_2)$	–	1	2
$p_T(\ell_1 \ell_2 j_1 j_2 E_T^{\text{miss}})$	–	4	
$H_T^{\text{ratio}}(\ell_1 \ell_2, \ell_1 \ell_2 j_1 j_2 E_T^{\text{miss}})$	–	7	
$H_T^{\text{ratio}}(\ell_1 \ell_2, \ell_1 \ell_2 j_1 E_T^{\text{miss}})$	–	8	
$p_T(j_2)$	–		3
$m(\ell_2 j_2)$	–		5

performance is achieved. LightGBM can report the importance based on how much the performance is improved by using a particular variable. The top three variables from each region according to this importance metric is given where the sum of gains for all variables is normalized to one. Distributions of the three highest ranked variables for each region are shown in Fig. 2. The BDT outputs are shown in Fig. 3. The prefit uncertainty shown in each distribution includes the complete set of uncertainties described in Sec. VI. The BDT range used in the fit described in Sec. VII is indicated by vertical dashed lines. The MC predictions describe the data well, consistent with the total systematic uncertainties.

VI. SYSTEMATIC UNCERTAINTIES

Systematic uncertainties are divided into experimental and theoretical sources. Each uncertainty is assigned a Gaussian distributed nuisance parameter that allows the uncertainty to be constrained by data.

A. Experimental uncertainties

Sources of experimental uncertainty include the uncertainties in the lepton efficiencies, the lepton energy scale and resolution, the E_T^{miss} soft-term calculation, the jet energy scale (JES) and resolution (JER), the JVT, the b -tagging efficiency, the pileup reweighting and the luminosity measurement. Among these, the dominant sources of uncertainty are those in the determination of JES and JER.

The differences between the electron (muon) trigger, reconstruction and isolation efficiencies in data and those in MC simulation are corrected for by scale factors derived from dedicated $Z \rightarrow ee$ ($Z \rightarrow \mu\mu$) enriched control samples using a tag-and-probe method [68,69].

The JES is calibrated using simulation and *in situ* techniques [73]. The JES uncertainty is decomposed into a set of 30 uncorrelated components. The contributing effects are from pileup, jet flavor composition and response, single particle detector response, η intercalibration, *in situ* measurement, and the properties of jets not completely contained inside of the calorimeter volume. The JER uncertainty is represented by eight components accounting for differences between data and MC simulation [73]. The uncertainties in the b -tagging calibration are determined separately for b -jets, c -jets, and light-flavor jets [80–82]. A total of 19 components, accounting for differences between data and simulation, are used (nine for b -jets, four for c - and light jets, and two for the MC-based extrapolation to high- p_T jets). These uncertainty factors are applied as changes to the scale factor weights on a per-event basis.

The energy scale and resolution uncertainties for hard objects (leptons and jets) are propagated to the E_T^{miss} through the recomputation of its corresponding terms. Therefore, the impact is evaluated when the event selections are reapplied after having shifted the lepton or jet energy. The soft track related uncertainties are derived from comparisons between data and MC simulation of the p_T balance between the hard and soft E_T^{miss} components using Z + jets events [76].

The uncertainty in the combined 2015–2018 integrated luminosity is 0.83% [83], derived from the calibration of the luminosity scale using x - y beam-separation scans, and using the LUCID-2 detector for the baseline luminosity measurements [26].

B. Theoretical uncertainties

Uncertainties stemming from theoretical models are estimated by comparing a set of predicted distributions produced with different modeling assumptions.

One of the most important theoretical uncertainties is the interference between tW and $t\bar{t}$ processes. The uncertainty is evaluated by comparing the DR and DS schemes as implemented in POWHEG BOX2 while the $t\bar{t}$ sample remains unchanged. The uncertainty is symmetrized.

The uncertainty due to the choice of the matching scheme is assessed by comparing the nominal generator setup with an alternative setup for $t\bar{t}$ and tW , using MADGRAPH5_AMC@NLO [84] with the NNPDF3.0NLO PDF set for the hard-scattering calculation. These are interfaced with PYTHIA8.230 using the A14 tune and the NNPDF23LO PDF set. This uncertainty is symmetrized.

The uncertainty in parton showering and hadronization is evaluated by comparing POWHEG BOX2+ PYTHIA8 and

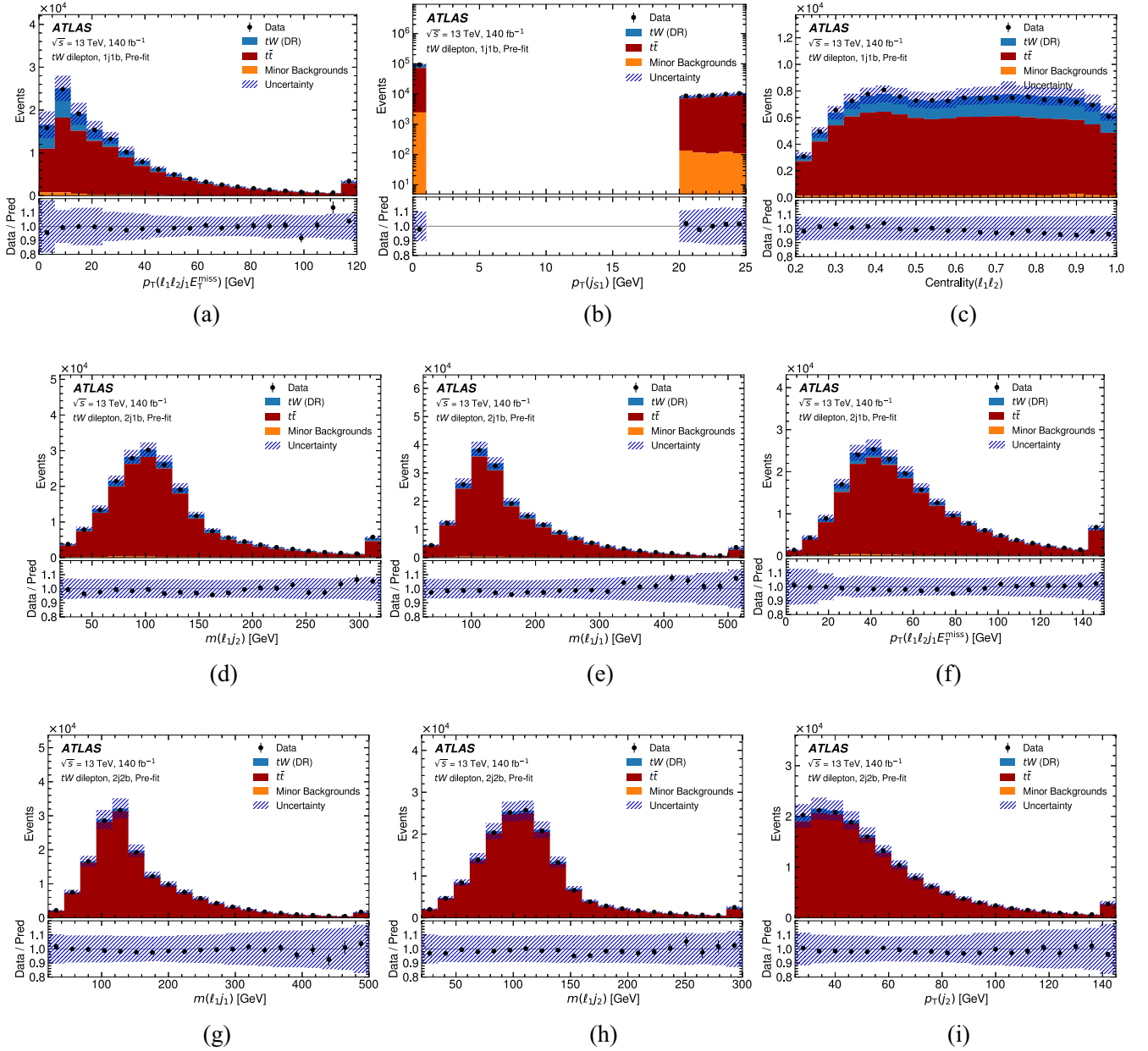


FIG. 2. BDT input distributions for the three highest ranked variables (defined in Table IV) from the 1j1b region [(a)–(c)], the 2j1b region [(d)–(f)], and the 2j2b region [(g)–(i)] before the fit. The “minor background” includes Z + jets, diboson, and misidentified/nonprompt lepton contributions. The first and last bin include the underflow and overflow, respectively. The upper panels give the yields in number of events per bin, while the lower panels give the ratios of the numbers of observed events to the total prediction in each bin. The uncertainty bands represent both statistical and systematic uncertainties, where all sources of systematic uncertainty are assumed to be uncorrelated.

POWHEG BOX2+ HERWIG7 samples for $t\bar{t}$ and tW . A total normalization uncertainty is constructed from the difference between the total yields predicted by the two models. A migration uncertainty is constructed by normalizing the overall yields of the two samples to be the same and comparing the yields in individual regions (one nuisance parameter for tW and one for $t\bar{t}$). Shape uncertainties are defined in each of the three analysis regions and assumed to be uncorrelated.

Initial and final state radiation (ISR/FSR) uncertainties are evaluated using internal weights stored in the nominal $t\bar{t}$ and tW POWHEG BOX2+ PYTHIA8 samples. The uncertainty due to missing higher-order QCD corrections in the matrix-element computation is estimated by independently varying the renormalization and factorization scales by factors of 2.0 and 0.5 relative to the central value. The nominal tuning used in the parton shower generator (called the A14 tune) is also varied up (called the VAR3CUP variation) and down

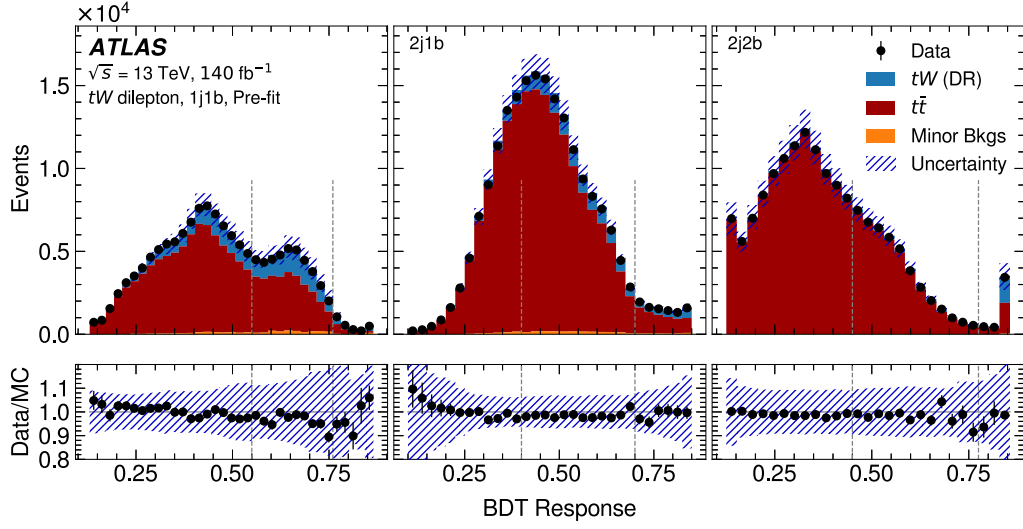


FIG. 3. The pre-fit BDT response distributions for the three regions used in the fit. The BDT range used in the fit described in Sec. VII is indicated by vertical dashed lines. The first and last bins include the underflow and overflow, respectively. The uncertainty bands represent both statistical and systematic uncertainties, where all sources of systematic uncertainty are assumed to be uncorrelated.

(called the VAR3CDOWN variation). The FSR uncertainty is evaluated by varying the scale μ_{FSR} by factors of 2.0 and 0.5 relative to the central value. These uncertainties are taken to be uncorrelated across regions and samples. The uncertainty due to the scale choice for matching the matrix-element calculation of the $t\bar{t}$ process to the parton shower is estimated by using an additional $t\bar{t}$ sample produced with the h_{damp} parameter set to $3.0 m_{\text{top}}$ instead of $1.5 m_{\text{top}}$, while keeping all other generator settings the same as in the nominal sample of $t\bar{t}$ events. This uncertainty is treated uncorrelated across regions and labeled “hdamp” in the following.

The PDF uncertainties are evaluated using the 30 eigenvectors of the PDF4LHC15 combined PDF set [85], taking into account the different effects on the $t\bar{t}$, tW , Z + jets, and inclusive Z processes and their correlations.

For the $t\bar{t}$ process, a one-sided symmetrized uncertainty is constructed in all analysis regions by comparing the nominal distribution after the top-quark p_{T} reweighting with the distribution before the reweighting.

The modeling uncertainties in the minor background normalizations are estimated as follows. An overall uncertainty of 11% is applied to Z + jets events in the two regions with one b -jet, and a 17% uncertainty is applied in

TABLE V. Yields of each process, and total yields, before and after the fit, in each fit region. The prefit uncertainties include statistical and systematic uncertainties while the uncertainties stemming from the theoretical calculation of the tW and $t\bar{t}$ processes are not included. The postfit uncertainties include statistical and systematic uncertainties, as well as the uncertainties in μ_{tW} and $\mu_{t\bar{t}}$. The postfit errors in the total prediction are reduced compared with the sum in quadrature of the individual uncertainties due to correlations resulting from the fit.

	1j1b	2j1b	2j2b
Prefit tW	$13\,000 \pm 1400$	$11\,900 \pm 1200$	2000 ± 400
Prefit $t\bar{t}$	$28\,000 \pm 4000$	$112\,000 \pm 8000$	$43\,000 \pm 4000$
Prefit Z + jets	1130 ± 160	750 ± 100	38 ± 12
Prefit diboson	380 ± 80	570 ± 130	8.5 ± 1.3
Prefit nonprompt	140 ± 70	450 ± 220	54 ± 27
Prefit total prediction	$43\,000 \pm 5000$	$126\,000 \pm 8000$	$45\,000 \pm 4000$
Postfit tW	$12\,500 \pm 2000$	$11\,400 \pm 2200$	2000 ± 400
Postfit $t\bar{t}$	$27\,400 \pm 2000$	$110\,300 \pm 2200$	$42\,100 \pm 500$
Postfit Z + jets	1100 ± 120	750 ± 80	38 ± 6
Postfit diboson	380 ± 80	570 ± 120	8.6 ± 1.1
Postfit nonprompt	140 ± 70	450 ± 220	53 ± 27
Postfit total prediction	$41\,600 \pm 210$	$123\,500 \pm 400$	$44\,150 \pm 210$
Data	41 591	123 531	44 149

the region with two b -jets [86]. A 22% uncertainty is applied to diboson events with one b -jet, and a 13% uncertainty used for diboson events with two b -jets, based on comparisons between SHERPA and POWHEG+PYTHIA models [87]. A 50% uncertainty is applied to the normalization of the backgrounds from nonprompt and misidentified leptons [87]. All minor backgrounds normalization uncertainties are uncorrelated across regions, and found to have a relatively minor impact on the final measurements due to the small contributions from these processes.

VII. FIT STRATEGY

BDT distributions of the observed data, simulated samples, and systematic uncertainty templates, are used together in a binned profile-likelihood fit to extract the measured tW and $t\bar{t}$ cross sections. The fit to all of the bins of all three regions is used to calculate the expected yields of each process. The core components of the likelihood function are Poisson distribution terms that account for the probability of observing the expected yields in data, and additional (Gaussian distribution) terms parametrized by nuisance parameters that account for variations from the central value of each source of systematic uncertainty. The strength parameters for both the processes, μ_{tW} and $\mu_{t\bar{t}}$, defined as the ratio of the measured cross section to that of the theoretical prediction, are free parameters of the fit. The strength parameters for all other (minor) processes are Gaussian distributed and constrained by their respective systematic uncertainties to their SM expectations.

Sources of uncertainty are removed from the fit if their effects are determined to be below a certain threshold. Specifically, a threshold of 0.05% is applied to normalization effects, and for shape effects, at least one bin must vary by more than 0.1%.

A challenge presented by the DR versus DS uncertainty arises from its nature as a two-point systematic uncertainty, making its constraint difficult to justify. Given that the DS scheme includes doubly resonant diagrams while the DR scheme does not, the DS sample tends to contain more events similar to $t\bar{t}$. Selectively excluding certain ranges of the BDT response distributions helps mitigate the stringent constraint while retaining a similar level of sensitivity, benefitting from the large available data sample. Therefore, additional cuts on the BDT response are applied to reduce the large impact of this uncertainty and its undesired constraint by the fit.

The impact of another two-point systematic uncertainty, the $t\bar{t}$ parton shower uncertainty, in this measurement is notable as $t\bar{t}$ is the dominant background. The showering algorithm can lead to variations in the kinematic properties and final-state particles of the $t\bar{t}$ events and consequently on the BDT distribution. Therefore, the BDT distribution range is further reduced by also taking the parton showering effects into account.

This optimization alleviates the stringent constraints imposed on the nuisance parameters of both the tW DR vs DS uncertainty and the $t\bar{t}$ parton shower uncertainty, changing the postfit uncertainty to the prefit uncertainty ratios from an initial 30–40% across fit regions to a more relaxed 60–90%. The postfit error of μ_{tW} increases from 13% to 19% with these selections on the BDT responses. The fractions of tW and $t\bar{t}$ events satisfying the additional selection cuts are 53% and 41%, respectively. The final fit range for each region can be seen in Sec. V.

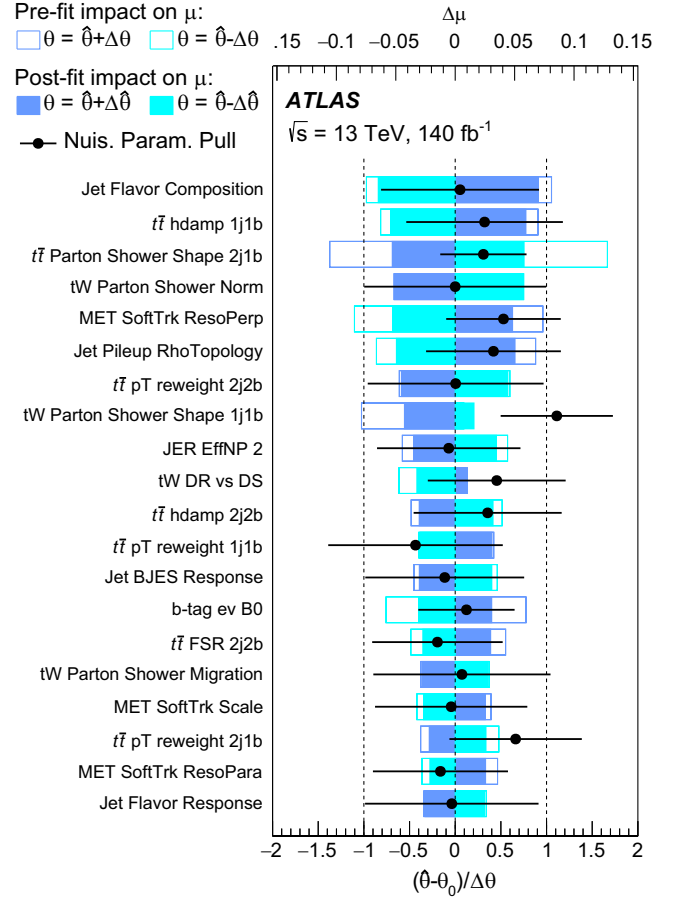


FIG. 4. Ranking of the top 20 nuisance parameters by their most significant postfit impact on μ_{tW} in the fit, after applying the additional BDT selection criteria shown in Fig. 3. The empty and filled blue rectangles represent respectively the prefit and postfit impacts on μ_{tW} and are referring to the upper scale. The impact of a nuisance parameter, $\Delta\mu$, is computed by comparing the nominal best-fit value of μ_{tW} with the fit result obtained when fixing the respective nuisance parameter to its best-fit value, $\hat{\theta}$, shifted by its prefit (postfit) uncertainties $\pm\Delta\theta$ ($\pm\Delta\hat{\theta}$). The black points show the pulls of the nuisance parameters relative to their nominal values, θ_0 . The pulls and their corresponding postfit errors, expressed as $\Delta\hat{\theta}/\Delta\theta$, are also depicted on the lower scale. “MET SoftTrk ResoPerp (ResoPara)” denotes the E_T^{miss} uncertainty in the soft-track p_T resolution smearing perpendicular (parallel) to the E_T^{miss} direction.

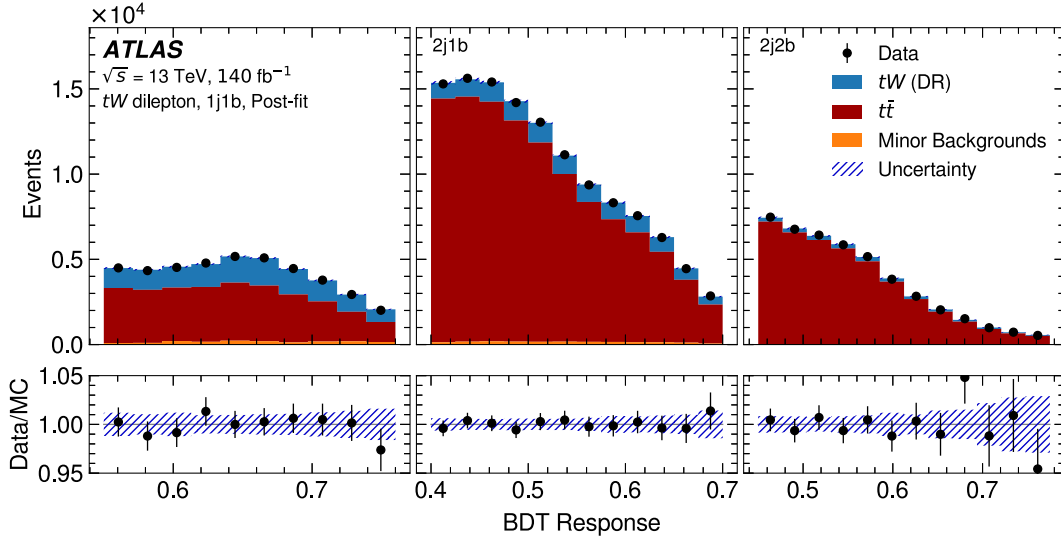


FIG. 5. The postfit BDT response distributions for the three regions used in the fit, after applying the additional BDT selection criteria shown in Fig. 3. The uncertainty bands represent both statistical and systematic uncertainties, with each source of systematic uncertainty taking into account correlations with other sources.

VIII. RESULTS

A. Measurement of the inclusive cross section

The observed and predicted yields after the BDT cuts in the three regions are shown in Table V. Good agreement is observed between data and prediction.

The ten nuisance parameters with the largest postfit impact on μ_{tW} are shown in Fig. 4. Due to the additional BDT selection criteria applied, the impact of the DR vs DS uncertainties are significantly reduced as is reflected in the ranking. No unacceptable constraint is observed and the only significant pull comes from the tW parton shower in the 1j1b region. The dominant uncertainties are in the signal and background modeling, jet reconstruction, and E_T^{miss} . Some of these modeling uncertainties are estimated from a comparison between two alternative MC generators that crucially provide a conservative coverage of the uncertainty stemming from the modeling of the processes.

After fitting to data the observed signal strengths are $\mu_{tW} = 0.95^{+0.19}_{-0.18}$ for tW and $\mu_{t\bar{t}} = 0.99^{+0.07}_{-0.06}$ for $t\bar{t}$. The fit value for μ_{tW} corresponds to a measured cross section of

$$\sigma_{tW} = 75^{+15}_{-14} \text{ pb} = 75 \pm 1(\text{stat})^{+15}_{-14}(\text{syst}) \pm 1(\text{lumi}) \text{ pb.}$$

to be compared with the theory prediction of $\sigma_{tW}^{\text{theory}} = 79.3^{+1.9}_{-1.8}(\text{scale}) \pm 2.2(\text{PDF}) \text{ pb}$. The additional BDT selection criteria do not introduce any bias in the final result, which has an uncertainty of 19%, compared to 13% without these criteria applied. They make the final result less sensitive to modeling uncertainties and assumptions, resulting in a more robust measurement. The observed (expected) significance is 5.3 (5.8) standard deviations calculated using the asymptotic

approximation [88]. The uncertainty in the measured cross section is reduced by around 40% compared with the previous measurement [18].

TABLE VI. Impact of relative uncertainties in the tW cross section σ_{tW} , broken down into major categories. For each category the impact is calculated by performing a fit where the nuisance parameters in the category are fixed to their best-fit values, and then subtracting the resulting uncertainty in the parameter of interest in quadrature from the uncertainty from the nominal fit. The symmetric impact is given for simplicity. “MC statistical uncertainty” is derived from the nuisance parameters associated with the Poisson distribution terms that represent the effect of the limited size of the MC samples. “Data statistical uncertainty” is derived as the subtraction in quadrature of the “Total uncertainty” and “Total systematic uncertainty”. The total systematic uncertainty is not equal to the sum in quadrature of the individual contributions due to correlations resulting from the fit.

Uncertainty source	$\Delta\sigma_{tW}/\sigma_{tW}$ [%]
$t\bar{t}$ modeling	13.2
Jet energy scale	12.0
E_T^{miss} reconstruction and calibration	11.0
tW modeling	7.9
Jet energy resolution	7.0
Jet flavor tagging	3.7
Pileup	2.5
Lepton (e and μ) reconstruction and calibration	1.9
Other background modeling	0.9
Luminosity	0.8
PDF (tW and $t\bar{t}$)	0.6
MC statistical uncertainty	4.7
Total systematic uncertainty	19.2
Data statistical uncertainty	1.4
Total uncertainty	19.3

The postfit BDT response distributions are shown in Fig. 5. The postfit uncertainties are significantly smaller compared with those in the prefit distributions of Fig. 3 due to the correlations between sources of systematic uncertainty and constraints imposed by the data.

The impact of the uncertainties in the tW signal strength, broken down into major categories, is summarized in Table VI. The statistical uncertainty in the measurement is estimated by performing the fit after fixing all nuisance parameters to their postfit values. The total systematic uncertainty is calculated by subtracting in quadrature the statistical component of the uncertainty from the total.

B. Constraints on $|f_{LV}V_{tb}|$

The inclusive cross section depends on the magnitude of the CKM matrix element V_{tb} . Assuming that tW -channel production through $|V_{ts}|$ and $|V_{td}|$ is small, the ratio of the measured cross section to the theoretical prediction is equal to $|f_{LV}V_{tb}|^2$, where the left-handed form factor f_{LV} could be modified by new physics or radiative corrections through anomalous coupling contributions. By assuming that the CKM matrix elements $|V_{td}|$ and $|V_{ts}|$ are much smaller than $|V_{tb}|$ and a $V-A$ interaction in the Wtb vertex, the measured cross section gives $|f_{LV}V_{tb}| = 0.97 \pm 0.10$, consistent with the SM prediction of unity. In addition to the uncertainty in the measurement, the uncertainty in the tW cross section calculation is taken into account and is found to be negligible.

IX. CONCLUSION

A measurement of the tW cross section using data collected with the ATLAS detector from 2015 to 2018 in pp collisions at a center-of-mass energy of $\sqrt{s} = 13$ TeV delivered by the LHC is presented. The full data sample corresponds to an integrated luminosity of 140 fb^{-1} . The tW final state used for this measurement comprises two oppositely charged leptons ($e^\pm\mu^\mp$ events) and missing transverse momentum from the two W -boson decays, and one b -jet from the top-quark decay. BDTs are used to separate the signal from the dominant $t\bar{t}$ background.

The cross section for the production of a W boson in association with a single top quark is measured to be

$$\sigma_{tW} = 75_{-14}^{+15} \text{ pb} = 75 \pm 1 \text{ (stat)}_{-14}^{+15} \text{ (syst)} \pm 1 \text{ (lumi)} \text{ pb},$$

which is in good agreement with the SM prediction of $\sigma_{tW}^{\text{theory}} = 79.3_{-1.8}^{+1.9}(\text{scale}) \pm 2.2(\text{PDF}) \text{ pb}$. The uncertainty in the measured cross section is reduced by around 40% compared with the previous ATLAS measurement using a partial run 2 dataset. The stringent constraints imposed on the nuisance parameters of both the tW DR vs DS uncertainty and the $t\bar{t}$ parton shower uncertainty are largely reduced by excluding bins of the BDT response in the fit

compared with the previous analysis, which leads to a more reliable measurement at the cost of a certain degradation of the precision. The measured cross section allows a direct extraction of the form factor times the CKM matrix element, $|f_{LV}V_{tb}| = 0.97 \pm 0.10$, which is consistent with the SM prediction of unity.

ACKNOWLEDGMENTS

We thank CERN for the very successful operation of the LHC and its injectors, as well as the support staff at CERN and at our institutions worldwide without whom ATLAS could not be operated efficiently. The crucial computing support from all WLCG partners is acknowledged gratefully, in particular from CERN, the ATLAS Tier-1 facilities at TRIUMF/SFU (Canada), NDGF (Denmark, Norway, Sweden), CC-IN2P3 (France), KIT/GridKA (Germany), INFN-CNAF (Italy), NL-T1 (Netherlands), PIC (Spain), RAL (UK), and BNL (USA), the Tier-2 facilities worldwide and large non-WLCG resource providers. Major contributors of computing resources are listed in Ref. [89]. We gratefully acknowledge the support of ANPCyT, Argentina; YerPhI, Armenia; ARC, Australia; BMWFW and FWF, Austria; ANAS, Azerbaijan; CNPq and FAPESP, Brazil; NSERC, NRC and CFI, Canada; CERN; ANID, Chile; CAS, MOST and NSFC, China; Minciencias, Colombia; MEYS CR, Czech Republic; DNRF and DNSRC, Denmark; IN2P3-CNRS and CEA-DRF/IRFU, France; SRNSFG, Georgia; BMBF, HGF and MPG, Germany; GSRI, Greece; RGC and Hong Kong SAR, China; ISF and Benoziyo Center, Israel; INFN, Italy; MEXT and JSPS, Japan; CNRST, Morocco; NWO, Netherlands; RCN, Norway; MNiSW, Poland; FCT, Portugal; MNE/IFA, Romania; MESTD, Serbia; MSSR, Slovakia; ARIS and MVZI, Slovenia; DSI/NRF, South Africa; MICIU/AEI, Spain; SRC and Wallenberg Foundation, Sweden; SERI, SNSF and Cantons of Bern and Geneva, Switzerland; NSTC, Taipei; TENMAK, Türkiye; STFC/UKRI, United Kingdom; DOE and NSF, United States of America. Individual groups and members have received support from BCKDF, CANARIE, CRC and DRAC, Canada; CERN-CZ, FORTE and PRIMUS, Czech Republic; COST, ERC, ERDF, Horizon 2020, ICSC-NextGenerationEU and Marie Skłodowska-Curie Actions, European Union; Investissements d’Avenir Labex, Investissements d’Avenir IDEX and ANR, France; DFG and AvH Foundation, Germany; Herakleitos, Thales and Aristeia programmes cofinanced by EU-ESF and the Greek NSRF, Greece; BSF-NSF and MINERVA, Israel; NCN and NAWA, Poland; La Caixa Banking Foundation, CERCA Programme Generalitat de Catalunya and PROMETEO and GenT Programmes Generalitat Valenciana, Spain; Göran Gustafssons Stiftelse, Sweden; The Royal Society and Leverhulme Trust, United Kingdom. In addition, individual members wish to acknowledge support from Armenia: Yerevan Physics

Institute (FAPERJ); CERN: European Organization for Nuclear Research (CERN PJAS); Chile: Agencia Nacional de Investigación y Desarrollo (Grants No. FONDECYT 1230812, No. FONDECYT 1230987, No. FONDECYT 1240864); China: Chinese Ministry of Science and Technology (MOST-2023YFA1605700), National Natural Science Foundation of China (Grants No. NSFC-12175119, No. NSFC-12275265, No. NSFC-12075060); Czech Republic: Czech Science Foundation (Grant No. GACR-24-11373S), Ministry of Education Youth and Sports (Grant No. FORTE CZ.02.01.01/00/22_008/0004632), PRIMUS Research Programme (Grant No. PRIMUS/21/SCI/017); EU: H2020 European Research Council (Grant No. ERC-101002463); European Union: European Research Council (Grants No. ERC-948254, No. ERC-101089007), Horizon 2020 Framework Programme (Grant No. MUCCA-CHIST-ERA-19-XAI-00), European Union, Future Artificial Intelligence Research (Grant No. FAIR-NextGenerationEU PE00000013), Italian Center for High Performance Computing, Big Data and Quantum Computing (ICSC, NextGenerationEU); France: Agence Nationale de la Recherche (Grants No. ANR-20-CE31-0013, No. ANR-21-CE31-0013, No. ANR-21-CE31-0022, No. ANR-22-EDIR-0002), Investissements d’Avenir Labex (Grant No. ANR-11-LABX-0012); Germany: Baden-Württemberg Stiftung (BW Stiftung-Postdoc Eliteprogramme), Deutsche Forschungsgemeinschaft (Grants No. DFG-469666862, No. DFG-CR 312/5-2); Italy: Istituto Nazionale di Fisica Nucleare (ICSC, NextGenerationEU), Ministero dell’Università e della Ricerca (Grant No. PRIN-20223N7F8K-PNRR M4.C2.1.1); Japan: Japan Society for the Promotion of Science (Grants No. JSPS KAKENHI JP22H01227, No. JSPS KAKENHI JP22H04944, No. JSPS

KAKENHI JP22KK0227, No. JSPS KAKENHI JP23KK0245); Netherlands: Netherlands Organisation for Scientific Research (NWO Veni 2020-VI.Veni.202.179); Norway: Research Council of Norway (Grant No. RCN-314472); Poland: Ministry of Science and Higher Education (IDUB AGH, POB8, D4 no 9722), Polish National Agency for Academic Exchange (Grant No. PPN/PPO/2020/1/00002/U/00001), Polish National Science Centre (Grants No. NCN 2021/42/E/ST2/00350, No. NCN OPUS nr 2022/47/B/ST2/03059, No. NCN UMO-2019/34/E/ST2/00393, No. UMO-2020/37/B/ST2/01043, No. UMO-2021/40/C/ST2/00187, No. UMO-2022/47/O/ST2/00148, No. UMO-2023/49/B/ST2/04085); Slovenia: Slovenian Research Agency (ARIS Grant No. J1-3010); Spain: Generalitat Valenciana (Artemisa, FEDER, Grant No. IDIFEDER/2018/048), Ministry of Science and Innovation (Grants No. MCIN & NextGenEU PCI2022-135018-2, No. MICIN & FEDER PID2021-125273NB, No. RYC2019-028510-I, No. RYC2020-030254-I, No. RYC2021-031273-I, No. RYC2022-038164-I), PROMETEO and GenT Programmes Generalitat Valenciana (Grant No. CIDEGENT/2019/027); Sweden: Swedish Research Council (Swedish Research Council 2023-04654, Grants No. VR 2018-00482, No. VR 2022-03845, No. VR 2022-04683, No. VR 2023-03403, No. VR 2021-03651), Knut and Alice Wallenberg Foundation (Grants No. KAW 2018.0157, No. KAW 2018.0458, No. KAW 2019.0447, No. KAW 2022.0358); Switzerland: Swiss National Science Foundation (Grant No. SNSF-PCEFP2_194658); United Kingdom: Leverhulme Trust (Leverhulme Trust Grant No. RPG-2020-004), Royal Society (Grant No. NIF-R1-231091); United States of America: U.S. Department of Energy (Grant No. ECA DE-AC02-76SF00515), Neubauer Family Foundation.

-
- [1] L. Evans and P. Bryant, LHC machine, *J. Instrum.* **3**, S08001 (2008).
- [2] V.M. Abazov *et al.* (D0 Collaboration), Combination of searches for anomalous top quark couplings with 5.4 fb^{-1} of $p\bar{p}$ collisions, *Phys. Lett. B* **713**, 165 (2012).
- [3] J. Alwall *et al.*, Is $V_{tb} \simeq 1$?, *Eur. Phys. J. C* **49**, 791 (2007).
- [4] ATLAS Collaboration, Measurement of t -channel production of single top quarks and antiquarks in pp collisions at 13 TeV using the full ATLAS Run 2 data sample, *J. High Energy Phys.* **05** (2024) 305.
- [5] T. M. P. Tait and C.-P. Yuan, Single top quark production as a window to physics beyond the Standard Model, *Phys. Rev. D* **63**, 014018 (2000).
- [6] Q.-H. Cao, J. Wudka, and C.-P. Yuan, Search for new physics via single-top production at the LHC, *Phys. Lett. B* **658**, 50 (2007).
- [7] ATLAS Collaboration, Search for heavy diboson resonances in semileptonic final states in pp collisions at $\sqrt{s} = 13 \text{ TeV}$ with the ATLAS detector, *Eur. Phys. J. C* **80**, 1165 (2020).
- [8] ATLAS Collaboration, Search for heavy resonances decaying into a pair of Z bosons in the $\ell^+\ell^-\ell'^+\ell'^-$ and $\ell^+\ell^-\nu\bar{\nu}$ final states using 139 fb^{-1} of proton–proton collisions at $\sqrt{s} = 13 \text{ TeV}$ with the ATLAS detector, *Eur. Phys. J. C* **81**, 332 (2021).
- [9] N. Kidonakis and N. Yamanaka, Higher-order corrections for tW production at high-energy hadron colliders, *J. High Energy Phys.* **05** (2021) 278.

- [10] R. D. Ball *et al.*, The PDF4LHC21 combination of global PDF fits for the LHC Run III, *J. Phys. G* **49**, 080501 (2022).
- [11] S. Frixione, E. Laenen, P. Motylinski, C. White, and B. R. Webber, Single-top hadroproduction in association with a W boson, *J. High Energy Phys.* **07** (2008) 029.
- [12] ATLAS Collaboration, Probing the quantum interference between singly and doubly resonant top-quark production in pp collisions at $\sqrt{s} = 13$ TeV with the ATLAS detector, *Phys. Rev. Lett.* **121**, 152002 (2018).
- [13] ATLAS Collaboration, Evidence for the associated production of a W boson and a top quark in ATLAS at $\sqrt{s} = 7$ TeV, *Phys. Lett. B* **716**, 142 (2012).
- [14] CMS Collaboration, Evidence for associated production of a single top quark and W boson in pp collisions at $\sqrt{s} = 7$ TeV, *Phys. Rev. Lett.* **110**, 022003 (2013).
- [15] CMS Collaboration, Observation of the associated production of a single top quark and a W boson in pp collisions at $\sqrt{s} = 8$ TeV, *Phys. Rev. Lett.* **112**, 231802 (2014).
- [16] ATLAS Collaboration, Measurement of the production cross-section of a single top quark in association with a W boson at 8 TeV with the ATLAS experiment, *J. High Energy Phys.* **01** (2016) 064.
- [17] ATLAS Collaboration, Measurement of single top-quark production in association with a W boson in the single-lepton channel at $\sqrt{s} = 8$ TeV with the ATLAS detector, *Eur. Phys. J. C* **81**, 720 (2021).
- [18] ATLAS Collaboration, Measurement of the cross-section for producing a W boson in association with a single top quark in pp collisions at $\sqrt{s} = 13$ TeV with ATLAS, *J. High Energy Phys.* **01** (2018) 063.
- [19] ATLAS Collaboration, Measurement of differential cross-sections of a single top quark produced in association with a W boson at $\sqrt{s} = 13$ TeV with ATLAS, *Eur. Phys. J. C* **78**, 186 (2018).
- [20] CMS Collaboration, Measurement of the production cross section for single top quarks in association with W bosons in proton–proton collisions at $\sqrt{s} = 13$ TeV, *J. High Energy Phys.* **10** (2018) 117.
- [21] CMS Collaboration, Observation of tW production in the single-lepton channel in pp collisions at $\sqrt{s} = 13$ TeV, *J. High Energy Phys.* **11** (2021) 111.
- [22] CMS Collaboration, Measurement of inclusive and differential cross sections for single top quark production in association with a W boson in proton–proton collisions at $\sqrt{s} = 13$ TeV, *J. High Energy Phys.* **07** (2023) 046.
- [23] ATLAS Collaboration, The ATLAS experiment at the CERN Large Hadron Collider, *J. Instrum.* **3**, S08003 (2008).
- [24] ATLAS Collaboration, ATLAS insertable B-layer: Technical design report, Reports No. ATLAS-TDR-19, No. CERN-LHCC-2010-013, 2010, <https://cds.cern.ch/record/1291633>; Addendum: Reports No. ATLAS-TDR-19-ADD-1, No. CERN-LHCC-2012-009, 2012, <https://cds.cern.ch/record/1451888>.
- [25] B. Abbott *et al.*, Production and integration of the ATLAS insertable B-layer, *J. Instrum.* **13**, T05008 (2018).
- [26] G. Avoni *et al.*, The new LUCID-2 detector for luminosity measurement and monitoring in ATLAS, *J. Instrum.* **13**, P07017 (2018).
- [27] ATLAS Collaboration, Performance of the ATLAS trigger system in 2015, *Eur. Phys. J. C* **77**, 317 (2017).
- [28] ATLAS Collaboration, Software and computing for Run 3 of the ATLAS experiment at the LHC, [arXiv:2404.06335](https://arxiv.org/abs/2404.06335).
- [29] T. Sjöstrand, S. Mrenna, and P. Skands, A brief introduction to PYTHIA8.1, *Comput. Phys. Commun.* **178**, 852 (2008).
- [30] R. D. Ball *et al.* (NNPDF Collaboration), Parton distributions with LHC data, *Nucl. Phys.* **B867**, 244 (2013).
- [31] ATLAS Collaboration, The PYTHIA8 A3 tune description of ATLAS minimum bias and inelastic measurements incorporating the Donnachie–Landshoff diffractive model, Report No. ATL-PHYS-PUB-2016-017, 2016, <https://cds.cern.ch/record/2206965>.
- [32] D. J. Lange, The EvtGen particle decay simulation package, *Nucl. Instrum. Methods Phys. Res., Sect. A* **462**, 152 (2001).
- [33] E. Re, Single-top Wt -channel production matched with parton showers using the POWHEG method, *Eur. Phys. J. C* **71**, 1547 (2011).
- [34] P. Nason, A new method for combining NLO QCD with shower Monte Carlo algorithms, *J. High Energy Phys.* **11** (2004) 040.
- [35] S. Frixione, P. Nason, and C. Oleari, Matching NLO QCD computations with parton shower simulations: The POWHEG method, *J. High Energy Phys.* **11** (2007) 070.
- [36] S. Alioli, P. Nason, C. Oleari, and E. Re, A general framework for implementing NLO calculations in shower Monte Carlo programs: The POWHEG BOX, *J. High Energy Phys.* **06** (2010) 043.
- [37] ATLAS Collaboration, Studies on top-quark Monte Carlo modelling for Top2016, Report No. ATL-PHYS-PUB-2016-020, 2016, <https://cds.cern.ch/record/2216168>.
- [38] T. Sjöstrand *et al.*, An introduction to PYTHIA8.2, *Comput. Phys. Commun.* **191**, 159 (2015).
- [39] ATLAS Collaboration, ATLAS PYTHIA8 tunes to 7 TeV data, Report No. ATL-PHYS-PUB-2014-021, 2014, <https://cds.cern.ch/record/1966419>.
- [40] S. Frixione, G. Ridolfi, and P. Nason, A positive-weight next-to-leading-order Monte Carlo for heavy flavour hadroproduction, *J. High Energy Phys.* **09** (2007) 126.
- [41] M. Beneke, P. Falgari, S. Klein, and C. Schwinn, Hadronic top-quark pair production with NNLL threshold resummation, *Nucl. Phys.* **B855**, 695 (2012).
- [42] M. Cacciari, M. Czakon, M. Mangano, A. Mitov, and P. Nason, Top-pair production at hadron colliders with next-to-next-to-leading logarithmic soft-gluon resummation, *Phys. Lett. B* **710**, 612 (2012).
- [43] P. Bärnreuther, M. Czakon, and A. Mitov, Percent-level-precision physics at the tevatron: Next-to-next-to-leading order QCD corrections to $q\bar{q} \rightarrow t\bar{t} + X$, *Phys. Rev. Lett.* **109**, 132001 (2012).
- [44] M. Czakon and A. Mitov, NNLO corrections to top-pair production at hadron colliders: the all-fermionic scattering channels, *J. High Energy Phys.* **12** (2012) 054.
- [45] M. Czakon and A. Mitov, NNLO corrections to top pair production at hadron colliders: The quark-gluon reaction, *J. High Energy Phys.* **01** (2013) 080.
- [46] M. Czakon, P. Fiedler, and A. Mitov, Total top-quark pair-production cross section at hadron colliders through $O(\alpha_s^4)$, *Phys. Rev. Lett.* **110**, 252004 (2013).

- [47] M. Czakon and A. Mitov, Top++: A program for the calculation of the top-pair cross-section at hadron colliders, *Comput. Phys. Commun.* **185**, 2930 (2014).
- [48] M. Bähr *et al.*, HERWIG++ physics and manual, *Eur. Phys. J. C* **58**, 639 (2008).
- [49] J. Bellm *et al.*, HERWIG7.0/HERWIG++3.0 release note, *Eur. Phys. J. C* **76**, 196 (2016).
- [50] L. A. Harland-Lang, A. D. Martin, P. Motylinski, and R. S. Thorne, Parton distributions in the LHC era: MMHT 2014 PDFs, *Eur. Phys. J. C* **75**, 204 (2015).
- [51] ATLAS Collaboration, Measurement of the $t\bar{t}$ production cross-section and lepton differential distributions in $e\mu$ dilepton events from pp collisions at $\sqrt{s} = 13$ TeV with the ATLAS detector, *Eur. Phys. J. C* **80**, 528 (2020).
- [52] M. Czakon *et al.*, Top-pair production at the LHC through NNLO QCD and NLO EW, *J. High Energy Phys.* **10** (2017) 186.
- [53] E. Bothmann *et al.*, Event generation with SHERPA2.2, *SciPost Phys.* **7**, 034 (2019).
- [54] T. Gleisberg and S. Höche, Comix, a new matrix element generator, *J. High Energy Phys.* **12** (2008) 039.
- [55] F. Cascioli, P. Maierhöfer, and S. Pozzorini, Scattering amplitudes with open loops, *Phys. Rev. Lett.* **108**, 111601 (2012).
- [56] A. Denner, S. Dittmaier, and L. Hofer, Collier: A fortran-based complex one-loop library in extended regularizations, *Comput. Phys. Commun.* **212**, 220 (2017).
- [57] S. Schumann and F. Krauss, A parton shower algorithm based on Catani–Seymour dipole factorisation, *J. High Energy Phys.* **03** (2008) 038.
- [58] S. Höche, F. Krauss, M. Schönherr, and F. Siegert, A critical appraisal of NLO + PS matching methods, *J. High Energy Phys.* **09** (2012) 049.
- [59] S. Höche, F. Krauss, M. Schönherr, and F. Siegert, QCD matrix elements + parton showers. The NLO case, *J. High Energy Phys.* **04** (2013) 027.
- [60] S. Catani, F. Krauss, B. R. Webber, and R. Kuhn, QCD matrix elements + parton showers, *J. High Energy Phys.* **11** (2001) 063.
- [61] S. Höche, F. Krauss, S. Schumann, and F. Siegert, QCD matrix elements and truncated showers, *J. High Energy Phys.* **05** (2009) 053.
- [62] ATLAS Collaboration, The ATLAS simulation infrastructure, *Eur. Phys. J. C* **70**, 823 (2010).
- [63] S. Agostinelli *et al.*, Geant4—a simulation toolkit, *Nucl. Instrum. Methods Phys. Res., Sect. A* **506**, 250 (2003).
- [64] ATLAS Collaboration, The simulation principle and performance of the ATLAS fast calorimeter simulation FastCaloSim, Report No. ATL-PHYS-PUB-2010-013, 2010, <https://cds.cern.ch/record/1300517>.
- [65] ATLAS Collaboration, Performance of electron and photon triggers in ATLAS during LHC Run 2, *Eur. Phys. J. C* **80**, 47 (2020).
- [66] ATLAS Collaboration, Performance of the ATLAS muon triggers in Run 2, *J. Instrum.* **15**, P09015 (2020).
- [67] ATLAS Collaboration, Vertex reconstruction performance of the ATLAS detector at $\sqrt{s} = 13$ TeV, Report No. ATL-PHYS-PUB-2015-026, 2015, <https://cds.cern.ch/record/2037717>.
- [68] ATLAS Collaboration, Electron and photon performance measurements with the ATLAS detector using the 2015–2017 LHC proton–proton collision data, *J. Instrum.* **14**, P12006 (2019).
- [69] ATLAS Collaboration, Muon reconstruction and identification efficiency in ATLAS using the full Run 2 pp collision data set at $\sqrt{s} = 13$ TeV, *Eur. Phys. J. C* **81**, 578 (2021).
- [70] ATLAS Collaboration, Jet reconstruction and performance using particle flow with the ATLAS detector, *Eur. Phys. J. C* **77**, 466 (2017).
- [71] M. Cacciari, G. P. Salam, and G. Soyez, The anti- k_t jet clustering algorithm, *J. High Energy Phys.* **04** (2008) 063.
- [72] M. Cacciari, G. P. Salam, and G. Soyez, FastJet user manual, *Eur. Phys. J. C* **72**, 1896 (2012).
- [73] ATLAS Collaboration, Jet energy scale and resolution measured in proton–proton collisions at $\sqrt{s} = 13$ TeV with the ATLAS detector, *Eur. Phys. J. C* **81**, 689 (2021).
- [74] ATLAS Collaboration, Performance of pile-up mitigation techniques for jets in pp collisions at $\sqrt{s} = 8$ TeV using the ATLAS detector, *Eur. Phys. J. C* **76**, 581 (2016).
- [75] ATLAS Collaboration, ATLAS flavour-tagging algorithms for the LHC Run 2 pp collision dataset, *Eur. Phys. J. C* **83**, 681 (2023).
- [76] ATLAS Collaboration, The performance of missing transverse momentum reconstruction and its significance with the ATLAS detector using 140 fb $^{-1}$ of $\sqrt{s} = 13$ TeV pp collisions, [arXiv:2402.05858](https://arxiv.org/abs/2402.05858).
- [77] G. Ke *et al.*, LightGBM: A highly efficient gradient boosting decision tree, *Advances in Neural Information Processing Systems 30*, edited by I. Guyon *et al.* (Curran Associates, Inc., 2017), <http://papers.nips.cc/paper/6907-lightgbm-highly-efficient-gradient-boosting-decision-tree.pdf>.
- [78] A. Kolmogorov, 19++. Sulla determinazione empirica di una legge di distribuzione, *Giornale dell’Istituto Nazionale degli Attuari* **4**, 91 (1933).
- [79] N. Smirnov, Sur les écarts de la courbe de distribution empirique, *Mat. Sb.* **48**, 3 (1939).
- [80] ATLAS Collaboration, ATLAS b -jet identification performance and efficiency measurement with $t\bar{t}$ events in pp collisions at $\sqrt{s} = 13$ TeV, *Eur. Phys. J. C* **79**, 970 (2019).
- [81] ATLAS Collaboration, Measurement of the c -jet mistagging efficiency in $t\bar{t}$ events using pp collision data at $\sqrt{s} = 13$ TeV collected with the ATLAS detector, *Eur. Phys. J. C* **82**, 95 (2022).
- [82] ATLAS Collaboration, Calibration of the light-flavour jet mistagging efficiency of the b -tagging algorithms with $Z + jets$ events using 139 fb $^{-1}$ of ATLAS proton–proton collision data at $\sqrt{s} = 13$ TeV, *Eur. Phys. J. C* **83**, 728 (2023).
- [83] ATLAS Collaboration, Luminosity determination in pp collisions at $\sqrt{s} = 13$ TeV using the ATLAS detector at the LHC, *Eur. Phys. J. C* **83**, 982 (2023).
- [84] J. Alwall *et al.*, The automated computation of tree-level and next-to-leading order differential cross sections, and their matching to parton shower simulations, *J. High Energy Phys.* **07** (2014) 079.
- [85] J. Butterworth *et al.*, PDF4LHC recommendations for LHC Run II, *J. Phys. G* **43**, 023001 (2016).
- [86] ATLAS Collaboration, Measurements of the production cross-section for a Z boson in association with b -jets in

- proton–proton collisions at $\sqrt{s} = 13$ TeV with the ATLAS detector, *J. High Energy Phys.* **07** (2020) 044.
- [87] ATLAS Collaboration, Measurement of the $t\bar{t}$ production cross-section using $e\mu$ events with b -tagged jets in pp collisions at $\sqrt{s} = 13$ TeV with the ATLAS detector, *Phys. Lett. B* **761**, 136 (2016); **772**, 879(E) (2017).
- [88] G. Cowan, K. Cranmer, E. Gross, and O. Vitells, Asymptotic formulae for likelihood-based tests of new physics, *Eur. Phys. J. C* **71**, 1554 (2011).
- [89] ATLAS Collaboration, ATLAS computing acknowledgements, Report No. ATL-SOFT-PUB-2023-001, 2023, <https://cds.cern.ch/record/2869272>.

G. Aad¹⁰⁴, E. Aakvaag¹⁷, B. Abbott¹²³, S. Abdelhameed^{119a}, K. Abeling⁵⁶, N. J. Abicht⁵⁰, S. H. Abidi³⁰, M. Aboelela⁴⁵, A. Aboulhorma^{36e}, H. Abramowicz¹⁵⁴, H. Abreu¹⁵³, Y. Abulaiti¹²⁰, B. S. Acharya^{70a,70b,b}, A. Ackermann^{64a}, C. Adam Bourdarios⁴, L. Adamczyk^{87a}, S. V. Addepalli²⁷, M. J. Addison¹⁰³, J. Adelman¹¹⁸, A. Adiguzel^{22c}, T. Adye¹³⁷, A. A. Affolder¹³⁹, Y. Afik⁴⁰, M. N. Agaras¹³, J. Agarwala^{74a,74b}, A. Aggarwal¹⁰², C. Agheorghiesei^{28c}, F. Ahmadov^{39,c}, W. S. Ahmed¹⁰⁶, S. Ahuja⁹⁷, X. Ai^{63e}, G. Aielli^{77a,77b}, A. Aikot¹⁶⁶, M. Ait Tamlihat^{36e}, B. Aitbenchikh^{36a}, M. Akbiyik¹⁰², T. P. A. Åkesson¹⁰⁰, A. V. Akimov³⁸, D. Akiyama¹⁷¹, N. N. Akolkar²⁵, S. Aktas^{22a}, K. Al Houry⁴², G. L. Alberghi^{24b}, J. Albert¹⁶⁸, P. Albicocco⁵⁴, G. L. Albouy⁶¹, S. Alderweireldt⁵³, Z. L. Alegria¹²⁴, M. Aleksa³⁷, I. N. Aleksandrov³⁹, C. Alexa^{28b}, T. Alexopoulos¹⁰, F. Alfonsi^{24b}, M. Algren⁵⁷, M. Alhroob¹⁷⁰, B. Ali¹³⁵, H. M. J. Ali⁹³, S. Ali³², S. W. Alibocus⁹⁴, M. Aliev^{34c}, G. Alimonti^{72a}, W. Alkahi⁵⁶, C. Allaire⁶⁷, B. M. M. Allbrooke¹⁴⁹, J. F. Allen⁵³, C. A. Allendes Flores^{140f}, P. P. Allport²¹, A. Aloisio^{73a,73b}, F. Alonso⁹², C. Alpigiani¹⁴¹, Z. M. K. Alsolami⁹³, M. Alvarez Estevez¹⁰¹, A. Alvarez Fernandez¹⁰², M. Alves Cardoso⁵⁷, M. G. Alviggi^{73a,73b}, M. Aly¹⁰³, Y. Amaral Coutinho^{84b}, A. Ambler¹⁰⁶, C. Amelung³⁷, M. Amerl¹⁰³, C. G. Ames¹¹¹, D. Amidei¹⁰⁸, B. Amini⁵⁵, K. J. Amirie¹⁵⁸, S. P. Amor Dos Santos^{133a}, K. R. Amos¹⁶⁶, D. Amperiadou¹⁵⁵, S. An⁸⁵, V. Ananiev¹²⁸, C. Anastopoulos¹⁴², T. Andeen¹¹, J. K. Anders³⁷, A. C. Anderson⁶⁰, S. Y. Andreato^{48a,48b}, A. Andreazza^{72a,72b}, S. Angelidakis⁹, A. Angerami⁴², A. V. Anisenkov³⁸, A. Annovi^{75a}, C. Antel⁵⁷, E. Antipov¹⁴⁸, M. Antonelli⁵⁴, F. Anulli^{76a}, M. Aoki⁸⁵, T. Aoki¹⁵⁶, M. A. Aparo¹⁴⁹, L. Aperio Bella⁴⁹, C. Appelt¹⁹, A. Apyan²⁷, S. J. Arbiol Val⁸⁸, C. Arcangeletti⁵⁴, A. T. H. Arce⁵², J-F. Arguin¹¹⁰, S. Argyropoulos⁵⁵, J.-H. Arling⁴⁹, O. Arnaez⁴, H. Arnold¹⁴⁸, G. Artoni^{76a,76b}, H. Asada¹¹³, K. Asai¹²¹, S. Asai¹⁵⁶, N. A. Asbah³⁷, R. A. Ashby Pickering¹⁷⁰, K. Assamagan³⁰, R. Astalos^{29a}, K. S. V. Astrand¹⁰⁰, S. Atashi¹⁶², R. J. Atkin^{34a}, M. Atkinson¹⁶⁵, H. Atmani^{36f}, P. A. Atmasiddha¹³¹, K. Augsten¹³⁵, S. Auricchio^{73a,73b}, A. D. Auriol²¹, V. A. Austrup¹⁰³, G. Avolio³⁷, K. Axiotis⁵⁷, G. Azuelos^{110,d}, D. Babal^{29b}, H. Bachacou¹³⁸, K. Bachas^{155,e}, A. Bachi³⁵, F. Backman^{48a,48b}, A. Badea⁴⁰, T. M. Baer¹⁰⁸, P. Bagnaia^{76a,76b}, M. Bahmani¹⁹, D. Bahner⁵⁵, K. Bai¹²⁶, J. T. Baines¹³⁷, L. Baines⁹⁶, O. K. Baker¹⁷⁵, E. Bakos¹⁶, D. Bakshi Gupta⁸, L. E. Balabram Filho^{84b}, V. Balakrishnan¹²³, R. Balasubramanian¹¹⁷, E. M. Baldin³⁸, P. Balek^{87a}, E. Ballabene^{24b,24a}, F. Balli¹³⁸, L. M. Baltes^{64a}, W. K. Balunas³³, J. Balz¹⁰², I. Bamwidhi^{119b}, E. Banas⁸⁸, M. Bandieramonte¹³², A. Bandyopadhyay²⁵, S. Bansal²⁵, L. Barak¹⁵⁴, M. Barakat⁴⁹, E. L. Barberio¹⁰⁷, D. Barberis^{58b,58a}, M. Barbero¹⁰⁴, M. Z. Barel¹¹⁷, T. Barillari¹¹², M-S. Barisits³⁷, T. Barklow¹⁴⁶, P. Baron¹²⁵, D. A. Baron Moreno¹⁰³, A. Baroncelli^{63a}, A. J. Barr¹²⁹, J. D. Barr⁹⁸, F. Barreiro¹⁰¹, J. Barreiro Guimarães da Costa¹⁴, U. Barron¹⁵⁴, M. G. Barros Teixeira^{133a}, S. Barsov³⁸, F. Bartels^{64a}, R. Bartoldus¹⁴⁶, A. E. Barton⁹³, P. Bartos^{29a}, A. Basan¹⁰², M. Baselga⁵⁰, A. Bassalat^{67,f}, M. J. Basso^{159a}, S. Bataju⁴⁵, R. Bate¹⁶⁷, R. L. Bates⁶⁰, S. Batlamous¹⁰¹, B. Batool¹⁴⁴, M. Battaglia¹³⁹, D. Battulga¹⁹, M. Bauce^{76a,76b}, M. Bauer⁸⁰, P. Bauer²⁵, L. T. Bazzano Hurrell³¹, J. B. Beacham⁵², T. Beau¹³⁰, J. Y. Beauchamp⁹², P. H. Beauchemin¹⁶¹, P. Bechtel²⁵, H. P. Beck^{20,g}, K. Becker¹⁷⁰, A. J. Beddall⁸³, V. A. Bednyakov³⁹, C. P. Bee¹⁴⁸, L. J. Beemster¹⁶, T. A. Beermann³⁷, M. Begalli^{84d}, M. Begel³⁰, A. Behera¹⁴⁸, J. K. Behr⁴⁹, J. F. Beirer³⁷, F. Beisiegel²⁵, M. Belfkir^{119b}, G. Bella¹⁵⁴, L. Bellagamba^{24b}, A. Bellerive³⁵, P. Bellos²¹, K. Beloborodov³⁸, D. Bencheikroun^{36a}, F. Bendebba^{36a}, Y. Benhammou¹⁵⁴, K. C. Benkendorfer⁶², L. Beresford⁴⁹, M. Beretta⁵⁴, E. Bergeas Kuutmann¹⁶⁴, N. Berger⁴, B. Bergmann¹³⁵, J. Beringer^{18a}, G. Bernardi⁵, C. Bernius¹⁴⁶, F. U. Bernlochner²⁵, F. Bernon^{37,104}, A. Berrocal Guardia¹³, T. Berry⁹⁷, P. Berta¹³⁶, A. Berthold⁵¹, S. Bethke¹¹², A. Betti^{76a,76b}, A. J. Bevan⁹⁶, N. K. Bhalla⁵⁵, S. Bhatta¹⁴⁸, D. S. Bhattacharya¹⁶⁹, P. Bhattarai¹⁴⁶, K. D. Bhide⁵⁵, V. S. Bhopatkar¹²⁴, R. M. Bianchi¹³², G. Bianco^{24b,24a}, O. Biebel¹¹¹, R. Bielski¹²⁶, M. Biglietti^{78a}, C. S. Billingsley⁴⁵, Y. Bimgdi^{36f}, M. Bindi⁵⁶, A. Bingul^{22b}, C. Bini^{76a,76b}

G. A. Bird³³ M. Birman¹⁷² M. Biros¹³⁶ S. Biryukov¹⁴⁹ T. Bisanz⁵⁰ E. Bisceglie^{44b,44a} J. P. Biswal¹³⁷
D. Biswas¹⁴⁴ I. Bloch⁴⁹ A. Blue⁶⁰ U. Blumenschein⁹⁶ J. Blumenthal¹⁰² V. S. Bobrovnikov³⁸ M. Boehler⁵⁵
B. Boehm¹⁶⁹ D. Bogavac³⁷ A. G. Bogdanchikov³⁸ L. S. Boggia¹³⁰ C. Bohm^{48a} V. Boisvert⁹⁷ P. Bokan³⁷
T. Bold^{87a} M. Bomben⁵ M. Bona⁹⁶ M. Boonekamp¹³⁸ C. D. Booth⁹⁷ A. G. Borbély⁶⁰ I. S. Bordulev³⁸
G. Borissov⁹³ D. Bortoletto¹²⁹ D. Boscherini^{24b} M. Bosman¹³ J. D. Bossio Sola³⁷ K. Bouaouda^{36a}
N. Bouchhar¹⁶⁶ L. Boudet⁴ J. Boudreau¹³² E. V. Bouhova-Thacker⁹³ D. Boumediene⁴¹ R. Bouquet^{58b,58a}
A. Boveia¹²² J. Boyd³⁷ D. Boye³⁰ I. R. Boyko³⁹ L. Bozianu⁵⁷ J. Bracinik²¹ N. Brahimi⁴ G. Brandt¹⁷⁴
O. Brandt³³ F. Braren⁴⁹ B. Brau¹⁰⁵ J. E. Brau¹²⁶ R. Brenner¹⁷² L. Brenner¹¹⁷ R. Brenner¹⁶⁴ S. Bressler¹⁷²
G. Brianti^{79a,79b} D. Britton⁶⁰ D. Britzger¹¹² I. Brock²⁵ R. Brock¹⁰⁹ G. Brooijmans⁴² E. M. Brooks^{159b}
E. Brost³⁰ L. M. Brown¹⁶⁸ L. E. Bruce⁶² T. L. Bruckler¹²⁹ P. A. Bruckman de Renstrom⁸⁸ B. Brüers⁴⁹
A. Bruni^{24b} G. Bruni^{24b} M. Bruschi^{24b} N. Brusino^{76a,76b} T. Buanes¹⁷ Q. Buat¹⁴¹ D. Buchin¹¹²
A. G. Buckley⁶⁰ O. Bulekov³⁸ B. A. Bullard¹⁴⁶ S. Burdin⁹⁴ C. D. Burgard⁵⁰ A. M. Burger³⁷ B. Burghgrave⁸
O. Burlayenko⁵⁵ J. Burleson¹⁶⁵ J. T. P. Burr³³ J. C. Burzynski¹⁴⁵ E. L. Busch⁴² V. Büscher¹⁰² P. J. Bussey⁶⁰
J. M. Butler²⁶ C. M. Buttar⁶⁰ J. M. Butterworth⁹⁸ W. Buttinger¹³⁷ C. J. Buxo Vazquez¹⁰⁹ A. R. Buzykaev³⁸
S. Cabrera Urbán¹⁶⁶ L. Cadamuro⁶⁷ D. Caforio⁵⁹ H. Cai¹³² Y. Cai^{14,114c} Y. Cai^{114a} V. M. M. Cairo³⁷
O. Cakir^{3a} N. Calace³⁷ P. Calafiura^{18a} G. Calderini¹³⁰ P. Calfayan⁶⁹ G. Callea⁶⁰ L. P. Caloba^{84b} D. Calvet⁴¹
S. Calvet⁴¹ M. Calvetti^{75a,75b} R. Camacho Toro¹³⁰ S. Camarda³⁷ D. Camarero Munoz²⁷ P. Camarri^{77a,77b}
M. T. Camerlingo^{73a,73b} D. Cameron³⁷ C. Camincher¹⁶⁸ M. Campanelli⁹⁸ A. Camplani⁴³ V. Canale^{73a,73b}
A. C. Canbay^{3a} E. Canonero⁹⁷ J. Cantero¹⁶⁶ Y. Cao¹⁶⁵ F. Capocasa²⁷ M. Capua^{44b,44a} A. Carbone^{72a,72b}
R. Cardarelli^{77a} J. C. J. Cardenas⁸ G. Carducci^{44b,44a} T. Carli³⁷ G. Carlino^{73a} J. I. Carlotto¹³
B. T. Carlson^{132,h} E. M. Carlson^{168,159a} J. Carmignani⁹⁴ L. Carminati^{72a,72b} A. Carnelli¹³⁸ M. Carnesale^{76a,76b}
S. Caron¹¹⁶ E. Carquin^{140f} S. Carrá^{72a} G. Carratta^{24b,24a} A. M. Carroll¹²⁶ T. M. Carter⁵³ M. P. Casado^{13,i}
M. Caspar⁴⁹ F. L. Castillo⁴ L. Castillo Garcia¹³ V. Castillo Gimenez¹⁶⁶ N. F. Castro^{133a,133e} A. Catinaccio³⁷
J. R. Catmore¹²⁸ T. Cavaliere⁴ V. Cavaliere³⁰ N. Cavalli^{24b,24a} L. J. Caviedes Betancourt^{23b}
Y. C. Cakmecioglu⁴⁹ E. Celebi⁸³ S. Cella³⁷ F. Celli¹²⁹ M. S. Centonze^{71a,71b} V. Cepaitis⁵⁷ K. Cerny¹²⁵
A. S. Cerqueira^{84a} A. Cerri¹⁴⁹ L. Cerrito^{77a,77b} F. Cerutti^{18a} B. Cervato¹⁴⁴ A. Cervelli^{24b} G. Cesarini⁵⁴
S. A. Cetin⁸³ D. Chakraborty¹¹⁸ J. Chan^{18a} W. Y. Chan¹⁵⁶ J. D. Chapman³³ E. Chapon¹³⁸
B. Chargeishvili^{152b} D. G. Charlton²¹ M. Chatterjee²⁰ C. Chauhan¹³⁶ Y. Che^{114a} S. Chekanov⁶
S. V. Chekulaev^{159a} G. A. Chelkov^{39,j} A. Chen¹⁰⁸ B. Chen¹⁵⁴ B. Chen¹⁶⁸ H. Chen^{114a} H. Chen³⁰
J. Chen^{63c} J. Chen¹⁴⁵ M. Chen¹²⁹ S. Chen¹⁵⁶ S. J. Chen^{114a} X. Chen^{63c} X. Chen^{15,k} Y. Chen^{63a}
C. L. Cheng¹⁷³ H. C. Cheng^{65a} S. Cheong¹⁴⁶ A. Cheplakov³⁹ E. Cheremushkina⁴⁹ E. Cherepanova¹¹⁷
R. Cherkaoui El Moursli^{36e} E. Cheu⁷ K. Cheung⁶⁶ L. Chevalier¹³⁸ V. Chiarella⁵⁴ G. Chiarelli^{75a}
N. Chiedde¹⁰⁴ G. Chiodini^{71a} A. S. Chisholm²¹ A. Chitan^{28b} M. Chitishvili¹⁶⁶ M. V. Chizhov^{39,l} K. Choi¹¹
Y. Chou¹⁴¹ E. Y. S. Chow¹¹⁶ K. L. Chu¹⁷² M. C. Chu^{65a} X. Chu^{14,114c} Z. Chubinidze⁵⁴ J. Chudoba¹³⁴
J. J. Chwastowski⁸⁸ D. Cieri¹¹² K. M. Ciesla^{87a} V. Cindro⁹⁵ A. Ciocio^{18a} F. Ciroto^{73a,73b} Z. H. Citron¹⁷²
M. Citterio^{72a} D. A. Ciubotaru^{28b} A. Clark⁵⁷ P. J. Clark⁵³ N. Clarke Hall⁹⁸ C. Clarry¹⁵⁸
J. M. Clavijo Columbie⁴⁹ S. E. Clawson⁴⁹ C. Clement^{48a,48b} Y. Coadou¹⁰⁴ M. Cobal^{70a,70c} A. Coccaro^{58b}
R. F. Coelho Barrue^{133a} R. Coelho Lopes De Sa¹⁰⁵ S. Coelli^{72a} B. Cole⁴² J. Collot⁶¹ P. Conde Muiño^{133a,133g}
M. P. Connell^{34c} S. H. Connell^{34c} E. I. Conroy¹²⁹ F. Conventi^{73a,m} H. G. Cooke²¹ A. M. Cooper-Sarkar¹²⁹
F. A. Corchia^{24b,24a} A. Cordeiro Oudot Choi¹³⁰ L. D. Corpe⁴¹ M. Corradi^{76a,76b} F. Corriveau^{106,n}
A. Cortes-Gonzalez¹⁹ M. J. Costa¹⁶⁶ F. Costanza⁴ D. Costanzo¹⁴² B. M. Cote¹²² J. Couthures⁴ G. Cowan⁹⁷
K. Cranmer¹⁷³ D. Cremonini^{24b,24a} S. Crépe-Renaudin⁶¹ F. Crescioli¹³⁰ M. Cristinziani¹⁴⁴
M. Cristoforetti^{79a,79b} V. Croft¹¹⁷ J. E. Crosby¹²⁴ G. Crosetti^{44b,44a} A. Cueto¹⁰¹ H. Cui⁹⁸ Z. Cui⁷
W. R. Cunningham⁶⁰ F. Curcio¹⁶⁶ J. R. Curran⁵³ P. Czodrowski³⁷ M. J. Da Cunha Sargedas De Sousa^{58b,58a}
J. V. Da Fonseca Pinto^{84b} C. Da Via¹⁰³ W. Dabrowski^{87a} T. Dado³⁷ S. Dahbi¹⁵¹ T. Dai¹⁰⁸ D. Dal Santo²⁰
C. Dallapiccola¹⁰⁵ M. Dam⁴³ G. D'amen³⁰ V. D'Amico¹¹¹ J. Damp¹⁰² J. R. Dandoy³⁵ D. Dannheim³⁷
M. Danninger¹⁴⁵ V. Dao¹⁴⁸ G. Darbo^{58b} S. J. Das^{30,o} F. Dattola⁴⁹ S. D'Auria^{72a,72b} A. D'Avanzo^{73a,73b}
C. David^{34a} T. Davidek¹³⁶ I. Dawson⁹⁶ H. A. Day-hall¹³⁵ K. De⁸ R. De Asmundis^{73a} N. De Biase⁴⁹
S. De Castro^{24b,24a} N. De Groot¹¹⁶ P. de Jong¹¹⁷ H. De la Torre¹¹⁸ A. De Maria^{114a} A. De Salvo^{76a}

- U. De Sanctis^{77a,77b} F. De Santis^{71a,71b} A. De Santo¹⁴⁹ J. B. De Vivie De Regie⁶¹ D. V. Dedovich³⁹ J. Degens⁹⁴
 A. M. Deiana⁴⁵ F. Del Corso^{24b,24a} J. Del Peso¹⁰¹ F. Del Rio^{64a} L. Delagrangé¹³⁰ F. Deliot¹³⁸
 C. M. Delitzsch⁵⁰ M. Della Pietra^{73a,73b} D. Della Volpe⁵⁷ A. Dell'Acqua³⁷ L. Dell'Asta^{72a,72b} M. Delmastro⁴
 P. A. Delsart⁶¹ S. Demers¹⁷⁵ M. Demichev³⁹ S. P. Denisov³⁸ L. D'Erano⁴¹ D. Derendarz⁸⁸ F. Derue¹³⁰
 P. Dervan⁹⁴ K. Desch²⁵ C. Deutsch²⁵ F. A. Di Bello^{58b,58a} A. Di Ciaccio^{77a,77b} L. Di Ciaccio⁴
 A. Di Domenico^{76a,76b} C. Di Donato^{73a,73b} A. Di Girolamo³⁷ G. Di Gregorio³⁷ A. Di Luca^{79a,79b}
 B. Di Micco^{78a,78b} R. Di Nardo^{78a,78b} K. F. Di Petrillo⁴⁰ M. Diamantopoulou³⁵ F. A. Dias¹¹⁷ T. Dias Do Vale¹⁴⁵
 M. A. Diaz^{140a,140b} F. G. Diaz Capriles²⁵ A. R. Didenko³⁹ M. Didenko¹⁶⁶ E. B. Diehl¹⁰⁸ S. Díez Cornell⁴⁹
 C. Diez Pardos¹⁴⁴ C. Dimitriadi¹⁶⁴ A. Dimitrievska²¹ J. Dingfelder²⁵ T. Dingley¹²⁹ I-M. Dinu^{28b}
 S. J. Dittmeier^{64b} F. Dittus³⁷ M. Divisek¹³⁶ B. Dixit⁹⁴ F. Djama¹⁰⁴ T. Djobava^{152b} C. Doglioni^{103,100}
 A. Dohnalova^{29a} J. Dolejsi¹³⁶ Z. Dolezal¹³⁶ K. Domijan^{87a} K. M. Dona⁴⁰ M. Donadelli^{84d} B. Dong¹⁰⁹
 J. Donini⁴¹ A. D'Onofrio^{73a,73b} M. D'Onofrio⁹⁴ J. Dopke¹³⁷ A. Doria^{73a} N. Dos Santos Fernandes^{133a}
 P. Dougan¹⁰³ M. T. Dova⁹² A. T. Doyle⁶⁰ M. A. Draguet¹²⁹ E. Dreyer¹⁷² I. Drivas-koulouris¹⁰
 M. Drnevich¹²⁰ M. Drozdova⁵⁷ D. Du^{63a} T. A. du Pree¹¹⁷ F. Dubinin³⁸ M. Dubovsky^{29a} E. Duchovni¹⁷²
 G. Duckeck¹¹¹ O. A. Ducu^{28b} D. Duda⁵³ A. Dudarev³⁷ E. R. Duden²⁷ M. D'uffizi¹⁰³ L. Duflost⁶⁷
 M. Dührssen³⁷ I. Duminica^{28g} A. E. Dumitriu^{28b} M. Dunford^{64a} S. Dungs⁵⁰ K. Dunne^{48a,48b} A. Duperrin¹⁰⁴
 H. Duran Yildiz^{3a} M. Düren⁵⁹ A. Durglishvili^{152b} B. L. Dwyer¹¹⁸ G. I. Dyckes^{18a} M. Dyndal^{87a}
 B. S. Dziedzic³⁷ Z. O. Earnshaw¹⁴⁹ G. H. Eberwein¹²⁹ B. Eckerova^{29a} S. Eggebrecht⁵⁶
 E. Egidio Purcino De Souza^{84e} L. F. Ehrke⁵⁷ G. Eigen¹⁷ K. Einsweiler^{18a} T. Ekelof¹⁶⁴ P. A. Ekman¹⁰⁰
 S. El Farkh^{36b} Y. El Ghazali^{63a} H. El Jarrari³⁷ A. El Moussaouy^{36a} V. Ellajosyula¹⁶⁴ M. Ellert¹⁶⁴
 F. Ellinghaus¹⁷⁴ N. Ellis³⁷ J. Elmsheuser³⁰ M. Elsayw^{119a} M. Elsing³⁷ D. Emelianov¹³⁷ Y. Enari⁸⁵
 I. Ene^{18a} S. Epari¹³ P. A. Erland⁸⁸ D. Ernani Martins Neto⁸⁸ M. Errenst¹⁷⁴ M. Escalier⁶⁷ C. Escobar¹⁶⁶
 E. Etzion¹⁵⁴ G. Evans^{133a} H. Evans⁶⁹ L. S. Evans⁹⁷ A. Ezhilov³⁸ S. Ezzarqtouni^{36a} F. Fabbri^{24b,24a}
 L. Fabbri^{24b,24a} G. Facini⁹⁸ V. Fadeyev¹³⁹ R. M. Fakhrutdinov³⁸ D. Fakoudis¹⁰² S. Falciano^{76a}
 L. F. Falda Ulhoa Coelho³⁷ F. Fallavollita¹¹² G. Falsetti^{44b,44a} J. Faltova¹³⁶ C. Fan¹⁶⁵ K. Y. Fan^{65b} Y. Fan¹⁴
 Y. Fang^{14,114c} M. Fanti^{72a,72b} M. Faraj^{70a,70b} Z. Farazpay⁹⁹ A. Farbin⁸ A. Farilla^{78a} T. Farooque¹⁰⁹
 S. M. Farrington⁵³ F. Fassi^{36e} D. Fassouliotis⁹ M. Fauci Giannelli^{77a,77b} W. J. Fawcett³³ L. Fayard⁶⁷
 P. Federic¹³⁶ P. Federicova¹³⁴ O. L. Fedin^{38j} M. Feickert¹⁷³ L. Feligioni¹⁰⁴ D. E. Fellers¹²⁶ C. Feng^{63b}
 Z. Feng¹¹⁷ M. J. Fenton¹⁶² L. Ferencz⁴⁹ R. A. M. Ferguson⁹³ S. I. Fernandez Luengo^{140f}
 P. Fernandez Martinez¹³ M. J. V. Fernoux¹⁰⁴ J. Ferrando⁹³ A. Ferrari¹⁶⁴ P. Ferrari^{117,116} R. Ferrari^{74a}
 D. Ferrere⁵⁷ C. Ferretti¹⁰⁸ D. Fiacco^{76a,76b} F. Fiedler¹⁰² P. Fiedler¹³⁵ A. Filipčić⁹⁵ E. K. Filmer¹
 F. Filthaut¹¹⁶ M. C. N. Fiolhais^{133a,133c,p} L. Fiorini¹⁶⁶ W. C. Fisher¹⁰⁹ T. Fitschen¹⁰³ P. M. Fitzhugh¹³⁸
 I. Fleck¹⁴⁴ P. Fleischmann¹⁰⁸ T. Flick¹⁷⁴ M. Flores^{34d,q} L. R. Flores Castillo^{65a} L. Flores Sanz De Acedo³⁷
 F. M. Follega^{79a,79b} N. Fomin³³ J. H. Foo¹⁵⁸ A. Formica¹³⁸ A. C. Forti¹⁰³ E. Fortin³⁷ A. W. Fortman^{18a}
 M. G. Foti^{18a} L. Fountas^{9,f} D. Fournier⁶⁷ H. Fox⁹³ P. Francavilla^{75a,75b} S. Francescato⁶² S. Franchellucci⁵⁷
 M. Franchini^{24b,24a} S. Franchino^{64a} D. Francis³⁷ L. Franco¹¹⁶ V. Franco Lima³⁷ L. Franconi⁴⁹ M. Franklin⁶²
 G. Frattari²⁷ Y. Y. Frid¹⁵⁴ J. Friend⁶⁰ N. Fritzsche³⁷ A. Froch⁵⁵ D. Froidevaux³⁷ J. A. Frost¹²⁹ Y. Fu^{63a}
 S. Fuenzalida Garrido^{140f} M. Fujimoto¹⁰⁴ K. Y. Fung^{65a} E. Furtado De Simas Filho^{84e} M. Furukawa¹⁵⁶
 J. Fuster¹⁶⁶ A. Gaa⁵⁶ A. Gabrielli^{24b,24a} A. Gabrielli¹⁵⁸ P. Gadow³⁷ G. Gagliardi^{58b,58a} L. G. Gagnon^{18a}
 S. Gaid¹⁶³ S. Galantzan¹⁵⁴ J. Gallagher¹ E. J. Gallas¹²⁹ B. J. Gallop¹³⁷ K. K. Gan¹²² S. Ganguly¹⁵⁶
 Y. Gao⁵³ F. M. Garay Walls^{140a,140b} B. Garcia³⁰ C. García¹⁶⁶ A. Garcia Alonso¹¹⁷ A. G. Garcia Caffaro¹⁷⁵
 J. E. García Navarro¹⁶⁶ M. Garcia-Sciveres^{18a} G. L. Gardner¹³¹ R. W. Gardner⁴⁰ N. Garelli¹⁶¹ D. Garg⁸¹
 R. B. Garg¹⁴⁶ J. M. Gargan⁵³ C. A. Garner¹⁵⁸ C. M. Garvey^{34a} V. K. Gassmann¹⁶¹ G. Gaudio^{74a} V. Gautam¹³
 P. Gauzzi^{76a,76b} J. Gavranovic⁹⁵ I. L. Gavrilenko³⁸ A. Gavriluk³⁸ C. Gay¹⁶⁷ G. Gaycken¹²⁶ E. N. Gazis¹⁰
 A. A. Geanta^{28b} C. M. Gee¹³⁹ A. Gekow¹²² C. Gemme^{58b} M. H. Genest⁶¹ A. D. Gentry¹¹⁵ S. George⁹⁷
 W. F. George²¹ T. Gerialis⁴⁷ P. Gessinger-Befurt³⁷ M. E. Geyik¹⁷⁴ M. Ghani¹⁷⁰ K. Ghorbanian⁹⁶
 A. Ghosal¹⁴⁴ A. Ghosh¹⁶² A. Ghosh⁷ B. Giacobbe^{24b} S. Giagu^{76a,76b} T. Giani¹¹⁷ A. Giannini^{63a}
 S. M. Gibson⁹⁷ M. Gignac¹³⁹ D. T. Gil^{87b} A. K. Gilbert^{87a} B. J. Gilbert⁴² D. Gillberg³⁵ G. Gilles¹¹⁷
 L. Ginabat¹³⁰ D. M. Gingrich^{2,d} M. P. Giordani^{70a,70c} P. F. Giraud¹³⁸ G. Giugliarelli^{70a,70c} D. Giugni^{72a}

F. Giuli³⁷, I. Gkialas^{9,r}, L. K. Gladilin³⁸, C. Glasman¹⁰¹, G. R. Gledhill¹²⁶, G. Glemža⁴⁹, M. Glisic¹²⁶, I. Gnesi^{44b,s}, Y. Go³⁰, M. Goblirsch-Kolb³⁷, B. Gocke⁵⁰, D. Godin¹¹⁰, B. Gokturk^{22a}, S. Goldfarb¹⁰⁷, T. Golling⁵⁷, M. G. D. Gololo^{34g}, D. Golubkov³⁸, J. P. Gombas¹⁰⁹, A. Gomes^{133a,133b}, G. Gomes Da Silva¹⁴⁴, A. J. Gomez Delegido¹⁶⁶, R. Gonçalo^{133a}, L. Gonella²¹, A. Gongadze^{152c}, F. Gonnella²¹, J. L. Gonski¹⁴⁶, R. Y. González Andana⁵³, S. González de la Hoz¹⁶⁶, R. Gonzalez Lopez⁹⁴, C. Gonzalez Renteria^{18a}, M. V. Gonzalez Rodrigues⁴⁹, R. Gonzalez Suarez¹⁶⁴, S. Gonzalez-Sevilla⁵⁷, L. Goossens³⁷, B. Gorini³⁷, E. Gorini^{71a,71b}, A. Gorišek⁹⁵, T. C. Gosart¹³¹, A. T. Goshaw⁵², M. I. Gostkin³⁹, S. Goswami¹²⁴, C. A. Gottardo³⁷, S. A. Gotz¹¹¹, M. Gouighri^{36b}, V. Goumarre⁴⁹, A. G. Goussiou¹⁴¹, N. Govender^{34c}, R. P. Grabarczyk¹²⁹, I. Grabowska-Bold^{87a}, K. Graham³⁵, E. Gramstad¹²⁸, S. Grancagnolo^{71a,71b}, C. M. Grant^{1,138}, P. M. Gravila^{28f}, F. G. Gravili^{71a,71b}, H. M. Gray^{18a}, M. Greco^{71a,71b}, M. J. Green¹, C. Grefe²⁵, A. S. Grefsrud¹⁷, I. M. Gregor⁴⁹, K. T. Greif¹⁶², P. Grenier¹⁴⁶, S. G. Grewe¹¹², A. A. Grillo¹³⁹, K. Grimm³², S. Grinstein^{13,t}, J.-F. Grivaz⁶⁷, E. Gross¹⁷², J. Grosse-Knetter⁵⁶, L. Guan¹⁰⁸, J. G. R. Guerrero Rojas¹⁶⁶, G. Guerrieri³⁷, R. Gugel¹⁰², J. A. M. Guhit¹⁰⁸, A. Guida¹⁹, E. Guillon¹⁷⁰, S. Guindon³⁷, F. Guo^{14,114c}, J. Guo^{63c}, L. Guo⁴⁹, Y. Guo¹⁰⁸, R. Gupta¹³², S. Gurbuz²⁵, S. S. Gurdasani⁵⁵, G. Gustavino^{76a,76b}, P. Gutierrez¹²³, L. F. Gutierrez Zagazeta¹³¹, M. Gutsche⁵¹, C. Gutschow⁹⁸, C. Gwenlan¹²⁹, C. B. Gwilliam⁹⁴, E. S. Haaland¹²⁸, A. Haas¹²⁰, M. Habedank⁴⁹, C. Haber^{18a}, H. K. Hadavand⁸, A. Hadeef⁵¹, S. Hadzic¹¹², A. I. Hagan⁹³, J. J. Hahn¹⁴⁴, E. H. Haines⁹⁸, M. Haleem¹⁶⁹, J. Haley¹²⁴, J. J. Hall¹⁴², G. D. Hallewell¹⁰⁴, L. Halser²⁰, K. Hamano¹⁶⁸, M. Hamer²⁵, G. N. Hamity⁵³, E. J. Hampshire⁹⁷, J. Han^{63b}, K. Han^{63a}, L. Han^{114a}, L. Han^{63a}, S. Han^{18a}, Y. F. Han¹⁵⁸, K. Hanagaki⁸⁵, M. Hance¹³⁹, D. A. Hangal⁴², H. Hanif¹⁴⁵, M. D. Hank¹³¹, J. B. Hansen⁴³, P. H. Hansen⁴³, D. Harada⁵⁷, T. Harenberg¹⁷⁴, S. Harkusha³⁸, M. L. Harris¹⁰⁵, Y. T. Harris²⁵, J. Harrison¹³, N. M. Harrison¹²², P. F. Harrison¹⁷⁰, N. M. Hartman¹¹², N. M. Hartmann¹¹¹, R. Z. Hasan^{97,137}, Y. Hasegawa¹⁴³, F. Haslbeck¹²⁹, S. Hassan¹⁷, R. Hauser¹⁰⁹, C. M. Hawkes²¹, R. J. Hawking³⁷, Y. Hayashi¹⁵⁶, D. Hayden¹⁰⁹, C. Hayes¹⁰⁸, R. L. Hayes¹¹⁷, C. P. Hays¹²⁹, J. M. Hays⁹⁶, H. S. Hayward⁹⁴, F. He^{63a}, M. He^{14,114c}, Y. He⁴⁹, Y. He⁹⁸, N. B. Heatley⁹⁶, V. Hedberg¹⁰⁰, A. L. Heggelund¹²⁸, N. D. Hehir^{96,a}, C. Heidegger⁵⁵, K. K. Heidegger⁵⁵, J. Heilman³⁵, S. Heim⁴⁹, T. Heim^{18a}, J. G. Heinlein¹³¹, J. J. Heinrich¹²⁶, L. Heinrich^{112,u}, J. Hejbal¹³⁴, A. Held¹⁷³, S. Hellesund¹⁷, C. M. Helling¹⁶⁷, S. Hellman^{48a,48b}, R. C. W. Henderson⁹³, L. Henkelmann³³, A. M. Henriques Correia³⁷, H. Herde¹⁰⁰, Y. Hernández Jiménez¹⁴⁸, L. M. Herrmann²⁵, T. Herrmann⁵¹, G. Herten⁵⁵, R. Hertenberger¹¹¹, L. Hervas³⁷, M. E. Hesping¹⁰², N. P. Hessey^{159a}, M. Hidaoui^{36b}, N. Hidic¹³⁶, E. Hill¹⁵⁸, S. J. Hillier²¹, J. R. Hinds¹⁰⁹, F. Hinterkeuser²⁵, M. Hirose¹²⁷, S. Hirose¹⁶⁰, D. Hirschbuehl¹⁷⁴, T. G. Hitchings¹⁰³, B. Hiti⁹⁵, J. Hobbs¹⁴⁸, R. Hobincu^{28e}, N. Hod¹⁷², M. C. Hodgkinson¹⁴², B. H. Hodgkinson¹²⁹, A. Hoecker³⁷, D. D. Hofer¹⁰⁸, J. Hofer⁴⁹, T. Holm²⁵, M. Holzbock³⁷, L. B. A. H. Hommels³³, B. P. Honan¹⁰³, J. J. Hong⁶⁹, J. Hong^{63c}, T. M. Hong¹³², B. H. Hooberman¹⁶⁵, W. H. Hopkins⁶, M. C. Hoppesch¹⁶⁵, Y. Horii¹¹³, S. Hou¹⁵¹, A. S. Howard⁹⁵, J. Howarth⁶⁰, J. Hoya⁶, M. Hrabovsky¹²⁵, A. Hrynevich⁴⁹, T. Hryn'ova⁴, P. J. Hsu⁶⁶, S.-C. Hsu¹⁴¹, T. Hsu⁶⁷, M. Hu^{18a}, Q. Hu^{63a}, S. Huang^{65b}, X. Huang^{14,114c}, Y. Huang¹⁴², Y. Huang¹⁰², Y. Huang¹⁴, Z. Huang¹⁰³, Z. Hubacek¹³⁵, M. Huebner²⁵, F. Huegging²⁵, T. B. Huffman¹²⁹, C. A. Hugli⁴⁹, M. Huhtinen³⁷, S. K. Huiberts¹⁷, R. Hulsken¹⁰⁶, N. Huseynov^{12,v}, J. Huston¹⁰⁹, J. Huth⁶², R. Hyneman¹⁴⁶, G. Iacobucci⁵⁷, G. Iakovidis³⁰, L. Iconomidou-Fayard⁶⁷, J. P. Iddon³⁷, P. Iengo^{73a,73b}, R. Iguchi¹⁵⁶, Y. Iiyama¹⁵⁶, T. Iizawa¹²⁹, Y. Ikegami⁸⁵, N. Ilic¹⁵⁸, H. Imam^{84c}, M. Ince Lezki⁵⁷, T. Ingebretsen Carlson^{48a,48b}, J. M. Inglis⁹⁶, G. Introzzi^{74a,74b}, M. Iodice^{78a}, V. Ippolito^{76a,76b}, R. K. Irwin⁹⁴, M. Ishino¹⁵⁶, W. Islam¹⁷³, C. Issever^{19,49}, S. Istin^{22a,w}, H. Ito¹⁷¹, R. Iuppa^{79a,79b}, A. Ivina¹⁷², J. M. Izen⁴⁶, V. Izzo^{73a}, P. Jacka¹³⁴, P. Jackson¹, C. S. Jagfeld¹¹¹, G. Jain^{159a}, P. Jain⁴⁹, K. Jakobs⁵⁵, T. Jakoubek¹⁷², J. Jamieson⁶⁰, W. Jang¹⁵⁶, M. Javurkova¹⁰⁵, P. Jawahar¹⁰³, L. Jeanty¹²⁶, J. Jejelava^{152a,x}, P. Jenni^{55,y}, C. E. Jessiman³⁵, C. Jia^{63b}, J. Jia¹⁴⁸, X. Jia^{14,114c}, Z. Jia^{114a}, C. Jiang⁵³, S. Jiggins⁴⁹, J. Jimenez Pena¹³, S. Jin^{114a}, A. Jinaru^{28b}, O. Jinnouchi¹⁵⁷, P. Johansson¹⁴², K. A. Johns⁷, J. W. Johnson¹³⁹, F. A. Jolly⁴⁹, D. M. Jones¹⁴⁹, E. Jones⁴⁹, K. S. Jones⁸, P. Jones³³, R. W. L. Jones⁹³, T. J. Jones⁹⁴, H. L. Joos^{56,37}, R. Joshi¹²², J. Jovicevic¹⁶, X. Ju^{18a}, J. J. Junggeburth¹⁰⁵, T. Junkermann^{64a}, A. Juste Rozas^{13,t}, M. K. Juzek⁸⁸, S. Kabana^{140e}, A. Kaczmarska⁸⁸, M. Kado¹¹², H. Kagan¹²², M. Kagan¹⁴⁶, A. Kahn¹³¹, C. Kahra¹⁰², T. Kaji¹⁵⁶, E. Kajomovitz¹⁵³, N. Kakati¹⁷², I. Kalaitzidou⁵⁵, C. W. Kalderon³⁰, N. J. Kang¹³⁹, D. Kar^{34g}, K. Karava¹²⁹, M. J. Kareem^{159b}, E. Karentzos⁵⁵, O. Karkout¹¹⁷, S. N. Karpov³⁹

Z. M. Karpova³⁹, V. Kartvelishvili⁹³, A. N. Karyukhin³⁸, E. Kasimi¹⁵⁵, J. Katzy⁴⁹, S. Kaur³⁵, K. Kawade¹⁴³, M. P. Kawale¹²³, C. Kawamoto⁸⁹, T. Kawamoto^{63a}, E. F. Kay³⁷, F. I. Kaya¹⁶¹, S. Kazakos¹⁰⁹, V. F. Kazanin³⁸, Y. Ke¹⁴⁸, J. M. Keaveney^{34a}, R. Keeler¹⁶⁸, G. V. Kehris⁶², J. S. Keller³⁵, A. S. Kelly⁹⁸, J. J. Kempster¹⁴⁹, P. D. Kennedy¹⁰², O. Kepka¹³⁴, B. P. Kerridge¹³⁷, S. Kersten¹⁷⁴, B. P. Kerševan⁹⁵, L. Keszeghova^{29a}, S. Ketabchi Haghighat¹⁵⁸, R. A. Khan¹³², A. Khanov¹²⁴, A. G. Kharlamov³⁸, T. Kharlamova³⁸, E. E. Khoda¹⁴¹, M. Kholodenko^{133a}, T. J. Khoo¹⁹, G. Khorialiuli¹⁶⁹, J. Khubua^{152b,a}, Y. A. R. Khwaira¹³⁰, B. Kibirige^{34g}, D. Kim⁶, D. W. Kim^{48a,48b}, Y. K. Kim⁴⁰, N. Kimura⁹⁸, M. K. Kingston⁵⁶, A. Kirchhoff⁵⁶, C. Kirfel²⁵, F. Kirfel²⁵, J. Kirk¹³⁷, A. E. Kiryunin¹¹², C. Kitsaki¹⁰, O. Kivernyk²⁵, M. Klassen¹⁶¹, C. Klein³⁵, L. Klein¹⁶⁹, M. H. Klein⁴⁵, S. B. Klein⁵⁷, U. Klein⁹⁴, P. Klimek³⁷, A. Klimentov³⁰, T. Klioutchnikova³⁷, P. Kluit¹¹⁷, S. Kluth¹¹², E. Kneringer⁸⁰, T. M. Knight¹⁵⁸, A. Knue⁵⁰, D. Kobylanski¹⁷², S. F. Koch¹²⁹, M. Kocian¹⁴⁶, P. Kodyš¹³⁶, D. M. Koeck¹²⁶, P. T. Koenig²⁵, T. Koffas³⁵, O. Kolay⁵¹, I. Koletsou⁴, T. Komarek⁸⁸, K. Köneke⁵⁵, A. X. Y. Kong¹, T. Kono¹²¹, N. Konstantinidis⁹⁸, P. Kontaxakis⁵⁷, B. Konya¹⁰⁰, R. Kopeliansky⁴², S. Koperny^{87a}, K. Korcyl⁸⁸, K. Kordas^{155,z}, A. Korn⁹⁸, S. Korn⁵⁶, I. Korolkov¹³, N. Korotkova³⁸, B. Kortman¹¹⁷, O. Kortner¹¹², S. Kortner¹¹², W. H. KostECKa¹¹⁸, V. V. Kostyukhin¹⁴⁴, A. Kotsokchagia³⁷, A. Kotwal⁵², A. Koulouris³⁷, A. Kourkoumeli-Charalampidi^{74a,74b}, C. Kourkoumelis⁹, E. Kourlitis^{112,u}, O. Kovanda¹²⁶, R. Kowalewski¹⁶⁸, W. Kozanecki¹²⁶, A. S. Kozhin³⁸, V. A. Kramarenko³⁸, G. Kramberger⁹⁵, P. Kramer¹⁰², M. W. Krasny¹³⁰, A. Krasznahorkay³⁷, A. C. Kraus¹¹⁸, J. W. Kraus¹⁷⁴, J. A. Kremer⁴⁹, T. Kresse⁵¹, L. Kretschmann¹⁷⁴, J. Kretschmar⁹⁴, K. Kreul¹⁹, P. Krieger¹⁵⁸, M. Krivos¹³⁶, K. Krizka²¹, K. Kroeninger⁵⁰, H. Kroha¹¹², J. Kroll¹³⁴, J. Kroll¹³¹, K. S. Krowpman¹⁰⁹, U. Kruchonak³⁹, H. Krüger²⁵, N. Krumnack⁸², M. C. Kruse⁵², O. Kuchinskaia³⁸, S. Kuday^{3a}, S. Kuehn³⁷, R. Kuesters⁵⁵, T. Kuhl⁴⁹, V. Kukhtin³⁹, Y. Kulchitsky^{38,j}, S. Kuleshov^{140d,140b}, M. Kumar^{34g}, N. Kumari⁴⁹, P. Kumari^{159b}, A. Kupco¹³⁴, T. Kupfer⁵⁰, A. Kupich³⁸, O. Kuprash⁵⁵, H. Kurashige⁸⁶, L. L. Kurchaninov^{159a}, O. Kurdyshev⁶⁷, Y. A. Kurochkin³⁸, A. Kurova³⁸, M. Kuze¹⁵⁷, A. K. Kvam¹⁰⁵, J. Kvita¹²⁵, T. Kwan¹⁰⁶, N. G. Kyriacou¹⁰⁸, L. A. O. Laatu¹⁰⁴, C. Lacasta¹⁶⁶, F. Lacava^{76a,76b}, H. Lacker¹⁹, D. Lacour¹³⁰, N. N. Lad⁹⁸, E. Ladygin³⁹, A. Lafarge⁴¹, B. Laforge¹³⁰, T. Lagouri¹⁷⁵, F. Z. Lahbabi^{36a}, S. Lai⁵⁶, J. E. Lambert¹⁶⁸, S. Lammers⁶⁹, W. Lampl⁷, C. Lampoudis^{155,z}, G. Lamprinoudis¹⁰², A. N. Lancaster¹¹⁸, E. Lançon³⁰, U. Landgraf⁵⁵, M. P. J. Landon⁹⁶, V. S. Lang⁵⁵, O. K. B. Langrekken¹²⁸, A. J. Lankford¹⁶², F. Lanni³⁷, K. Lantzsch²⁵, A. Lanza^{74a}, J. F. Laporte¹³⁸, T. Lari^{72a}, F. Lasagni Manghi^{24b}, M. Lassnig³⁷, V. Latonova¹³⁴, A. Laurier¹⁵³, S. D. Lawlor¹⁴², Z. Lawrence¹⁰³, R. Lazaridou¹⁷⁰, M. Lazzaroni^{72a,72b}, B. Le¹⁰³, E. M. Le Boulicaut⁵², L. T. Le Pottier^{18a}, B. Leban^{24b,24a}, A. Lebedev⁸², M. LeBlanc¹⁰³, F. Ledroit-Guillon⁶¹, S. C. Lee¹⁵¹, S. Lee^{48a,48b}, T. F. Lee⁹⁴, L. L. Leeuw^{34c}, H. P. Lefebvre⁹⁷, M. Lefebvre¹⁶⁸, C. Leggett^{18a}, G. Lehmann Miotto³⁷, M. Leigh⁵⁷, W. A. Leight¹⁰⁵, W. Leinonen¹¹⁶, A. Leisos^{155,aa}, M. A. L. Leite^{84c}, C. E. Leitgeb¹⁹, R. Leitner¹³⁶, K. J. C. Leney⁴⁵, T. Lenz²⁵, S. Leone^{75a}, C. Leonidopoulos⁵³, A. Leopold¹⁴⁷, R. Les¹⁰⁹, C. G. Lester³³, M. Levchenko³⁸, J. Levêque⁴, L. J. Levinson¹⁷², G. Levrini^{24b,24a}, M. P. Lewicki⁸⁸, C. Lewis¹⁴¹, D. J. Lewis⁴, L. Lewitt¹⁴², A. Li⁵, B. Li^{63b}, C. Li^{63a}, C-Q. Li¹¹², H. Li^{63a}, H. Li^{63b}, H. Li^{114a}, H. Li¹⁵, H. Li^{63b}, J. Li^{63c}, K. Li¹⁴¹, L. Li^{63c}, M. Li^{14,114c}, S. Li^{14,114c}, S. Li^{63d,63c}, T. Li⁵, X. Li¹⁰⁶, Z. Li¹²⁹, Z. Li¹⁵⁶, Z. Li^{14,114c}, Z. Li^{63a}, S. Liang^{14,114c}, Z. Liang¹⁴, M. Liberatore¹³⁸, B. Liberti^{77a}, K. Lie^{65c}, J. Lieber Marin^{84e}, H. Lien⁶⁹, H. Lin¹⁰⁸, K. Lin¹⁰⁹, R. E. Lindley⁷, J. H. Lindon², J. Ling⁶², E. Lipeles¹³¹, A. Lipniacka¹⁷, A. Lister¹⁶⁷, J. D. Little⁶⁹, B. Liu¹⁴, B. X. Liu^{114b}, D. Liu^{63d,63c}, E. H. L. Liu²¹, J. B. Liu^{63a}, J. K. K. Liu³³, K. Liu^{63d}, K. Liu^{63d,63c}, M. Liu^{63a}, M. Y. Liu^{63a}, P. Liu¹⁴, Q. Liu^{63d,141,63c}, X. Liu^{63a}, X. Liu^{63b}, Y. Liu^{114b,114c}, Y. L. Liu^{63b}, Y. W. Liu^{63a}, S. L. Lloyd⁹⁶, E. M. Lobodzinska⁴⁹, P. Loch⁷, T. Lohse¹⁹, K. Lohwasser¹⁴², E. Loiacono⁴⁹, M. Lokajicek^{134,a}, J. D. Lomas²¹, J. D. Long¹⁶⁵, I. Longarini¹⁶², R. Longo¹⁶⁵, I. Lopez Paz⁶⁸, A. Lopez Solis⁴⁹, N. A. Lopez-canelas⁷, N. Lorenzo Martinez⁴, A. M. Lory¹¹¹, M. Losada^{119a}, G. Löschcke Centeno¹⁴⁹, O. Loseva³⁸, X. Lou^{48a,48b}, X. Lou^{14,114c}, A. Lounis⁶⁷, P. A. Love⁹³, G. Lu^{14,114c}, M. Lu⁶⁷, S. Lu¹³¹, Y. J. Lu⁶⁶, H. J. Lubatti¹⁴¹, C. Luci^{76a,76b}, F. L. Lucio Alves^{114a}, F. Luehring⁶⁹, I. Luise¹⁴⁸, O. Lukianchuk⁶⁷, O. Lundberg¹⁴⁷, B. Lund-Jensen^{147,a}, N. A. Luongo⁶, M. S. Lutz³⁷, A. B. Lux²⁶, D. Lynn³⁰, R. Lysak¹³⁴, E. Lytken¹⁰⁰, V. Lyubushkin³⁹, T. Lyubushkina³⁹, M. M. Lyukova¹⁴⁸, M. Firdaus M. Soberi⁵³, H. Ma³⁰, K. Ma^{63a}, L. L. Ma^{63b}, W. Ma^{63a}, Y. Ma¹²⁴, J. C. MacDonald¹⁰², P. C. Machado De Abreu Farias^{84e}, R. Madar⁴¹, T. Madula⁹⁸, J. Maeda⁸⁶, T. Maeno³⁰, H. Maguire¹⁴², V. Maiboroda¹³⁸, A. Maio^{133a,133b,133d}, K. Maj^{87a}

O. Majersky⁴⁹, S. Majewski¹²⁶, N. Makovec⁶⁷, V. Maksimovic¹⁶, B. Malaescu¹³⁰, Pa. Malecki⁸⁸, V. P. Maleev³⁸, F. Malek^{61,bb}, M. Mali⁹⁵, D. Malito⁹⁷, U. Mallik^{81,a}, S. Maltezos¹⁰, S. Malyukov³⁹, J. Mamuzic¹³, G. Mancini⁵⁴, M. N. Mancini²⁷, G. Manco^{74a,74b}, J. P. Mandalia⁹⁶, S. S. Mandary¹⁴⁹, I. Mandić⁹⁵, L. Manhaes de Andrade Filho^{84a}, I. M. Maniatis¹⁷², J. Manjarres Ramos⁹¹, D. C. Mankad¹⁷², A. Mann¹¹¹, S. Manzoni³⁷, L. Mao^{63c}, X. Mapekula^{34c}, A. Marantis^{155,aa}, G. Marchiori⁵, M. Marcisovsky¹³⁴, C. Marcon^{72a}, M. Marinescu²¹, S. Marium⁴⁹, M. Marjanovic¹²³, A. Markhoos⁵⁵, M. Markovitch⁶⁷, E. J. Marshall⁹³, Z. Marshall^{18a}, S. Marti-Garcia¹⁶⁶, J. Martin⁹⁸, T. A. Martin¹³⁷, V. J. Martin⁵³, B. Martin dit Latour¹⁷, L. Martinelli^{76a,76b}, M. Martinez^{13,t}, P. Martinez Agullo¹⁶⁶, V. I. Martinez Outschoorn¹⁰⁵, P. Martinez Suarez¹³, S. Martin-Haugh¹³⁷, G. Martinovicova¹³⁶, V. S. Martoiu^{28b}, A. C. Martyniuk⁹⁸, A. Marzin³⁷, D. Mascione^{79a,79b}, L. Masetti¹⁰², J. Masik¹⁰³, A. L. Maslennikov³⁸, P. Massarotti^{73a,73b}, P. Mastrandrea^{75a,75b}, A. Mastroberardino^{44b,44a}, T. Masubuchi¹²⁷, T. Mathisen¹⁶⁴, J. Matousek¹³⁶, J. Maurer^{28b}, A. J. Maury⁶⁷, B. Maček⁹⁵, D. A. Maximov³⁸, A. E. May¹⁰³, R. Mazini¹⁵¹, I. Maznas¹¹⁸, M. Mazza¹⁰⁹, S. M. Mazza¹³⁹, E. Mazzeo^{72a,72b}, C. Mc Ginn³⁰, J. P. Mc Gowan¹⁶⁸, S. P. Mc Kee¹⁰⁸, C. C. McCracken¹⁶⁷, E. F. McDonald¹⁰⁷, A. E. McDougall¹¹⁷, J. A. Mcfayden¹⁴⁹, R. P. McGovern¹³¹, R. P. McKenzie^{34g}, T. C. McLachlan⁴⁹, D. J. McLaughlin⁹⁸, S. J. McMahon¹³⁷, C. M. Mcpartland⁹⁴, R. A. McPherson^{168,n}, S. Mehlhase¹¹¹, A. Mehta⁹⁴, D. Melini¹⁶⁶, B. R. Mellado Garcia^{34g}, A. H. Melo⁵⁶, F. Meloni⁴⁹, A. M. Mendes Jacques Da Costa¹⁰³, H. Y. Meng¹⁵⁸, L. Meng⁹³, S. Menke¹¹², M. Mentink³⁷, E. Meoni^{44b,44a}, G. Mercado¹¹⁸, S. Merianos¹⁵⁵, C. Merlassino^{70a,70c}, L. Merola^{73a,73b}, C. Meroni^{72a,72b}, J. Metcalfe⁶, A. S. Mete⁶, E. Meuser¹⁰², C. Meyer⁶⁹, J-P. Meyer¹³⁸, R. P. Middleton¹³⁷, L. Mijović⁵³, G. Mikenberg¹⁷², M. Mikesikova¹³⁴, M. Mikuž⁹⁵, H. Mildner¹⁰², A. Milic³⁷, D. W. Miller⁴⁰, E. H. Miller¹⁴⁶, L. S. Miller³⁵, A. Milov¹⁷², D. A. Milstead^{48a,48b}, T. Min^{114a}, A. A. Minaenko³⁸, I. A. Minashvili^{152b}, L. Mince⁶⁰, A. I. Mincer¹²⁰, B. Mindur^{87a}, M. Mineev³⁹, Y. Mino⁸⁹, L. M. Mir¹³, M. Miralles Lopez⁶⁰, M. Mironova^{18a}, M. C. Missio¹¹⁶, A. Mitra¹⁷⁰, V. A. Mitsou¹⁶⁶, Y. Mitsumori¹¹³, O. Miu¹⁵⁸, P. S. Miyagawa⁹⁶, T. Mkrtychyan^{64a}, M. Mlinarevic⁹⁸, T. Mlinarevic⁹⁸, M. Mlynarikova³⁷, S. Mobius²⁰, P. Mogg¹¹¹, M. H. Mohamed Farook¹¹⁵, A. F. Mohammed^{14,114c}, S. Mohapatra⁴², G. Mokgatitwane^{34g}, L. Moleri¹⁷², B. Mondal¹⁴⁴, S. Mondal¹³⁵, K. Mönig⁴⁹, E. Monnier¹⁰⁴, L. Monsonis Romero¹⁶⁶, J. Montejo Berlingen¹³, A. Montella^{48a,48b}, M. Montella¹²², F. Montekali^{78a,78b}, F. Monticelli⁹², S. Monzani^{70a,70c}, A. Morancho Tarda⁴³, N. Morange⁶⁷, A. L. Moreira De Carvalho⁴⁹, M. Moreno Llácer¹⁶⁶, C. Moreno Martinez⁵⁷, J. M. Moreno Perez^{23b}, P. Morettini^{58b}, S. Morgenstern³⁷, M. Morii⁶², M. Morinaga¹⁵⁶, F. Morodei^{76a,76b}, L. Morvaj³⁷, P. Moschovakos³⁷, B. Moser¹²⁹, M. Mosidze^{152b}, T. Moskalets⁴⁵, P. Moskvitina¹¹⁶, J. Moss^{32,cc}, P. Moszkowicz^{87a}, A. Moussa^{36d}, E. J. W. Moyse¹⁰⁵, O. Mtintsilana^{34g}, S. Muanza¹⁰⁴, J. Mueller¹³², D. Muenstermann⁹³, R. Müller³⁷, G. A. Mullier¹⁶⁴, A. J. Mullin³³, J. J. Mullin¹³¹, D. P. Mungo¹⁵⁸, D. Munoz Perez¹⁶⁶, F. J. Munoz Sanchez¹⁰³, M. Murin¹⁰³, W. J. Murray^{170,137}, M. Muškinja⁹⁵, C. Mwewa³⁰, A. G. Myagkov^{38,j}, A. J. Myers⁸, G. Myers¹⁰⁸, M. Myska¹³⁵, B. P. Nachman^{18a}, O. Nackenhorst⁵⁰, K. Nagai¹²⁹, K. Nagano⁸⁵, J. L. Nagle^{30,o}, E. Nagy¹⁰⁴, A. M. Nairz³⁷, Y. Nakahama⁸⁵, K. Nakamura⁸⁵, K. Nakkalil⁵, H. Nanjo¹²⁷, E. A. Narayanan¹¹⁵, I. Naryshkin³⁸, L. Nasella^{72a,72b}, M. Naseri³⁵, S. Nasri^{119b}, C. Nass²⁵, G. Navarro^{23a}, J. Navarro-Gonzalez¹⁶⁶, R. Nayak¹⁵⁴, A. Nayaz¹⁹, P. Y. Nechaeva³⁸, S. Nechaeva^{24b,24a}, F. Nechansky⁴⁹, L. Nedic¹²⁹, T. J. Neep²¹, A. Negri^{74a,74b}, M. Negrini^{24b}, C. Nellist¹¹⁷, C. Nelson¹⁰⁶, K. Nelson¹⁰⁸, S. Nemecek¹³⁴, M. Nessi^{37,dd}, M. S. Neubauer¹⁶⁵, F. Neuhaus¹⁰², J. Neundorff⁴⁹, P. R. Newman²¹, C. W. Ng¹³², Y. W. Y. Ng⁴⁹, B. Ngair^{119a}, H. D. N. Nguyen¹¹⁰, R. B. Nickerson¹²⁹, R. Nicolaidou¹³⁸, J. Nielsen¹³⁹, M. Niemeyer⁵⁶, J. Niermann⁵⁶, N. Nikiforou³⁷, V. Nikolaenko^{38,j}, I. Nikolic-Audit¹³⁰, K. Nikolopoulos²¹, P. Nilsson³⁰, I. Ninca⁴⁹, G. Ninio¹⁵⁴, A. Nisati^{76a}, N. Nishu², R. Nisius¹¹², J-E. Nitschke⁵¹, E. K. Nkadimeng^{34g}, T. Nobe¹⁵⁶, T. Nommensen¹⁵⁰, M. B. Norfolk¹⁴², B. J. Norman³⁵, M. Noury^{36a}, J. Novak⁹⁵, T. Novak⁹⁵, L. Novotny¹³⁵, R. Novotny¹¹⁵, L. Nozka¹²⁵, K. Ntekas¹⁶², N. M. J. Nunes De Moura Junior^{84b}, J. Ocariz¹³⁰, A. Ochi⁸⁶, I. Ochoa^{133a}, S. Oerdek^{49,ee}, J. T. Offermann⁴⁰, A. Ogrodnik¹³⁶, A. Oh¹⁰³, C. C. Ohm¹⁴⁷, H. Oide⁸⁵, R. Oishi¹⁵⁶, M. L. Ojeda⁴⁹, Y. Okumura¹⁵⁶, L. F. Oleiro Seabra^{133a}, I. Oleksiyuk⁵⁷, S. A. Olivares Pino^{140d}, G. Oliveira Correa¹³, D. Oliveira Damazio³⁰, J. L. Oliver¹⁶², Ö. O. Öncel⁵⁵, A. P. O'Neill²⁰, A. Onofre^{133a,133e}, P. U. E. Onyisi¹¹, M. J. Oreglia⁴⁰, G. E. Orellana⁹², D. Orestano^{78a,78b}, N. Orlando¹³, R. S. Orr¹⁵⁸, L. M. Osojnak¹³¹, R. Ospanov^{63a}, G. Otero y Garzon³¹, H. Otono⁹⁰, P. S. Ott^{64a}, G. J. Ottino^{18a}, M. Ouchrif^{36d}, F. Ould-Saada¹²⁸

T. Ovsiannikova¹⁴¹ M. Owen⁶⁰ R. E. Owen¹³⁷ V. E. Ozcan^{22a} F. Ozturk⁸⁸ N. Ozturk⁸ S. Ozturk⁸³
H. A. Pacey¹²⁹ A. Pacheco Pages¹³ C. Padilla Aranda¹³ G. Padovano^{76a,76b} S. Pagan Griso^{18a} G. Palacino⁶⁹
A. Palazzo^{71a,71b} J. Pampel²⁵ J. Pan¹⁷⁵ T. Pan^{65a} D. K. Panchal¹¹ C. E. Pandini¹¹⁷ J. G. Panduro Vazquez¹³⁷
H. D. Pandya¹ H. Pang¹⁵ P. Pani⁴⁹ G. Panizzo^{70a,70c} L. Panwar¹³⁰ L. Paolozzi⁵⁷ S. Parajuli¹⁶⁵
A. Paramonov⁶ C. Paraskevopoulos⁵⁴ D. Paredes Hernandez^{65b} A. Paretì^{74a,74b} K. R. Park⁴² T. H. Park¹⁵⁸
M. A. Parker³³ F. Parodi^{58b,58a} E. W. Parrish¹¹⁸ V. A. Parrish⁵³ J. A. Parsons⁴² U. Parzefall⁵⁵
B. Pascual Dias¹¹⁰ L. Pascual Dominguez¹⁰¹ E. Pasqualucci^{76a} S. Passaggio^{58b} F. Pastore⁹⁷ P. Patel⁸⁸
U. M. Patel⁵² J. R. Pater¹⁰³ T. Pauly³⁷ C. I. Pazos¹⁶¹ J. Pearkes¹⁴⁶ M. Pedersen¹²⁸ R. Pedro^{133a}
S. V. Peleganchuk³⁸ O. Penc³⁷ E. A. Pender⁵³ S. Peng¹⁵ G. D. Penn¹⁷⁵ K. E. Pensi¹¹¹ M. Penzin³⁸
B. S. Peralva^{84d} A. P. Pereira Peixoto¹⁴¹ L. Pereira Sanchez¹⁴⁶ D. V. Perepelitsa^{30,o} G. Perera¹⁰⁵
E. Perez Codina^{159a} M. Perganti¹⁰ H. Pernegger³⁷ S. Perrella^{76a,76b} O. Perrin⁴¹ K. Peters⁴⁹ R. F. Y. Peters¹⁰³
B. A. Petersen³⁷ T. C. Petersen⁴³ E. Petit¹⁰⁴ V. Petousis¹³⁵ C. Petridou^{155,z} T. Petru¹³⁶ A. Petrukhin¹⁴⁴
M. Pettee^{18a} A. Petukhov³⁸ K. Petukhova³⁷ R. Pezoa^{140f} L. Pezzotti³⁷ G. Pezzullo¹⁷⁵ T. M. Pham¹⁷³
T. Pham¹⁰⁷ P. W. Phillips¹³⁷ G. Piacquadio¹⁴⁸ E. Pianori^{18a} F. Piazza¹²⁶ R. Piegai³¹ D. Pietreanu^{28b}
A. D. Pilkington¹⁰³ M. Pinamonti^{70a,70c} J. L. Pinfeld² B. C. Pinheiro Pereira^{133a} J. Pinol Bel¹³
A. E. Pinto Pinoargote¹³⁸ L. Pintucci^{70a,70c} K. M. Piper¹⁴⁹ A. Pirttikoski⁵⁷ D. A. Pizzi³⁵ L. Pizzimento^{65b}
A. Pizzini¹¹⁷ M.-A. Pleier³⁰ V. Pleskot¹³⁶ E. Plotnikova³⁹ G. Poddar⁹⁶ R. Poettgen¹⁰⁰ L. Poggioli¹³⁰
I. Pokharel⁵⁶ S. Polacek¹³⁶ G. Polesello^{74a} A. Poley^{145,159a} A. Polini^{24b} C. S. Pollard¹⁷⁰ Z. B. Pollock¹²²
E. Pompa Pacchi^{76a,76b} N. I. Pond⁹⁸ D. Ponomarenko⁶⁹ L. Pontecorvo³⁷ S. Popa^{28a} G. A. Popeneciu^{28d}
A. Poreba³⁷ D. M. Portillo Quintero^{159a} S. Pospisil¹³⁵ M. A. Postill¹⁴² P. Postolache^{28c} K. Potamianos¹⁷⁰
P. A. Potepa^{87a} I. N. Potrap³⁹ C. J. Potter³³ H. Potti¹⁵⁰ J. Poveda¹⁶⁶ M. E. Pozo Astigarraga³⁷
A. Prades Ibanez^{77a,77b} J. Pretel¹⁶⁸ D. Price¹⁰³ M. Primavera^{71a} L. Primomo^{70a,70c} M. A. Principe Martin¹⁰¹
R. Privara¹²⁵ T. Procter⁶⁰ M. L. Proffitt¹⁴¹ N. Proklova¹³¹ K. Prokofiev^{65c} G. Proto¹¹² J. Proudfoot⁶
M. Przybycien^{87a} W. W. Przygoda^{87b} A. Psallidas⁴⁷ J. E. Puddefoot¹⁴² D. Pudzha⁵⁵ D. Pyatiizbyantseva³⁸
J. Qian¹⁰⁸ D. Qichen¹⁰³ Y. Qin¹³ T. Qiu⁵³ A. Quadt⁵⁶ M. Queitsch-Maitland¹⁰³ G. Quetant⁵⁷
R. P. Quinn¹⁶⁷ G. Rabanal Bolanos⁶² D. Rafanoharana⁵⁵ F. Raffaelli^{77a,77b} F. Ragusa^{72a,72b} J. L. Rainbolt⁴⁰
J. A. Raine⁵⁷ S. Rajagopalan³⁰ E. Ramakoti³⁸ L. Rambelli^{58b,58a} I. A. Ramirez-Berend³⁵ K. Ran^{49,114c}
D. S. Rankin¹³¹ N. P. Rapheeha^{34g} H. Rasheed^{28b} V. Raskina¹³⁰ D. F. Rassloff^{64a} A. Rastogi^{18a} S. Rave¹⁰²
S. Ravera^{58b,58a} B. Ravina⁵⁶ I. Ravinovich¹⁷² M. Raymond³⁷ A. L. Read¹²⁸ N. P. Readioff¹⁴²
D. M. Rebuzzi^{74a,74b} G. Redlinger³⁰ A. S. Reed¹¹² K. Reeves²⁷ J. A. Reidelsturz¹⁷⁴ D. Reikher¹²⁶ A. Rej⁵⁰
C. Rembser³⁷ M. Renda^{28b} F. Renner⁴⁹ A. G. Rennie¹⁶² A. L. Rescia⁴⁹ S. Resconi^{72a} M. Ressegotti^{58b,58a}
S. Rettie³⁷ J. G. Reyes Rivera¹⁰⁹ E. Reynolds^{18a} O. L. Rezanova³⁸ P. Reznicek¹³⁶ H. Riani^{36d} N. Ribaric⁹³
E. Ricci^{79a,79b} R. Richter¹¹² S. Richter^{48a,48b} E. Richter-Was^{87b} M. Ridel¹³⁰ S. Ridouani^{36d} P. Rieck¹²⁰
P. Riedler³⁷ E. M. Riefel^{48a,48b} J. O. Rieger¹¹⁷ M. Rijssenbeek¹⁴⁸ M. Rimoldi³⁷ L. Rinaldi^{24b,24a}
P. Rincke^{56,164} T. T. Rinn³⁰ M. P. Rinnagel¹¹¹ G. Ripellino¹⁶⁴ I. Riu¹³ J. C. Rivera Vergara¹⁶⁸
F. Rizatdinova¹²⁴ E. Rizvi⁹⁶ B. R. Roberts^{18a} S. S. Roberts¹³⁹ S. H. Robertson^{106,n} D. Robinson³³
M. Robles Manzano¹⁰² A. Robson⁶⁰ A. Rocchi^{77a,77b} C. Roda^{75a,75b} S. Rodriguez Bosca³⁷
Y. Rodriguez Garcia^{23a} A. Rodriguez Rodriguez⁵⁵ A. M. Rodríguez Vera¹¹⁸ S. Roe³⁷ J. T. Roemer³⁷
A. R. Roepe-Gier¹³⁹ O. Røhne¹²⁸ R. A. Rojas¹⁰⁵ C. P. A. Roland¹³⁰ J. Roloff³⁰ A. Romaniouk³⁸
E. Romano^{74a,74b} M. Romano^{24b} A. C. Romero Hernandez¹⁶⁵ N. Rompotis⁹⁴ L. Roos¹³⁰ S. Rosati^{76a}
B. J. Rosser⁴⁰ E. Rossi¹²⁹ E. Rossi^{73a,73b} L. P. Rossi⁶² L. Rossini⁵⁵ R. Rosten¹²² M. Rotaru^{28b} B. Rottler⁵⁵
C. Rougier⁹¹ D. Rousseau⁶⁷ D. Rousso⁴⁹ A. Roy¹⁶⁵ S. Roy-Garand¹⁵⁸ A. Rozanov¹⁰⁴ Z. M. A. Rozario⁶⁰
Y. Rozen¹⁵³ A. Rubio Jimenez¹⁶⁶ A. J. Ruby⁹⁴ V. H. Ruelas Rivera¹⁹ T. A. Ruggeri¹ A. Ruggiero¹²⁹
A. Ruiz-Martinez¹⁶⁶ A. Rummler³⁷ Z. Rurikova⁵⁵ N. A. Rusakovich³⁹ H. L. Russell¹⁶⁸ G. Russo^{76a,76b}
J. P. Rutherford⁷ S. Rutherford Colmenares³³ M. Rybar¹³⁶ E. B. Rye¹²⁸ A. Ryzhov⁴⁵ J. A. Sabater Iglesias⁵⁷
H. F-W. Sadrozinski¹³⁹ F. Safai Tehrani^{76a} B. Safarzadeh Samani¹³⁷ S. Saha¹ M. Sahinsoy⁸³ A. Saibel¹⁶⁶
M. Saimpert¹³⁸ M. Saito¹⁵⁶ T. Saito¹⁵⁶ A. Sala^{72a,72b} D. Salamani³⁷ A. Salnikov¹⁴⁶ J. Salt¹⁶⁶
A. Salvador Salas¹⁵⁴ D. Salvatore^{44b,44a} F. Salvatore¹⁴⁹ A. Salzburger³⁷ D. Sammel⁵⁵ E. Sampson⁹³
D. Sampsonidis^{155,z} D. Sampsonidou¹²⁶ J. Sánchez¹⁶⁶ V. Sanchez Sebastian¹⁶⁶ H. Sandaker¹²⁸ C. O. Sander⁴⁹

J. A. Sandesara¹⁰⁵ M. Sandhoff¹⁷⁴ C. Sandoval^{23b} L. Sanfilippo^{64a} D. P. C. Sankey¹³⁷ T. Sano⁸⁹
A. Sansoni⁵⁴ L. Santi^{37,76b} C. Santoni⁴¹ H. Santos^{133a,133b} A. Santra¹⁷² E. Sanzani^{24b,24a} K. A. Saoucha¹⁶³
J. G. Saraiva^{133a,133d} J. Sardain⁷ O. Sasaki⁸⁵ K. Sato¹⁶⁰ C. Sauer^{64b} E. Sauvan⁴ P. Savard^{158,d} R. Sawada¹⁵⁶
C. Sawyer¹³⁷ L. Sawyer⁹⁹ C. Sbarra^{24b} A. Sbrizzi^{24b,24a} T. Scanlon⁹⁸ J. Schaarschmidt¹⁴¹ U. Schäfer¹⁰²
A. C. Schaffer^{67,45} D. Schaile¹¹¹ R. D. Schamberger¹⁴⁸ C. Scharf¹⁹ M. M. Schefer²⁰ V. A. Schegelsky³⁸
D. Scheirich¹³⁶ M. Schernau¹⁶² C. Scheulen⁵⁶ C. Schiavi^{58b,58a} M. Schioppa^{44b,44a} B. Schlag^{146,ff}
K. E. Schleicher⁵⁵ S. Schlenker³⁷ J. Schmeing¹⁷⁴ M. A. Schmidt¹⁷⁴ K. Schmieden¹⁰² C. Schmitt¹⁰²
N. Schmitt¹⁰² S. Schmitt⁴⁹ L. Schoeffel¹³⁸ A. Schoening^{64b} P. G. Scholer³⁵ E. Schopf¹²⁹ M. Schott²⁵
J. Schovancova³⁷ S. Schramm⁵⁷ T. Schroer⁵⁷ H-C. Schultz-Coulon^{64a} M. Schumacher⁵⁵ B. A. Schumm¹³⁹
Ph. Schune¹³⁸ A. J. Schuy¹⁴¹ H. R. Schwartz¹³⁹ A. Schwartzman¹⁴⁶ T. A. Schwarz¹⁰⁸ Ph. Schwemling¹³⁸
R. Schwienhorst¹⁰⁹ F. G. Sciacca²⁰ A. Sciandra³⁰ G. Sciolla²⁷ F. Scuri^{75a} C. D. Sebastiani⁹⁴ K. Sedlaczek¹¹⁸
S. C. Seidel¹¹⁵ A. Seiden¹³⁹ B. D. Seidlitz⁴² C. Seitz⁴⁹ J. M. Seixas^{84b} G. Sekhniaidze^{73a} L. Selem⁶¹
N. Semprini-Cesari^{24b,24a} D. Sengupta⁵⁷ V. Senthilkumar¹⁶⁶ L. Serin⁶⁷ M. Sessa^{77a,77b} H. Severini¹²³
F. Sforza^{58b,58a} A. Sfyrla⁵⁷ Q. Sha¹⁴ E. Shabalina⁵⁶ A. H. Shah³³ R. Shaheen¹⁴⁷ J. D. Shahinian¹³¹
D. Shaked Renous¹⁷² L. Y. Shan¹⁴ M. Shapiro^{18a} A. Sharma³⁷ A. S. Sharma¹⁶⁷ P. Sharma⁸¹ P. B. Shatalov³⁸
K. Shaw¹⁴⁹ S. M. Shaw¹⁰³ Q. Shen^{63c} D. J. Sheppard¹⁴⁵ P. Sherwood⁹⁸ L. Shi⁹⁸ X. Shi¹⁴ S. Shimizu⁸⁵
C. O. Shimmin¹⁷⁵ J. D. Shinner⁹⁷ I. P. J. Shipsey¹²⁹ S. Shirabe⁹⁰ M. Shiyakova^{39,gg} M. J. Shochet⁴⁰
D. R. Shope¹²⁸ B. Shrestha¹²³ S. Shrestha^{122,hh} M. J. Shroff¹⁶⁸ P. Sicho¹³⁴ A. M. Sickles¹⁶⁵
E. Sideras Haddad^{34g} A. C. Sidley¹¹⁷ A. Sidoti^{24b} F. Siegert⁵¹ Dj. Sijacki¹⁶ F. Sili⁹² J. M. Silva⁵³
I. Silva Ferreira^{84b} M. V. Silva Oliveira³⁰ S. B. Silverstein^{48a} S. Simion⁶⁷ R. Simoniello³⁷ E. L. Simpson¹⁰³
H. Simpson¹⁴⁹ L. R. Simpson¹⁰⁸ N. D. Simpson¹⁰⁰ S. Simsek⁸³ S. Sindhu⁵⁶ P. Sinervo¹⁵⁸ S. Singh¹⁵⁸
S. Sinha⁴⁹ S. Sinha¹⁰³ M. Sioli^{24b,24a} I. Siral³⁷ E. Sitnikova⁴⁹ J. Sjölin^{48a,48b} A. Skaf⁵⁶ E. Skorda²¹
P. Skubic¹²³ M. Slawinska⁸⁸ V. Smakhtin¹⁷² B. H. Smart¹³⁷ S. Yu. Smirnov³⁸ Y. Smirnov³⁸ L. N. Smirnova^{38,j}
O. Smirnova¹⁰⁰ A. C. Smith⁴² D. R. Smith¹⁶² E. A. Smith⁴⁰ J. L. Smith¹⁰³ R. Smith¹⁴⁶ M. Smizanska⁹³
K. Smolek¹³⁵ A. A. Snesarev³⁸ S. R. Snider¹⁵⁸ H. L. Snoek¹¹⁷ S. Snyder³⁰ R. Sobie^{168,n} A. Soffer¹⁵⁴
C. A. Solans Sanchez³⁷ E. Yu. Soldatov³⁸ U. Soldevila¹⁶⁶ A. A. Solodkov³⁸ S. Solomon²⁷ A. Soloshenko³⁹
K. Solovieva⁵⁵ O. V. Solovyanov⁴¹ P. Sommer⁵¹ A. Sonay¹³ W. Y. Song^{159b} A. Sopczak¹³⁵ A. L. Sapiro⁹⁸
F. Sopkova^{29b} J. D. Sorenson¹¹⁵ I. R. Sotarriva Alvarez¹⁵⁷ V. Sothilingam^{64a} O. J. Soto Sandoval^{140c,140b}
S. Sottocornola⁶⁹ R. Soualah¹⁶³ Z. Soumami^{36e} D. South⁴⁹ N. Soybelman¹⁷² S. Spagnolo^{71a,71b}
M. Spalla¹¹² D. Sperlich⁵⁵ G. Spigo³⁷ B. Spisso^{73a,73b} D. P. Spiteri⁶⁰ M. Spousta¹³⁶ E. J. Staats³⁵
R. Stamen^{64a} A. Stampekis²¹ M. Standke²⁵ E. Stanecka⁸⁸ W. Stanek-Maslouska⁴⁹ M. V. Stange⁵¹
B. Stanislaus^{18a} M. M. Stanitzki⁴⁹ B. Stapf⁴⁹ E. A. Starchenko³⁸ G. H. Stark¹³⁹ J. Stark⁹¹ P. Staroba¹³⁴
P. Starovoitov^{64a} S. Stärz¹⁰⁶ R. Staszewski⁸⁸ G. Stavropoulos⁴⁷ A. Stefl³⁷ P. Steinberg³⁰ B. Stelzer^{145,159a}
H. J. Stelzer¹³² O. Stelzer-Chilton^{159a} H. Stenzel⁵⁹ T. J. Stevenson¹⁴⁹ G. A. Stewart³⁷ J. R. Stewart¹²⁴
M. C. Stockton³⁷ G. Stoicea^{28b} M. Stolarski^{133a} S. Stonjek¹¹² A. Straessner⁵¹ J. Strandberg¹⁴⁷
S. Strandberg^{48a,48b} M. Stratmann¹⁷⁴ M. Strauss¹²³ T. Streblner¹⁰⁴ P. Striznec^{29b} R. Ströhmer¹⁶⁹
D. M. Strom¹²⁶ R. Stroynowski⁴⁵ A. Strubig^{48a,48b} S. A. Stucci³⁰ B. Stugu¹⁷ J. Stupak¹²³ N. A. Styles⁴⁹
D. Su¹⁴⁶ S. Su^{63a} W. Su^{63d} X. Su^{63a} D. Suchy^{29a} K. Sugizaki¹⁵⁶ V. V. Sulim³⁸ M. J. Sullivan⁹⁴
D. M. S. Sultan¹²⁹ L. Sultanaliev³⁸ S. Sultansoy^{3b} T. Sumida⁸⁹ S. Sun¹⁷³ O. Sunneborn Gudnadottir¹⁶⁴
N. Sur¹⁰⁴ M. R. Sutton¹⁴⁹ H. Suzuki¹⁶⁰ M. Svatos¹³⁴ M. Swiatlowski^{159a} T. Swirski¹⁶⁹ I. Sykora^{29a}
M. Sykora¹³⁶ T. Sykora¹³⁶ D. Ta¹⁰² K. Tackmann^{49,ee} A. Taffard¹⁶² R. Tafirout^{159a} J. S. Tafoya Vargas⁶⁷
Y. Takubo⁸⁵ M. Talby¹⁰⁴ A. A. Talyshchev³⁸ K. C. Tam^{65b} N. M. Tamir¹⁵⁴ A. Tanaka¹⁵⁶ J. Tanaka¹⁵⁶
R. Tanaka⁶⁷ M. Tanasini¹⁴⁸ Z. Tao¹⁶⁷ S. Tapia Araya^{140f} S. Tapprogge¹⁰² A. Tarek Abouelfadl Mohamed¹⁰⁹
S. Tarem¹⁵³ K. Tariq¹⁴ G. Tarna^{28b} G. F. Tartarelli^{72a} M. J. Tartarin⁹¹ P. Tas¹³⁶ M. Tasevsky¹³⁴
E. Tassi^{44b,44a} A. C. Tate¹⁶⁵ G. Tateno¹⁵⁶ Y. Tayalati^{36e,ii} G. N. Taylor¹⁰⁷ W. Taylor^{159b}
R. Teixeira De Lima¹⁴⁶ P. Teixeira-Dias⁹⁷ J. J. Teoh¹⁵⁸ K. Terashi¹⁵⁶ J. Terron¹⁰¹ S. Terzo¹³ M. Testa⁵⁴
R. J. Teuscher^{158,n} A. Thaler⁸⁰ O. Theiner⁵⁷ N. Themistokleous⁵³ T. Theveneaux-Pelzer¹⁰⁴ O. Thielmann¹⁷⁴
D. W. Thomas⁹⁷ J. P. Thomas²¹ E. A. Thompson^{18a} P. D. Thompson²¹ E. Thomson¹³¹ R. E. Thornberry⁴⁵
C. Tian^{63a} Y. Tian⁵⁶ V. Tikhomirov^{38,j} Yu. A. Tikhonov³⁸ S. Timoshenko³⁸ D. Timoshyn¹³⁶ E. X. L. Ting¹

P. Tipton¹⁷⁵ A. Tishelman-Charny³⁰ S. H. Tlou^{34g} K. Todome¹⁵⁷ S. Todorova-Nova¹³⁶ S. Todt,⁵¹
 L. Toffolin^{70a,70c} M. Togawa⁸⁵ J. Tojo⁹⁰ S. Tokár^{29a} K. Tokushuku⁸⁵ O. Toldaiev⁶⁹ M. Tomoto^{85,113}
 L. Tompkins^{146,ff} K. W. Topolnicki^{87b} E. Torrence¹²⁶ H. Torres⁹¹ E. Torr  Pastor¹⁶⁶ M. Toscani³¹
 C. Tosciri⁴⁰ M. Tost¹¹ D. R. Tovey¹⁴² I. S. Trandafir^{28b} T. Trefzger¹⁶⁹ A. Tricoli³⁰ I. M. Trigger^{159a}
 S. Trincaz-Duvoid¹³⁰ D. A. Trischuk²⁷ B. Trocm ⁶¹ A. Tropina,³⁹ L. Truong^{34c} M. Trzebinski⁸⁸ A. Trzupke⁸⁸
 F. Tsai¹⁴⁸ M. Tsai¹⁰⁸ A. Tsiamis¹⁵⁵ P. V. Tsiareshka,³⁸ S. Tsigaridas^{159a} A. Tsirigotis^{155,aa} V. Tsiskaridze¹⁵⁸
 E. G. Tskhadadze^{152a} M. Tsopoulou¹⁵⁵ Y. Tsujikawa⁸⁹ I. I. Tsukerman³⁸ V. Tsulaia^{18a} S. Tsuno⁸⁵
 K. Tsuru¹²¹ D. Tsybychev¹⁴⁸ Y. Tu^{65b} A. Tudorache^{28b} V. Tudorache^{28b} A. N. Tuna⁶² S. Turchikhin^{58b,58a}
 I. Turk Cakir^{3a} R. Turra^{72a} T. Turtuvshin³⁹ P. M. Tuts⁴² S. Tzamarias^{155,z} E. Tzovara¹⁰² F. Ukegawa¹⁶⁰
 P. A. Ulloa Poblete^{140c,140b} E. N. Umaka³⁰ G. Unal³⁷ A. Undrus³⁰ G. Unel¹⁶² J. Urban^{29b} P. Urrejola^{140a}
 G. Usai⁸ R. Ushioda¹⁵⁷ M. Usman¹¹⁰ F. Ustuner⁵³ Z. Uysal⁸³ V. Vacek¹³⁵ B. Vachon¹⁰⁶ T. Vafeiadis³⁷
 A. Vaitkus⁹⁸ C. Valderanis¹¹¹ E. Valdes Santurio^{48a,48b} M. Valente^{159a} S. Valentineti^{24b,24a} A. Valero¹⁶⁶
 E. Valiente Moreno¹⁶⁶ A. Vallier⁹¹ J. A. Valls Ferrer¹⁶⁶ D. R. Van Arneman¹¹⁷ T. R. Van Daalen¹⁴¹
 A. Van Der Graaf⁵⁰ P. Van Gemmeren⁶ M. Van Rijnbach³⁷ S. Van Stroud⁹⁸ I. Van Vulpen¹¹⁷ P. Vana¹³⁶
 M. Vanadia^{77a,77b} W. Vandelli³⁷ E. R. Vandewall¹²⁴ D. Vannicola¹⁵⁴ L. Vannoli⁵⁴ R. Vari^{76a} E. W. Varnes⁷
 C. Varni^{18b} T. Varol¹⁵¹ D. Varouchas⁶⁷ L. Varriale¹⁶⁶ K. E. Varvell¹⁵⁰ M. E. Vasile^{28b} L. Vaslin,⁸⁵
 G. A. Vasquez¹⁶⁸ A. Vasyukov³⁹ L. M. Vaughan¹²⁴ R. Vavricka¹⁰² T. Vazquez Schroeder³⁷ J. Veatch³²
 V. Vecchio¹⁰³ M. J. Veen¹⁰⁵ I. Veliscek³⁰ L. M. Veloce¹⁵⁸ F. Veloso^{133a,133c} S. Veneziano^{76a} A. Ventura^{71a,71b}
 S. Ventura Gonzalez¹³⁸ A. Verbytskyi¹¹² M. Verducci^{75a,75b} C. Vergis⁹⁶ M. Verissimo De Araujo^{84b}
 W. Verkerke¹¹⁷ J. C. Vermeulen¹¹⁷ C. Vernieri¹⁴⁶ M. Vessella¹⁰⁵ M. C. Vetterli^{145,d} A. Vgenopoulos¹⁰²
 N. Viaux Maira^{140f} T. Vickey¹⁴² O. E. Vickey Boeriu¹⁴² G. H. A. Viehhauser¹²⁹ L. Vignani^{64b} M. Vigi¹¹²
 M. Villa^{24b,24a} M. Villaplana Perez¹⁶⁶ E. M. Villhauer,⁵³ E. Vilucchi⁵⁴ M. G. Vincter³⁵ A. Visibile,¹¹⁷ C. Vittori³⁷
 I. Vivarelli^{24b,24a} E. Voevodina¹¹² F. Vogel¹¹¹ J. C. Voigt⁵¹ P. Vokac¹³⁵ Yu. Volkotrub^{87b} J. Von Ahnen⁴⁹
 E. Von Toerne²⁵ B. Vormwald³⁷ V. Vorobel¹³⁶ K. Vorobev³⁸ M. Vos¹⁶⁶ K. Voss¹⁴⁴ M. Vozak¹¹⁷
 L. Vozdecky¹²³ N. Vranjes¹⁶ M. Vranjes Milosavljevic¹⁶ M. Vreeswijk¹¹⁷ N. K. Vu^{63d,63c} R. Vuillermet³⁷
 O. Vujanovic¹⁰² I. Vukotic⁴⁰ S. Wada¹⁶⁰ C. Wagner¹⁰⁵ J. M. Wagner^{18a} W. Wagner¹⁷⁴ S. Wahdan¹⁷⁴
 H. Wahlberg⁹² J. Walder¹³⁷ R. Walker¹¹¹ W. Walkowiak¹⁴⁴ A. Wall¹³¹ E. J. Wallin¹⁰⁰ T. Wamorkar⁶
 A. Z. Wang¹³⁹ C. Wang¹⁰² C. Wang¹¹ H. Wang^{18a} J. Wang^{65c} P. Wang⁹⁸ R. Wang⁶² R. Wang⁶
 S. M. Wang¹⁵¹ S. Wang^{63b} S. Wang¹⁴ T. Wang^{63a} W. T. Wang⁸¹ W. Wang¹⁴ X. Wang^{114a} X. Wang¹⁶⁵
 X. Wang^{63c} Y. Wang^{63d} Y. Wang^{114a} Y. Wang^{63a} Z. Wang¹⁰⁸ Z. Wang^{63d,52,63c} Z. Wang¹⁰⁸ A. Warburton¹⁰⁶
 R. J. Ward²¹ N. Warrack⁶⁰ S. Waterhouse⁹⁷ A. T. Watson²¹ H. Watson⁶⁰ M. F. Watson²¹ E. Watton^{60,137}
 G. Watts¹⁴¹ B. M. Waugh⁹⁸ J. M. Webb⁵⁵ C. Weber³⁰ H. A. Weber¹⁹ M. S. Weber²⁰ S. M. Weber^{64a}
 C. Wei^{63a} Y. Wei⁵⁵ A. R. Weidberg¹²⁹ E. J. Weik¹²⁰ J. Weingarten⁵⁰ C. Weiser⁵⁵ C. J. Wells⁴⁹ T. Wenaus³⁰
 B. Wendland⁵⁰ T. Wengler³⁷ N. S. Wenke,¹¹² N. Wermes²⁵ M. Wessels^{64a} A. M. Wharton⁹³ A. S. White⁶²
 A. White⁸ M. J. White¹ D. Whiteson¹⁶² L. Wickremasinghe¹²⁷ W. Wiedenmann¹⁷³ M. Wielers¹³⁷
 C. Wiglesworth⁴³ D. J. Wilbern,¹²³ H. G. Wilkens³⁷ J. J. H. Wilkinson³³ D. M. Williams⁴² H. H. Williams,¹³¹
 S. Williams³³ S. Willocq¹⁰⁵ B. J. Wilson¹⁰³ P. J. Windischhofer⁴⁰ F. I. Winkel³¹ F. Winklmeier¹²⁶
 B. T. Winter⁵⁵ J. K. Winter¹⁰³ M. Wittgen¹⁴⁶ M. Wobisch⁹⁹ T. Wojtkowski⁶¹ Z. Wolfs¹¹⁷ J. Wollrath,¹⁶²
 M. W. Wolter⁸⁸ H. Wolters^{133a,133c} M. C. Wong,¹³⁹ E. L. Woodward⁴² S. D. Worm⁴⁹ B. K. Wosiek⁸⁸
 K. W. Woźniak⁸⁸ S. Wozniowski⁵⁶ K. Wraight⁶⁰ C. Wu²¹ M. Wu^{114b} M. Wu¹¹⁶ S. L. Wu¹⁷³ X. Wu⁵⁷
 Y. Wu^{63a} Z. Wu⁴ J. Wuerzinger^{112,u} T. R. Wyatt¹⁰³ B. M. Wynne⁵³ S. Xella⁴³ L. Xia^{114a} M. Xia¹⁵
 M. Xie^{63a} S. Xin^{14,114c} A. Xiong¹²⁶ J. Xiong^{18a} D. Xu¹⁴ H. Xu^{63a} L. Xu^{63a} R. Xu¹³¹ T. Xu¹⁰⁸ Y. Xu¹⁵
 Z. Xu⁵³ Z. Xu^{114a} B. Yabsley¹⁵⁰ S. Yacoob^{34a} Y. Yamaguchi⁸⁵ E. Yamashita¹⁵⁶ H. Yamauchi¹⁶⁰
 T. Yamazaki^{18a} Y. Yamazaki⁸⁶ J. Yan,^{63c} S. Yan⁶⁰ Z. Yan¹⁰⁵ H. J. Yang^{63c,63d} H. T. Yang^{63a} S. Yang^{63a}
 T. Yang^{65c} X. Yang³⁷ X. Yang¹⁴ Y. Yang⁴⁵ Y. Yang^{63a} Z. Yang^{63a} W-M. Yao^{18a} H. Ye^{114a} H. Ye⁵⁶
 J. Ye¹⁴ S. Ye³⁰ X. Ye^{63a} Y. Yeh⁹⁸ I. Yeletsikh³⁹ B. Yeo^{18b} M. R. Yexley⁹⁸ T. P. Yildirim¹²⁹ P. Yin⁴²
 K. Yorita¹⁷¹ S. Younas^{28b} C. J. S. Young³⁷ C. Young¹⁴⁶ C. Yu^{14,114c} Y. Yu^{63a} J. Yuan^{14,114c} M. Yuan¹⁰⁸
 R. Yuan^{63d,63c} L. Yue⁹⁸ M. Zaazoua^{63a} B. Zabinski⁸⁸ E. Zaid,⁵³ Z. K. Zak⁸⁸ T. Zakareishvili¹⁶⁶ S. Zambito⁵⁷
 J. A. Zamora Saa^{140d,140b} J. Zang¹⁵⁶ D. Zanzi⁵⁵ O. Zaplatilek¹³⁵ C. Zeitnitz¹⁷⁴ H. Zeng¹⁴ J. C. Zeng¹⁶⁵

D. T. Zenger Jr.²⁷ O. Zenin³⁸ T. Ženiš^{29a} S. Zenz⁹⁶ S. Zerradi^{36a} D. Zerwas⁶⁷ M. Zhai^{14,114c} D. F. Zhang¹⁴²
 J. Zhang^{63b} J. Zhang⁶ K. Zhang^{14,114c} L. Zhang^{63a} L. Zhang^{114a} P. Zhang^{14,114c} R. Zhang¹⁷³ S. Zhang¹⁰⁸
 S. Zhang⁹¹ T. Zhang¹⁵⁶ X. Zhang^{63c} X. Zhang^{63b} Y. Zhang^{63c} Y. Zhang⁹⁸ Y. Zhang^{114a} Z. Zhang^{18a}
 Z. Zhang^{63b} Z. Zhang⁶⁷ H. Zhao¹⁴¹ T. Zhao^{63b} Y. Zhao¹³⁹ Z. Zhao^{63a} Z. Zhao^{63a} A. Zhemchugov³⁹
 J. Zheng^{114a} K. Zheng¹⁶⁵ X. Zheng^{63a} Z. Zheng¹⁴⁶ D. Zhong¹⁶⁵ B. Zhou¹⁰⁸ H. Zhou⁷ N. Zhou^{63c}
 Y. Zhou¹⁵ Y. Zhou^{114a} Y. Zhou⁷ C. G. Zhu^{63b} J. Zhu¹⁰⁸ X. Zhu^{63d} Y. Zhu^{63c} Y. Zhu^{63a} X. Zhuang¹⁴
 K. Zhukov⁶⁹ N. I. Zimine³⁹ J. Zinsser^{64b} M. Ziolkowski¹⁴⁴ L. Živković¹⁶ A. Zoccoli^{24b,24a} K. Zoch⁶²
 T. G. Zorbas¹⁴² O. Zormpa⁴⁷ W. Zou⁴² and L. Zwalinski³⁷

(ATLAS Collaboration)

¹*Department of Physics, University of Adelaide, Adelaide, Australia*

²*Department of Physics, University of Alberta, Edmonton, Alberta, Canada*

^{3a}*Department of Physics, Ankara University, Ankara, Türkiye*

^{3b}*Division of Physics, TOBB University of Economics and Technology, Ankara, Türkiye*

⁴*LAPP, Université Savoie Mont Blanc, CNRS/IN2P3, Annecy, France*

⁵*APC, Université Paris Cité, CNRS/IN2P3, Paris, France*

⁶*High Energy Physics Division, Argonne National Laboratory, Argonne, Illinois, USA*

⁷*Department of Physics, University of Arizona, Tucson, Arizona, USA*

⁸*Department of Physics, University of Texas at Arlington, Arlington, Texas, USA*

⁹*Physics Department, National and Kapodistrian University of Athens, Athens, Greece*

¹⁰*Physics Department, National Technical University of Athens, Zografou, Greece*

¹¹*Department of Physics, University of Texas at Austin, Austin, Texas, USA*

¹²*Institute of Physics, Azerbaijan Academy of Sciences, Baku, Azerbaijan*

¹³*Institut de Física d'Altes Energies (IFAE), Barcelona Institute of Science and Technology, Barcelona, Spain*

¹⁴*Institute of High Energy Physics, Chinese Academy of Sciences, Beijing, China*

¹⁵*Physics Department, Tsinghua University, Beijing, China*

¹⁶*Institute of Physics, University of Belgrade, Belgrade, Serbia*

¹⁷*Department for Physics and Technology, University of Bergen, Bergen, Norway*

^{18a}*Physics Division, Lawrence Berkeley National Laboratory, Berkeley, California, USA*

^{18b}*University of California, Berkeley, California, USA*

¹⁹*Institut für Physik, Humboldt Universität zu Berlin, Berlin, Germany*

²⁰*Albert Einstein Center for Fundamental Physics and Laboratory for High Energy Physics, University of Bern, Bern, Switzerland*

²¹*School of Physics and Astronomy, University of Birmingham, Birmingham, United Kingdom*

^{22a}*Department of Physics, Bogazici University, Istanbul, Türkiye*

^{22b}*Department of Physics Engineering, Gaziantep University, Gaziantep, Türkiye*

^{22c}*Department of Physics, Istanbul University, Istanbul, Türkiye*

^{23a}*Facultad de Ciencias y Centro de Investigaciones, Universidad Antonio Nariño, Bogotá, Colombia*

^{23b}*Departamento de Física, Universidad Nacional de Colombia, Bogotá, Colombia*

^{24a}*Dipartimento di Fisica e Astronomia A. Righi, Università di Bologna, Bologna, Italy*

^{24b}*INFN Sezione di Bologna, Italy*

²⁵*Physikalisches Institut, Universität Bonn, Bonn, Germany*

²⁶*Department of Physics, Boston University, Boston, Massachusetts, USA*

²⁷*Department of Physics, Brandeis University, Waltham, Massachusetts, USA*

^{28a}*Transilvania University of Brasov, Brasov, Romania*

^{28b}*Horia Hulubei National Institute of Physics and Nuclear Engineering, Bucharest, Romania*

^{28c}*Department of Physics, Alexandru Ioan Cuza University of Iasi, Iasi, Romania*

^{28d}*National Institute for Research and Development of Isotopic and Molecular Technologies, Physics Department, Cluj-Napoca, Romania*

^{28e}*National University of Science and Technology Politehnica, Bucharest, Romania*

^{28f}*West University in Timisoara, Timisoara, Romania*

^{28g}*Faculty of Physics, University of Bucharest, Bucharest, Romania*

^{29a}*Faculty of Mathematics, Physics and Informatics, Comenius University, Bratislava, Slovak Republic*

^{29b}*Department of Subnuclear Physics, Institute of Experimental Physics of the Slovak Academy of Sciences, Kosice, Slovak Republic*

³⁰*Physics Department, Brookhaven National Laboratory, Upton, New York, USA*

- ³¹*Universidad de Buenos Aires, Facultad de Ciencias Exactas y Naturales, Departamento de Física, y CONICET, Instituto de Física de Buenos Aires (IFIBA), Buenos Aires, Argentina*
- ³²*California State University, California, USA*
- ³³*Cavendish Laboratory, University of Cambridge, Cambridge, United Kingdom*
- ^{34a}*Department of Physics, University of Cape Town, Cape Town, South Africa*
- ^{34b}*iThemba Labs, Western Cape, South Africa*
- ^{34c}*Department of Mechanical Engineering Science, University of Johannesburg, Johannesburg, South Africa*
- ^{34d}*National Institute of Physics, University of the Philippines Diliman (Philippines), Philippines*
- ^{34e}*University of South Africa, Department of Physics, Pretoria, South Africa*
- ^{34f}*University of Zululand, KwaDlangezwa, South Africa*
- ^{34g}*School of Physics, University of the Witwatersrand, Johannesburg, South Africa*
- ³⁵*Department of Physics, Carleton University, Ottawa, Ontario, Canada*
- ^{36a}*Faculté des Sciences Ain Chock, Université Hassan II de Casablanca, Morocco*
- ^{36b}*Faculté des Sciences, Université Ibn-Tofail, Kénitra, Morocco*
- ^{36c}*Faculté des Sciences Semlalia, Université Cadi Ayyad, LPHEA-Marrakech, Morocco*
- ^{36d}*LPMR, Faculté des Sciences, Université Mohamed Premier, Oujda, Morocco*
- ^{36e}*Faculté des sciences, Université Mohammed V, Rabat, Morocco*
- ^{36f}*Institute of Applied Physics, Mohammed VI Polytechnic University, Ben Guerir, Morocco*
- ³⁷*CERN, Geneva, Switzerland*
- ³⁸*Affiliated with an institute covered by a cooperation agreement with CERN*
- ³⁹*Affiliated with an international laboratory covered by a cooperation agreement with CERN*
- ⁴⁰*Enrico Fermi Institute, University of Chicago, Chicago, Illinois, USA*
- ⁴¹*LPC, Université Clermont Auvergne, CNRS/IN2P3, Clermont-Ferrand, France*
- ⁴²*Nevis Laboratory, Columbia University, Irvington, New York, USA*
- ⁴³*Niels Bohr Institute, University of Copenhagen, Copenhagen, Denmark*
- ^{44a}*Dipartimento di Fisica, Università della Calabria, Rende, Italy*
- ^{44b}*INFN Gruppo Collegato di Cosenza, Laboratori Nazionali di Frascati, Italy*
- ⁴⁵*Physics Department, Southern Methodist University, Dallas, Texas, USA*
- ⁴⁶*Physics Department, University of Texas at Dallas, Richardson, Texas, USA*
- ⁴⁷*National Centre for Scientific Research “Demokritos”, Agia Paraskevi, Greece*
- ^{48a}*Department of Physics, Stockholm University, Sweden*
- ^{48b}*Oskar Klein Centre, Stockholm, Sweden*
- ⁴⁹*Deutsches Elektronen-Synchrotron DESY, Hamburg and Zeuthen, Germany*
- ⁵⁰*Fakultät Physik, Technische Universität Dortmund, Dortmund, Germany*
- ⁵¹*Institut für Kern- und Teilchenphysik, Technische Universität Dresden, Dresden, Germany*
- ⁵²*Department of Physics, Duke University, Durham, North Carolina, USA*
- ⁵³*SUPA—School of Physics and Astronomy, University of Edinburgh, Edinburgh, United Kingdom*
- ⁵⁴*INFN e Laboratori Nazionali di Frascati, Frascati, Italy*
- ⁵⁵*Physikalisches Institut, Albert-Ludwigs-Universität Freiburg, Freiburg, Germany*
- ⁵⁶*II. Physikalisches Institut, Georg-August-Universität Göttingen, Göttingen, Germany*
- ⁵⁷*Département de Physique Nucléaire et Corpusculaire, Université de Genève, Genève, Switzerland*
- ^{58a}*Dipartimento di Fisica, Università di Genova, Genova, Italy*
- ^{58b}*INFN Sezione di Genova, Italy*
- ⁵⁹*II. Physikalisches Institut, Justus-Liebig-Universität Giessen, Giessen, Germany*
- ⁶⁰*SUPA—School of Physics and Astronomy, University of Glasgow, Glasgow, United Kingdom*
- ⁶¹*LPSC, Université Grenoble Alpes, CNRS/IN2P3, Grenoble INP, Grenoble, France*
- ⁶²*Laboratory for Particle Physics and Cosmology, Harvard University, Cambridge, Massachusetts, USA*
- ^{63a}*Department of Modern Physics and State Key Laboratory of Particle Detection and Electronics, University of Science and Technology of China, Hefei, China*
- ^{63b}*Institute of Frontier and Interdisciplinary Science and Key Laboratory of Particle Physics and Particle Irradiation (MOE), Shandong University, Qingdao, China*
- ^{63c}*School of Physics and Astronomy, Shanghai Jiao Tong University, Key Laboratory for Particle Astrophysics and Cosmology (MOE), SKLPPC, Shanghai, China*
- ^{63d}*Tsung-Dao Lee Institute, Shanghai, China*
- ^{63e}*School of Physics and Microelectronics, Zhengzhou University, China*
- ^{64a}*Kirchhoff-Institut für Physik, Ruprecht-Karls-Universität Heidelberg, Heidelberg, Germany*
- ^{64b}*Physikalisches Institut, Ruprecht-Karls-Universität Heidelberg, Heidelberg, Germany*
- ^{65a}*Department of Physics, Chinese University of Hong Kong, Shatin, N.T., Hong Kong, China*
- ^{65b}*Department of Physics, University of Hong Kong, Hong Kong, China*

- ^{65c}*Department of Physics and Institute for Advanced Study, Hong Kong University of Science and Technology, Clear Water Bay, Kowloon, Hong Kong, China*
- ⁶⁶*Department of Physics, National Tsing Hua University, Hsinchu, Taiwan*
- ⁶⁷*IJCLab, Université Paris-Saclay, CNRS/IN2P3, 91405, Orsay, France*
- ⁶⁸*Centro Nacional de Microelectrónica (IMB-CNM-CSIC), Barcelona, Spain*
- ⁶⁹*Department of Physics, Indiana University, Bloomington, Indiana, USA*
- ^{70a}*INFN Gruppo Collegato di Udine, Sezione di Trieste, Udine, Italy*
- ^{70b}*ICTP, Trieste, Italy*
- ^{70c}*Dipartimento Politecnico di Ingegneria e Architettura, Università di Udine, Udine, Italy*
- ^{71a}*INFN Sezione di Lecce, Italy*
- ^{71b}*Dipartimento di Matematica e Fisica, Università del Salento, Lecce, Italy*
- ^{72a}*INFN Sezione di Milano, Italy*
- ^{72b}*Dipartimento di Fisica, Università di Milano, Milano, Italy*
- ^{73a}*INFN Sezione di Napoli, Italy*
- ^{73b}*Dipartimento di Fisica, Università di Napoli, Napoli, Italy*
- ^{74a}*INFN Sezione di Pavia, Italy*
- ^{74b}*Dipartimento di Fisica, Università di Pavia, Pavia, Italy*
- ^{75a}*INFN Sezione di Pisa, Italy*
- ^{75b}*Dipartimento di Fisica E. Fermi, Università di Pisa, Pisa, Italy*
- ^{76a}*INFN Sezione di Roma, Italy*
- ^{76b}*Dipartimento di Fisica, Sapienza Università di Roma, Roma, Italy*
- ^{77a}*INFN Sezione di Roma Tor Vergata, Italy*
- ^{77b}*Dipartimento di Fisica, Università di Roma Tor Vergata, Roma, Italy*
- ^{78a}*INFN Sezione di Roma Tre, Italy*
- ^{78b}*Dipartimento di Matematica e Fisica, Università Roma Tre, Roma, Italy*
- ^{79a}*INFN-TIFPA, Italy*
- ^{79b}*Università degli Studi di Trento, Trento, Italy*
- ⁸⁰*Universität Innsbruck, Department of Astro and Particle Physics, Innsbruck, Austria*
- ⁸¹*University of Iowa, Iowa City, Iowa, USA*
- ⁸²*Department of Physics and Astronomy, Iowa State University, Ames, Iowa, USA*
- ⁸³*Istinye University, Sariyer, Istanbul, Türkiye*
- ^{84a}*Departamento de Engenharia Elétrica, Universidade Federal de Juiz de Fora (UFJF), Juiz de Fora, Brazil*
- ^{84b}*Universidade Federal do Rio De Janeiro COPPE/EE/IF, Rio de Janeiro, Brazil*
- ^{84c}*Instituto de Física, Universidade de São Paulo, São Paulo, Brazil*
- ^{84d}*Rio de Janeiro State University, Rio de Janeiro, Brazil*
- ^{84e}*Federal University of Bahia, Bahia, Brazil*
- ⁸⁵*KEK, High Energy Accelerator Research Organization, Tsukuba, Japan*
- ⁸⁶*Graduate School of Science, Kobe University, Kobe, Japan*
- ^{87a}*AGH University of Krakow, Faculty of Physics and Applied Computer Science, Krakow, Poland*
- ^{87b}*Marian Smoluchowski Institute of Physics, Jagiellonian University, Krakow, Poland*
- ⁸⁸*Institute of Nuclear Physics Polish Academy of Sciences, Krakow, Poland*
- ⁸⁹*Faculty of Science, Kyoto University, Kyoto, Japan*
- ⁹⁰*Research Center for Advanced Particle Physics and Department of Physics, Kyushu University, Fukuoka, Japan*
- ⁹¹*L2IT, Université de Toulouse, CNRS/IN2P3, UPS, Toulouse, France*
- ⁹²*Instituto de Física La Plata, Universidad Nacional de La Plata and CONICET, La Plata, Argentina*
- ⁹³*Physics Department, Lancaster University, Lancaster, United Kingdom*
- ⁹⁴*Oliver Lodge Laboratory, University of Liverpool, Liverpool, United Kingdom*
- ⁹⁵*Department of Experimental Particle Physics, Jožef Stefan Institute and Department of Physics, University of Ljubljana, Ljubljana, Slovenia*
- ⁹⁶*School of Physics and Astronomy, Queen Mary University of London, London, United Kingdom*
- ⁹⁷*Department of Physics, Royal Holloway University of London, Egham, United Kingdom*
- ⁹⁸*Department of Physics and Astronomy, University College London, London, United Kingdom*
- ⁹⁹*Louisiana Tech University, Ruston, Louisiana, USA*
- ¹⁰⁰*Fysiska institutionen, Lunds universitet, Lund, Sweden*
- ¹⁰¹*Departamento de Física Teórica C-15 and CIAFF, Universidad Autónoma de Madrid, Madrid, Spain*
- ¹⁰²*Institut für Physik, Universität Mainz, Mainz, Germany*
- ¹⁰³*School of Physics and Astronomy, University of Manchester, Manchester, United Kingdom*
- ¹⁰⁴*CPPM, Aix-Marseille Université, CNRS/IN2P3, Marseille, France*

- ¹⁰⁵*Department of Physics, University of Massachusetts, Amherst, Massachusetts, USA*
- ¹⁰⁶*Department of Physics, McGill University, Montreal, Quebec, Canada*
- ¹⁰⁷*School of Physics, University of Melbourne, Victoria, Australia*
- ¹⁰⁸*Department of Physics, University of Michigan, Ann Arbor, Michigan, USA*
- ¹⁰⁹*Department of Physics and Astronomy, Michigan State University, East Lansing, Michigan, USA*
- ¹¹⁰*Group of Particle Physics, University of Montreal, Montreal, Quebec, Canada*
- ¹¹¹*Fakultät für Physik, Ludwig-Maximilians-Universität München, München, Germany*
- ¹¹²*Max-Planck-Institut für Physik (Werner-Heisenberg-Institut), München, Germany*
- ¹¹³*Graduate School of Science and Kobayashi-Maskawa Institute, Nagoya University, Nagoya, Japan*
- ^{114a}*Department of Physics, Nanjing University, Nanjing, China*
- ^{114b}*School of Science, Shenzhen Campus of Sun Yat-sen University, China*
- ^{114c}*University of Chinese Academy of Science (UCAS), Beijing, China*
- ¹¹⁵*Department of Physics and Astronomy, University of New Mexico, Albuquerque, New Mexico, USA*
- ¹¹⁶*Institute for Mathematics, Astrophysics and Particle Physics, Radboud University/Nikhef, Nijmegen, Netherlands*
- ¹¹⁷*Nikhef National Institute for Subatomic Physics and University of Amsterdam, Amsterdam, Netherlands*
- ¹¹⁸*Department of Physics, Northern Illinois University, DeKalb, Illinois, USA*
- ^{119a}*New York University Abu Dhabi, Abu Dhabi, United Arab Emirates*
- ^{119b}*United Arab Emirates University, Al Ain, United Arab Emirates*
- ¹²⁰*Department of Physics, New York University, New York, New York, USA*
- ¹²¹*Ochanomizu University, Otsuka, Bunkyo-ku, Tokyo, Japan*
- ¹²²*Ohio State University, Columbus, Ohio, USA*
- ¹²³*Homer L. Dodge Department of Physics and Astronomy, University of Oklahoma, Norman, Oklahoma, USA*
- ¹²⁴*Department of Physics, Oklahoma State University, Stillwater, Oklahoma, USA*
- ¹²⁵*Palacký University, Joint Laboratory of Optics, Olomouc, Czech Republic*
- ¹²⁶*Institute for Fundamental Science, University of Oregon, Eugene, Oregon, USA*
- ¹²⁷*Graduate School of Science, Osaka University, Osaka, Japan*
- ¹²⁸*Department of Physics, University of Oslo, Oslo, Norway*
- ¹²⁹*Department of Physics, Oxford University, Oxford, United Kingdom*
- ¹³⁰*LPNHE, Sorbonne Université, Université Paris Cité, CNRS/IN2P3, Paris, France*
- ¹³¹*Department of Physics, University of Pennsylvania, Philadelphia, Pennsylvania, USA*
- ¹³²*Department of Physics and Astronomy, University of Pittsburgh, Pittsburgh, Pennsylvania, USA*
- ^{133a}*Laboratório de Instrumentação e Física Experimental de Partículas—LIP, Lisboa, Portugal*
- ^{133b}*Departamento de Física, Faculdade de Ciências, Universidade de Lisboa, Lisboa, Portugal*
- ^{133c}*Departamento de Física, Universidade de Coimbra, Coimbra, Portugal*
- ^{133d}*Centro de Física Nuclear da Universidade de Lisboa, Lisboa, Portugal*
- ^{133e}*Departamento de Física, Universidade do Minho, Braga, Portugal*
- ^{133f}*Departamento de Física Teórica y del Cosmos, Universidad de Granada, Granada (Spain), Spain*
- ^{133g}*Departamento de Física, Instituto Superior Técnico, Universidade de Lisboa, Lisboa, Portugal*
- ¹³⁴*Institute of Physics of the Czech Academy of Sciences, Prague, Czech Republic*
- ¹³⁵*Czech Technical University in Prague, Prague, Czech Republic*
- ¹³⁶*Charles University, Faculty of Mathematics and Physics, Prague, Czech Republic*
- ¹³⁷*Particle Physics Department, Rutherford Appleton Laboratory, Didcot, United Kingdom*
- ¹³⁸*IRFU, CEA, Université Paris-Saclay, Gif-sur-Yvette, France*
- ¹³⁹*Santa Cruz Institute for Particle Physics, University of California Santa Cruz, Santa Cruz, California, USA*
- ^{140a}*Departamento de Física, Pontificia Universidad Católica de Chile, Santiago, Chile*
- ^{140b}*Millennium Institute for Subatomic physics at high energy frontier (SAPHIR), Santiago, Chile*
- ^{140c}*Instituto de Investigación Multidisciplinario en Ciencia y Tecnología, y Departamento de Física, Universidad de La Serena, Chile*
- ^{140d}*Universidad Andres Bello, Department of Physics, Santiago, Chile*
- ^{140e}*Instituto de Alta Investigación, Universidad de Tarapacá, Arica, Chile*
- ^{140f}*Departamento de Física, Universidad Técnica Federico Santa María, Valparaíso, Chile*
- ¹⁴¹*Department of Physics, University of Washington, Seattle, Washington, USA*
- ¹⁴²*Department of Physics and Astronomy, University of Sheffield, Sheffield, United Kingdom*
- ¹⁴³*Department of Physics, Shinshu University, Nagano, Japan*
- ¹⁴⁴*Department Physik, Universität Siegen, Siegen, Germany*
- ¹⁴⁵*Department of Physics, Simon Fraser University, Burnaby, British Columbia, Canada*
- ¹⁴⁶*SLAC National Accelerator Laboratory, Stanford, California, USA*

- ¹⁴⁷*Department of Physics, Royal Institute of Technology, Stockholm, Sweden*
- ¹⁴⁸*Departments of Physics and Astronomy, Stony Brook University, Stony Brook, New York, USA*
- ¹⁴⁹*Department of Physics and Astronomy, University of Sussex, Brighton, United Kingdom*
- ¹⁵⁰*School of Physics, University of Sydney, Sydney, Australia*
- ¹⁵¹*Institute of Physics, Academia Sinica, Taipei, Taiwan*
- ^{152a}*E. Andronikashvili Institute of Physics, Iv. Javakishvili Tbilisi State University, Tbilisi, Georgia*
- ^{152b}*High Energy Physics Institute, Tbilisi State University, Tbilisi, Georgia*
- ^{152c}*University of Georgia, Tbilisi, Georgia*
- ¹⁵³*Department of Physics, Technion, Israel Institute of Technology, Haifa, Israel*
- ¹⁵⁴*Raymond and Beverly Sackler School of Physics and Astronomy, Tel Aviv University, Tel Aviv, Israel*
- ¹⁵⁵*Department of Physics, Aristotle University of Thessaloniki, Thessaloniki, Greece*
- ¹⁵⁶*International Center for Elementary Particle Physics and Department of Physics, University of Tokyo, Tokyo, Japan*
- ¹⁵⁷*Department of Physics, Tokyo Institute of Technology, Tokyo, Japan*
- ¹⁵⁸*Department of Physics, University of Toronto, Toronto, Ontario, Canada*
- ^{159a}*TRIUMF, Vancouver, British Columbia, Canada*
- ^{159b}*Department of Physics and Astronomy, York University, Toronto, Ontario, Canada*
- ¹⁶⁰*Division of Physics and Tomonaga Center for the History of the Universe, Faculty of Pure and Applied Sciences, University of Tsukuba, Tsukuba, Japan*
- ¹⁶¹*Department of Physics and Astronomy, Tufts University, Medford, Massachusetts, USA*
- ¹⁶²*Department of Physics and Astronomy, University of California Irvine, Irvine, California, USA*
- ¹⁶³*University of Sharjah, Sharjah, United Arab Emirates*
- ¹⁶⁴*Department of Physics and Astronomy, University of Uppsala, Uppsala, Sweden*
- ¹⁶⁵*Department of Physics, University of Illinois, Urbana, Illinois, USA*
- ¹⁶⁶*Instituto de Física Corpuscular (IFIC), Centro Mixto Universidad de Valencia—CSIC, Valencia, Spain*
- ¹⁶⁷*Department of Physics, University of British Columbia, Vancouver, British Columbia, Canada*
- ¹⁶⁸*Department of Physics and Astronomy, University of Victoria, Victoria, British Columbia, Canada*
- ¹⁶⁹*Fakultät für Physik und Astronomie, Julius-Maximilians-Universität Würzburg, Würzburg, Germany*
- ¹⁷⁰*Department of Physics, University of Warwick, Coventry, United Kingdom*
- ¹⁷¹*Waseda University, Tokyo, Japan*
- ¹⁷²*Department of Particle Physics and Astrophysics, Weizmann Institute of Science, Rehovot, Israel*
- ¹⁷³*Department of Physics, University of Wisconsin, Madison, Wisconsin, USA*
- ¹⁷⁴*Fakultät für Mathematik und Naturwissenschaften, Fachgruppe Physik, Bergische Universität Wuppertal, Wuppertal, Germany*
- ¹⁷⁵*Department of Physics, Yale University, New Haven, Connecticut, USA*

^aDeceased.

^bAlso at Department of Physics, King's College London, London, United Kingdom.

^cAlso at Institute of Physics, Azerbaijan Academy of Sciences, Baku, Azerbaijan.

^dAlso at TRIUMF, Vancouver, British Columbia, Canada.

^eAlso at Department of Physics, University of Thessaly, Greece.

^fAlso at An-Najah National University, Nablus, Palestine.

^gAlso at Department of Physics, University of Fribourg, Fribourg, Switzerland.

^hAlso at Department of Physics, Westmont College, Santa Barbara, USA.

ⁱAlso at Departament de Física de la Universitat Autònoma de Barcelona, Barcelona, Spain.

^jAlso at Affiliated with an institute covered by a cooperation agreement with CERN.

^kAlso at The Collaborative Innovation Center of Quantum Matter (CICQM), Beijing, China.

^lAlso at Faculty of Physics, Sofia University, 'St. Kliment Ohridski', Sofia, Bulgaria.

^mAlso at Università di Napoli Parthenope, Napoli, Italy.

ⁿAlso at Institute of Particle Physics (IPP), Canada.

^oAlso at University of Colorado Boulder, Department of Physics, Colorado, USA.

^pAlso at Borough of Manhattan Community College, City University of New York, New York, New York, USA.

^qAlso at National Institute of Physics, University of the Philippines Diliman (Philippines), Philippines.

^rAlso at Department of Financial and Management Engineering, University of the Aegean, Chios, Greece.

^sAlso at Centro Studi e Ricerche Enrico Fermi, Italy.

^tAlso at Institutio Catalana de Recerca i Estudis Avancats, ICREA, Barcelona, Spain.

^uAlso at Technical University of Munich, Munich, Germany.

^vAlso at CMD-AC UNEC Research Center, Azerbaijan State University of Economics (UNEC), Azerbaijan.

^wAlso at Yeditepe University, Physics Department, Istanbul, Türkiye.

^xAlso at Institute of Theoretical Physics, Iliia State University, Tbilisi, Georgia.

^yAlso at CERN, Geneva, Switzerland.

^zAlso at Center for Interdisciplinary Research and Innovation (CIRI-AUTH), Thessaloniki, Greece.

^{aa}Also at Hellenic Open University, Patras, Greece.

^{bb}Also at Department of Physics, Stellenbosch University, South Africa.

^{cc}Also at Department of Physics, California State University, Sacramento, USA.

^{dd}Also at Département de Physique Nucléaire et Corpusculaire, Université de Genève, Genève, Switzerland.

^{ee}Also at Institut für Experimentalphysik, Universität Hamburg, Hamburg, Germany.

^{ff}Also at Department of Physics, Stanford University, Stanford, California, USA.

^{gg}Also at Institute for Nuclear Research and Nuclear Energy (INRNE) of the Bulgarian Academy of Sciences, Sofia, Bulgaria.

^{hh}Also at Washington College, Chestertown, Maryland, USA.

ⁱⁱAlso at Institute of Applied Physics, Mohammed VI Polytechnic University, Ben Guerir, Morocco.